Fakultät für Mathematik und Physik

Institut für Theoretische Physik

Lehrstuhl Prof. Dr. Hugo Reinhardt

Eberhard Karls
Universität
Tübingen

Coulomb Gauge Quark Propagator from Lattice Quantum Chromodynamics

Diplomarbeit
Universität Tübingen

Mario Schröck

30. Juli 2010

Betreuer:
Prof. Dr. H. Reinhardt

Zweitgutachter:
PD Dr. M. Quandt

Eigenständigkeitserklärung

Hiermit versichere ich, dass ich die vorliegende Diplomarbeit selbständig verfasst und keine anderen als die angegebenen Quellen und Hilfsmittel verwendet habe.

Tübingen, den 30. Juli 2010

Mario Schröck

Zusammenfassung[1]

Die Quantenchromodynamik (QCD) [1, 2] ist die Theorie der starken Wechselwirkung, welche für das Hadronenspektrum und somit für die ganze Materie in unserer Alltag, verantwortlich ist. Die QCD, als Quantenfeldtheorie und Teil des Standardmodells der Elementarteilchen, beschreibt die Wechselwirkung zwischen farbgeladenen Quarks und Gluonen. Hadronen wie z.B. das Proton, das Neutron oder das Pion, um die bekanntesten zu nennen, bestehen aus zwei bzw. drei Quarks, welche durch die Gluonen zusammengehalten werden, um dann ein farbneutrales Teilchen zu bilden. In den 1970er Jahren haben große Beschleunigerexperimente die Existenz der Quarks bestätigt, nichts desto trotz wurden einzelne Quarks nie in der Natur beobachtet. Man sagt, Quarks sind innerhalb farbneutraler Zusammensetzungen eingeschlossen, dieses Phänomen ist als *Quark Confinement* bekannt.

Bei darauffolgenden Experimenten entdeckte man, dass Quarks bei sehr kleinen Abständen – oder äquivalent sehr großen Energien – die starke Wechselwirkung nicht zu spüren scheinen, diese Eigenschaft wurde bekannt unter dem Namen *Asymptotische Freiheit* und ermöglichte den Physikern die Störungstheorie, welche Ergebnisse mit beeindruckender Genauigkeit in der Quantenelektrodynamik hervorbrachte, auf die QCD anzuwenden, innerhalb des Bereichs in dem die Kopplung als schwach angesehen werden kann. Jedoch finden Phänomene wie die spontane Brechung der chiralen Symmetrie, welche für Teilchen aus leichten Quarks den größten Massenbeitrag liefert, in der Niedrigimpulsregion statt und sind somit der Störungstheorie nicht zugänglich.

Im Jahre 1974 stellte Wilson [3] ein Formulierung von Eichtheorien auf einem diskreten Raumzeitgitter vor. Das Gitter, welches einen kleinstmöglichen Abstand – einen größtmöglichen Impuls – einführt, dient als Regulator für Quantenfeldtheorien. Heute ist das Gitter der vielversprechendste *ab initio* Ansatz um die Geheimnisse der Natur, welche der Dynamik von Quantenfeldtheorien unterliegen, mit der Hilfe von Supercomputern, zu lüften. QCD ist eine renormierbare Theorie und somit werden physikalische Observablen unabhängig vom *cutoff*,

1 Dieses Kapitel entspricht weitestgehend einer Übersetzung der Einleitung auf deutsch.

also im Fall des Gitters der Gitterkonstanten, wenn man sie gegen Null gehen lässt und somit der Kontinuumslimes vollzogen wird. Die Gitterformulierung der QCD ist von Natur aus nicht-perturbativ und somit gut geeignet um die volle Dynamik von Quarks und Gluonen zu studieren.

Die bekanntesten Eichungen in Eichtheorien sind die Landau- und die Coulomb-Eichung. Während die Landau-Eichung frei ersichtlich kovariant ist und somit räumliche und zeitliche Freiheitsgrade gleichermaßen behandelt, ist die Coulomb-Eichung auf natürliche Weise mit physikalischen Freiheitsgraden verbunden. Desweiteren bietet das Gribov-Zwanziger Szenario [4, 5, 6], ein gefälliges Bild des Confinements. Die Nichtkovarianz der Coulomb-Eichung macht technischen Fortschritt schwierig, dennoch haben in den letzten Jahren verschiedene Ansätze zu achtungsvollem Vorsprung geführt. Darunter sind ein Hamilton-basierte Ansatz, ein Dyson-Schwinger Funktionalintegralansatz und das Gitter zu nennen, siehe z.B. [7, 8, 9, 10, 11].

In dieser Arbeit untersuchen wir den Quarkpropagator, welcher die fermionische Zweipunktsfunktion der QCD ist, in Coulomb-Eichung auf dem Gitter. Im Laufe der Studie erforschen wir die Struktur des wechselwirkenden Propagators und dabei gewinnen wir wertvolle Einblicke in die Dynamik der QCD. Im ersten Anlauf analysieren wir den Quarkpropagator, mittels zweier Formulierungen von Fermionen auf dem Gitter, in sogenannter *quenched* Näherung. Das bedeutet, wir vernachlässigen Anfangs die Effekte von Seequarks. Darauffolgend vollziehen wir schließlich eine Studie welche dynamische Quarks beinhaltet. Desweiteren prüfen und beweisen wir Renormierbarkeit für den (statischen) Quarkpropagator in Coulomb-Eichung auf dem Gitter.

Unseres Wissens nach, wurden bisher keine Studien des Quarkpropagators in Coulomb-Eichung auf dem Gitter vollzogen, während die Literatur reich an Arbeiten über den Gitterquarkpropagator in Landau-Eichung ist, siehe z.B. [12, 13, 14, 15, 16, 17, 18].

Contents

Chapter 1

Introduction

Quantum Chromodynamics (QCD) [1, 2] is the theory of the strong interaction which is responsible for the hadron spectrum and therefore for all matter in our everyday life. QCD, being a quantum field theory and part of the standard model of elementary particles, describes the interactions between color-charged quarks and gluons. Hadrons, e.g., protons, neutrons and the pion, to name the most famous, are made up of two or three quarks, respectively, "glued" together by gluons to build a color-neutral particle. In the 1970s, large accelerator experiments confirmed the existence of the quarks, nevertheless, single quarks have never been observed in nature. Quarks are said to be *confined* within color-neutral composites.

Subsequent experiments found that at very small distances – or equivalently high momenta – the quarks seem not to be affected by the strong nuclear force. This phenomenon is known as *asymptotic freedom* and it enabled physicists to apply perturbation theory, which engendered calculations with astonishing precision in Quantum Electrodynamics (QED), to QCD, for the regime of weak coupling. Phenomena like spontaneous chiral symmetry breaking, though, which is responsible for the mass of light-quark composites, like the nucleons, occur in the low-momentum regime and therefore their exploration can not be tackled within perturbation theory.

In 1974, Wilson [3] proposed a formulation of gauge theories on a discrete space-time lattice. The lattice, introducing a smallest possible length or equivalently a largest momentum, serves as a regulator for quantum field theories. Today, lattice gauge theory is the most promising *ab initio* approach to reveal the secrets of nature, underlying the dynamics of quantum field theories, by numerics on large scale computers. QCD is a renormalizable theory and thus physical observables become independent of the cutoff once it is removed, i.e., once the continuum limit is taken on the lattice. Since the lattice formulation of QCD is inherently non-perturbative, it

is well suited for studying the full dynamics of quarks and gluons.

The most popular gauges of gauge theories are the Landau and the Coulomb gauge. Whereas the Landau gauge is manifestly covariant and consequently treats spatial and temporal degrees of freedom uniformly, the Coulomb gauge framework is naturally connected to physical degrees of freedom and the Gribov-Zwanziger scenario [4, 5, 6], features an appealing picture for confinement. Non-covariance of Coulomb gauge makes technical progress difficult, nevertheless, in the recent years various approaches enjoyed significant advance. Among them are to name a Hamilton-based approach, a Dyson-Schwinger based functional integral approach and the lattice, see, e.g., [7, 8, 9, 10, 11].

In this work, we examine the quark propagator, which is the fermionic two-point function of QCD, in Coulomb gauge on the lattice. Throughout this study we explore the structure of the interacting propagator and thereby we will gain valuable insights in the dynamics of QCD. As a first attempt, we explore the quark propagator using two kinds of fermion lattice formulations in quenched approximation, i.e., we initially neglect the effects of sea quarks. Thereafter, we eventually conduct a study including dynamical quarks. Furthermore, we will test and prove renormalizability of the (static) Coulomb gauge lattice quark propagator.

As to our knowledge, no previous studies of the lattice quark propagator in Coulomb gauge have been performed, whereas the literature contains extensive studies of the propagator in Landau gauge, see, e.g., [12, 13, 14, 15, 16, 17, 18].

The remainder of this work is as follows: in Chap. 2, we will introduce the path integral approach to quantization, based on ordinary quantum mechanics and we will reveal the connection of the path integral to ground state expectation values. In Chap. 3, we will consider the quantum mechanical harmonic oscillator as a scalar 0+1 dimensional quantum field theory and subsequently formulate the latter on a discrete temporal lattice. We will generalize this picture to relativistic bosonic fields, introduce fermions and gauge fields on the lattice and finally end up with a complete formulation of lattice QCD. During this journey, our focus will always lie on the two-point function of the theory under discussion. In Chap. 4, we will discuss the computation of the Coulomb gauge quark propagator on a discrete space-time lattice and its decomposition into spatial, temporal and massive components, in detail. In Chap. 5, we will present our various findings for the Coulomb gauge quark propagator and in Chap. 6, we will summarize and give an outlook on possible further studies.

Chapter 2

Path Integrals and Green's Functions

Within this preluding chapter we will introduce basic concepts from quantum mechanics to quantum field theory in order to collect the preliminaries needed for subsequent introduction of lattice field theory. This chapter is mainly leant to [19, 20, 21].

2.1 The path integral approach to quantum mechanics

In this section we derive the path integral representation of the propagator in quantum mechanics and show equality of the propagator, the transition amplitude and Green's function of Schrödinger's equation. After performing these steps in great detail for conventional Minkowski space, we state the corresponding results for Euclidean space where the time parameter is purely imaginary.

2.1.1 Real time formulation

In ordinary quantum mechanics, time evolution is described by Schrödinger's equation,

$$i\hbar\partial_t \left|\alpha,t\right\rangle = H \left|\alpha,t\right\rangle , \tag{2.1}$$

where the underlying system is fully characterized by a time-dependent Schrödinger state ket $|\alpha,t\rangle$ which is an element of a complex Hilbert space $\mathcal{H}$. The dimensionality of $\mathcal{H}$ is determined by the nature of the physical problem under consideration. The operator $H : \mathcal{H} \to \mathcal{H}$ is the Hamiltonian of the system. Suppose the latter is time-independent: then time evolution is

equivalently given by the following time-evolution operator,

$$U(t,t_0) = \mathrm{e}^{-iH(t-t_0)/\hbar}, \quad t \geq t_0, \tag{2.2}$$

which evolves a given state $|\alpha,t_0\rangle \equiv |\alpha\rangle$ at time t_0 towards later times t:

$$|\alpha,t\rangle = U(t,t_0)\,|\alpha\rangle\,. \tag{2.3}$$

In every Hilbert space, a scalar product is defined by $\langle\alpha|\beta\rangle$ whereby the state bra $\langle\alpha| \in \mathcal{H}^*$ is an element of the dual space of $\mathcal{H}$. Time evolution of a bra state is accomplished by the hermitian conjugate of $U(t,t_0)$, [1]

$$\langle\alpha|\,U^\dagger(t,t_0) = \langle\alpha,t|\,. \tag{2.4}$$

Using the coordinate basis $\{\langle\boldsymbol{x}|\}$ in $\mathcal{H}^*$, the scalar product for a given state ket, $\langle\boldsymbol{x}|\alpha,t\rangle$, can be interpreted as a scalar valued function of $\boldsymbol{x}$ which is known as wave function $\psi(\boldsymbol{x},t) \equiv \langle\boldsymbol{x}|\alpha,t\rangle$. One should acknowledge the fact that eigenstates of operators are time-independent in the Schrödinger picture.[2] Hence we can formally write (2.3) in coordinate space as

$$\begin{aligned}\psi(\boldsymbol{x},t) &= \int \mathrm{d}^3x'\ \langle\boldsymbol{x}|\,U(t,t')\,|\boldsymbol{x}'\rangle\,\psi(\boldsymbol{x}',t') \\ &\equiv \int \mathrm{d}^3x'\,K(\boldsymbol{x},t;\boldsymbol{x}',t')\psi(\boldsymbol{x}',t')\end{aligned} \tag{2.5}$$

where we used the completeness relation $\int \mathrm{d}^3x'\ |\boldsymbol{x}'\rangle\,\langle\boldsymbol{x}'| = \mathbb{1}$. From the above equation it can be seen that the transition amplitude $\langle\boldsymbol{x}|\,U(t,t')\,|\boldsymbol{x}'\rangle$ acts as a propagator $K(\boldsymbol{x},t;\boldsymbol{x}',t')$ for the wave function $\psi(\boldsymbol{x}',t')$, i.e., once an initial wave function $\psi(\boldsymbol{x}',t')$ is given, time evolution is completely determined by the propagator $K(\boldsymbol{x},t;\boldsymbol{x}',t')$ – supposed that the system is left undisturbed.

Since $\psi(\boldsymbol{x},t)$ is subject to Schrödinger's time-dependent wave equation, it is obvious from (2.5) that $K(\boldsymbol{x},t;\boldsymbol{x}',t')$ also fulfills it in the variables $\boldsymbol{x},t$. Furthermore, an apparent property of the transition amplitude is $\lim_{t\to t'}\langle\boldsymbol{x}|\,U(t,t')\,|\boldsymbol{x}'\rangle = \delta(\boldsymbol{x}-\boldsymbol{x}')$ and consequently the propagator equals the wave equation's Green's function up to a factor $i/\hbar$,

$$\left(-\frac{\hbar^2}{2m}\Delta + V(\boldsymbol{x}) - i\hbar\partial_t\right) K(\boldsymbol{x},t;\boldsymbol{x}',t') = -i\hbar\delta(\boldsymbol{x}-\boldsymbol{x}')\delta(t-t'), \tag{2.6}$$

with the causality boundary condition $K(\boldsymbol{x},t;\boldsymbol{x}',t') = 0$ for $t < t'$. Note that in (2.6) the

1 U is an unitary operator, $U^\dagger U = \mathbb{1}$, as long as H is hermitian.
2 Since we assume that H is time-independent.

potential $V(\boldsymbol{x})$ is a function of the coordinate operator $\boldsymbol{x}$ and $-i\hbar\nabla$ is the coordinate space representation of the momentum operator $\boldsymbol{p}$, thus $\boldsymbol{p}^2 = -\hbar^2\Delta$.

To simplify the following analysis, we restrict our setup to one spatial dimension, hence we consider a point particle of mass m moving along the x-axis under the influence of a potential $V(x)$. The corresponding Hamiltonian reads

$$H = \frac{p^2}{2m} + V(x). \tag{2.7}$$

Making use of the time-evolution operator's composition property, $U(t,t'') = U(t,t')U(t',t'')$, $t \geq t' \geq t''$, and, again, of the completeness relation in coordinate space, we can write

$$\langle x|\, U(t,t'')\, |x''\rangle = \int \mathrm{d}x'\ \langle x|\, U(t,t')\, |x'\rangle\, \langle x'|\, U(t',t'')\, |x''\rangle\,. \tag{2.8}$$

Obviously, we can repeat the aforementioned decomposition of the propagator an arbitrary number of times; we divide the time interval $[t',t]$ into N pieces of length $a = (t-t')/N$ resulting in

$$\langle x_N|\, U(t_N,t_0)\, |x_0\rangle = \int \mathrm{d}x_1 \int \mathrm{d}x_2\ \ldots \int \mathrm{d}x_{N-1} \prod_{i=0}^{N-1} \langle x_{i+1}|\, U(t_{i+1},t_i)\, |x_i\rangle\,. \tag{2.9}$$

In the last equation we have set $x' = x_0, t' = t_0$ and $x = x_N, t = t_N$ for the sake of a uniform notation. We want to further investigate a single factor of the right-hand side (r.h.s.) of (2.9). Therefore we will need the momentum operator's eigenfunctions, the plane waves,

$$\langle x'|p'\rangle = \frac{1}{\sqrt{2\pi\hbar}}\, \mathrm{e}^{ip'x'/\hbar}, \tag{2.10}$$

and moreover the Baker-Campbell-Hausdorff formula (see ,e.g., [19]) to obtain an approximation of the exponential of a sum of functions of the non-commuting operators x and p for small a,

$$\mathrm{e}^{-iaH/\hbar} \approx \mathrm{e}^{-iap^2/(2m\hbar)}\, \mathrm{e}^{-iaV(x)/\hbar}. \tag{2.11}$$

Therewith we can approximate each of the products of (2.9) according to

$$\begin{aligned}
\langle x_{i+1}|\, U(t_{i+1},t_i)\, |x_i\rangle &\approx \int \mathrm{d}p'\ \langle x_{i+1}|\, \mathrm{e}^{-iap^2/2m\hbar}\, |p'\rangle\, \langle p'|\, \mathrm{e}^{-iaV(x)/\hbar}\, |x_i\rangle \\
&\approx \frac{1}{2\pi\hbar} \int \mathrm{d}p'\ \mathrm{e}^{-ia\left[p'^2 - 2mp'(x_{i+1}-x_i)/a\right]/2m\hbar}\, \mathrm{e}^{-iaV(x_i)/\hbar} \\
&\approx \frac{1}{2\pi\hbar} \int \mathrm{d}p'\ \mathrm{e}^{-ia[p'-m(x_{i+1}-x_i)/a]^2/2m\hbar}\, \mathrm{e}^{im(x_{i+1}-x_i)^2/2\hbar a}\, \mathrm{e}^{-iaV(x_i)/\hbar}.
\end{aligned} \tag{2.12}$$

This integral is known as Fresnel integral and the integrand herein is not convergent: to ensure

convergence we slightly shift the time-step size into the complex plane, $a \to a - i\varepsilon$, so that the exponent gets suppressed for large p' values. After the integration we let $\varepsilon \to 0$. Then the value of above Gaussian integral is given by $\sqrt{2\pi\hbar m/ia}$ and thus

$$\langle x_{i+1}| U(t_{i+1},t_i) |x_i\rangle \approx \sqrt{\frac{m}{2\pi\hbar i a}}\, \mathrm{e}^{ia\left[m(x_{i+1}-x_i)^2/(2a^2)-V(x_i)\right]/\hbar}. \tag{2.13}$$

Inserting this back into the expression for the propagator, (2.9), yields

$$\langle x_N| U(t_N,t_0) |x_0\rangle \approx \int \mathrm{d}x_1 \int \mathrm{d}x_2 \ \ldots \int \mathrm{d}x_{N-1} \left(\frac{m}{2\pi\hbar i a}\right)^{N/2} \times \exp\left(i\frac{a}{\hbar}\sum_{i=0}^{N-1}\left[\frac{m\,(x_{i+1}-x_i)^2}{2a^2} - V(x_i)\right]\right). \tag{2.14}$$

We are now ready to formally take the continuum time limit, i.e., letting $a \to 0$ and $N \to \infty$, in order to achieve a path integral (PI) representation for the transition amplitude:

$$\langle x_N| U(t_N,t_0) |x_0\rangle = \int \mathcal{D}[x]\ \mathrm{e}^{iS[x,\dot{x}]/\hbar}. \tag{2.15}$$

In the last expression, we have *formally* defined the integration measure as

$$\int \mathcal{D}[x] \ = \lim_{a\to 0}\left(\frac{m}{2\pi\hbar i a}\right)^{N/2} \int \mathrm{d}x_1 \int \mathrm{d}x_2 \ \ldots \int \mathrm{d}x_{N-1}\,, \tag{2.16}$$

moreover, we have introduced the action

$$S\,[x,\dot{x}] = \int_{t_0}^{t_N} \mathrm{d}t\, L\,[x,\dot{x}] = \int_{t_0}^{t_N} \mathrm{d}t\ \left[\frac{m}{2}\dot{x}^2 - V(x)\right]. \tag{2.17}$$

$L\,[x,\dot{x}]$ is the Lagrangian of the system. It has to be pointed out that in (2.15) x is not an operator anymore but simply a number which depends on the time index. When formally taking the continuum time limit, x becomes a function of t and hence the Lagrangian, as well as the action, are functionals of *classical* trajectories $x(t)$. In (2.15), the points $x_0 = x(t_0)$ and $x_N = x(t_N)$ are held fixed and we integrate over all paths between these two points while every path is weighted by a factor $\exp\left(iS\,[x,\dot{x}]\,/\hbar\right)$. Before we further discuss the path integral representation, let us switch to the Euclidean time formulation.

2.1.2 Imaginary time formulation

The weighting factor of (2.15) consists of a highly oscillating phase which is clearly inappropriate for numerical calculations. In order to remove this phase factor we perform a so called Wick

rotation, that is we replace $t \to -i\tau$. As a consequence, the relative minus sign between temporal and spatial components in the Minkowski metric $g_{\mu\nu}$ vanishes. Hence the resulting metric is given by the Kronecker delta, $\delta_{\mu\nu}$, what makes the common reference to this formulation as *Euclidean* apparent. For a discussion of the equivalence of this formulation to the conventional Minkowskian formulation see ,e.g., [22]. In addition to continuing to imaginary times, we will from now on and for the rest of this work set $\hbar \equiv 1$.

In this new setup the time-evolution operator reads

$$U(\tau,\tau') = \mathrm{e}^{-H(\tau-\tau')}\,. \tag{2.18}$$

The connection of the propagator to the PI that we just derived in the real time formulation can be revealed in the same way straightforwardly in imaginary time. In particular, it is not necessary to shift a into the complex plane to solve the integral, as we did before. We simply state here the result [20],

$$\langle x_N|\, U(\tau_N,\tau_0)\, |x_0\rangle = \int \mathcal{D}[x]\ \mathrm{e}^{-S_E[x,\dot{x}]}, \tag{2.19}$$

where the integration measure is defined as in (2.16) but without the i in the denominator and the Euclidean action is given by

$$S_E\,[x,\dot{x}] = \int_{\tau_0}^{\tau_N} \mathrm{d}t\ \left[\frac{m}{2}\dot{x}^2 + V(x)\right]. \tag{2.20}$$

Mind the relative minus sign in front of the potential term in contradistinction to the real time case. In this formulation the interpretation of the PI is very clear: we integrate over all paths connecting the initial point x_0 with the final point x_N, whereas paths with a corresponding action close to the minimum – thus close to the classical solution – give the main contribution to the integral. Paths with a relatively large action become exponentially suppressed. This reveals a connection between quantum mechanics and the principle of least action from classical mechanics.

2.2 Vacuum expectation values via path integrals

In this section we will introduce basic concepts of quantum field theories, whereby our focus again lies on the connection between Green's functions and the path integral representation, since it is this connection from which the whole idea of lattice field theories stems from. With regard to what we worked out in the previous section, we will continue to consider ordinary quantum mechanics, although we interpret the latter as a 0+1 dimensional field theory. This

interpretation originates from the fact that a general (real) classic field ϕ is a function

$$\phi : \Omega \times T \to D, \quad (\boldsymbol{x},t) \mapsto \phi(\boldsymbol{x},t), \tag{2.21}$$

with $\Omega \subseteq \mathbb{R}^3$ and $T, D \subseteq \mathbb{R}$, opposed to a classical (one dimensional) trajectory of a point-particle

$$x : T \to D, \quad t \mapsto x(t). \tag{2.22}$$

Consequently, we can generalize our path integral studies for quantum mechanics later easily to (bosonic) quantum field theories by introducing additional spatial degrees of freedom.

We continue to work in the Euclidean formulation, nevertheless from now on we will write t instead of τ. Moreover, we will make use of the Heisenberg picture, where the connection between the time-independent Schrödinger operators A and the time-dependent Heisenberg operators $A(t)$ is given by

$$A(t) = \mathrm{e}^{Ht} \, A \, \mathrm{e}^{-Ht} \, . \tag{2.23}$$

Also note that eigenstates of operators evolve in the opposite direction of time in the Heisenberg picture, which can be attributed to following eigenvalue equation,

$$A(t)U^\dagger(t,t_0) \, |a'\rangle = U^\dagger(t,t_0)A \, |a'\rangle = a'U^\dagger(t,t_0) \, |a'\rangle \, . \tag{2.24}$$

Due to the complexity of quantum field theories one becomes content with studying only a few concrete processes of interactions [21]; in this fashion one does not seek the propagator of the whole system, as for simple quantum mechanical problems, instead one is interested in vacuum expectation values of time ordered products of field operators of the form

$$\langle 0| \, T \left(x(t_1) \, x(t_2) \ldots x(t_l) \right) |0\rangle \, . \tag{2.25}$$

The time-ordering operator T orders the field operators according to descending time from left to right. These vacuum expectation values are often referred to as Green's functions as well, we will uncover the reason therefore below. Let us assume for forthcoming analysis that time-ordering is already accomplished, i.e., we consider

$$\langle 0| \, x(t_1) \, x(t_2) \ldots x(t_l) \, |0\rangle \, , \quad t_1 \geq t_2 \geq \ldots \geq t_l. \tag{2.26}$$

Our aim is to construct a PI representation of (2.26) which we can evaluate numerically on a temporal lattice. Our starting point will be

$$\langle x,t| \, x(t_1) \ldots x(t_l) \, |x',t'\rangle \equiv \langle x| \, \mathrm{e}^{-Ht} \, x(t_1) \ldots x(t_l) \, \mathrm{e}^{Ht'} \, |x'\rangle \, , \tag{2.27}$$

which, as we will see, is connected to (2.26) in the limit of very large negative and positive values for t' and t, respectively. In order to show the aforementioned connection, we insert a complete set of energy eigenstates to the left of $\exp(-Ht')$ and the right of $\exp(Ht)$,

$$\begin{aligned}
&\sum_{n,m} \langle x|n\rangle \langle n| \, \mathrm{e}^{-Ht} \, x(t_1) \dots x(t_l) \, \mathrm{e}^{Ht'} \, |m\rangle \langle m|x'\rangle \\
&= \sum_{n,m} \varphi_n(x) \, \mathrm{e}^{-E_n t} \langle n| \, x(t_1) \dots x(t_l) \, |m\rangle \, \mathrm{e}^{E_m t'} \, \varphi_m^*(x') \\
&\xrightarrow[t' \to -\infty]{t \to \infty} \mathrm{e}^{-E_0(t-t')} \, \varphi_0(x) \varphi_0^*(x') \, \langle 0| \, x(t_1) \dots x(t_l) \, |0\rangle \, .
\end{aligned} \tag{2.28}$$

Where $\langle x|n\rangle \equiv \varphi_n(x)$ are the energy eigenfunctions. The last step is to be understood as letting t' and t take very large negative and positive values, so that under the assumption of a energy gap between the ground state and the first excited state, only the ground state survives. When we additionally write the left-hand side (l.h.s.) of (2.27), with the operators $x(t_i)$ replaced by the identity operator, into the denominator, we obtain

$$\frac{\langle x,t| \, x(t_1) \dots x(t_l) \, |x',t'\rangle}{\langle x,t|x',t'\rangle} \xrightarrow[t' \to -\infty]{t \to \infty} \langle 0| \, x(t_1) \dots x(t_l) \, |0\rangle \, . \tag{2.29}$$

Hence, in order to construct a PI representation of (2.26), we now focus on the l.h.s. of (2.29). The denominator's PI representation is already known from the previous section, since

$$\langle x,t|x',t'\rangle = \langle x| \, \mathrm{e}^{-H(t-t')} \, |x'\rangle = \langle x| \, U(t,t') \, |x'\rangle \, . \tag{2.30}$$

Concerning the numerator, we first extract the time-evolution operators from the coordinate space eigenstates and operators,

$$\begin{aligned}
&\langle x,t| \, x(t_1) \dots x(t_l) \, |x',t'\rangle \\
&= \langle x| \, \mathrm{e}^{-H(t-t_1)} \, x \, \mathrm{e}^{-H(t_1-t_2)} \dots \mathrm{e}^{-H(t_{l-1}-t_l)} \, x \, \mathrm{e}^{-H(t_l-t')} \, |x'\rangle \\
&= \int \mathrm{d}x_1 \, \dots \int \mathrm{d}x_{2l} \, \langle x| \, \mathrm{e}^{-H(t-t_1)} \, |x_1\rangle \prod_{i=1}^{l-1} \langle x_{2i-1}| \, x \, |x_{2i}\rangle \, \langle x_{2i}| \, \mathrm{e}^{-H(t_i-t_{i+1})} \, |x_{2i+1}\rangle \\
&\qquad\qquad \times \langle x_{2l-1}| \, x \, |x_{2l}\rangle \, \langle x_{2l}| \, \mathrm{e}^{-H(t_l-t')} \, |x'\rangle \, .
\end{aligned} \tag{2.31}$$

In the second step we inserted complete sets of coordinate operator eigenstates between each time-evolution operator and coordinate operator. It remains to extract the eigenvalues of the coordinate operator according to $\langle x_i| \, x \, |x_{i+1}\rangle = x_i \delta_{i,i+1}$ and relabeling of the indices to obtain

$$\int \mathrm{d}x_1 \, \dots \int \mathrm{d}x_l \, \langle x| \, \mathrm{e}^{-H(t-t_1)} \, |x_1\rangle \prod_{i=1}^{l-1} x_i \, \langle x_i| \, \mathrm{e}^{-H(t_i-t_{i+1})} \, |x_{i+1}\rangle \, x_l \, \langle x_l| \, \mathrm{e}^{-H(t_l-t')} \, |x'\rangle \, . \tag{2.32}$$

Lastly, we further decompose the factors $\langle x_i| \exp\left(-H(t_i - t_{i+1})\right) |x_{i+1}\rangle$, N-times, to be consistent with (2.9) and to achieve correspondence with the PI representation of the previous section. We therefore attain, after taking the continuum time limit, a formal PI representation of the l.h.s. of (2.29),

$$\frac{\langle x,t|\, x(t_1)\dots x(t_l)\, |x',t'\rangle}{\langle x,t|x',t'\rangle} = \frac{\int \mathcal{D}[x]\, x(t_1)\dots x(t_l)\, \mathrm{e}^{-S_E[x,\dot{x}]}}{\int \mathcal{D}[x]\ \mathrm{e}^{-S_E[x,\dot{x}]}}. \tag{2.33}$$

With regard to the l-point functions (2.26), we take the indicated limit to obtain the formal expression

$$\langle 0|\, x(t_1)\dots x(t_l)\, |0\rangle = \frac{\int \mathcal{D}[x]\, x(t_1)\dots x(t_l)\, \mathrm{e}^{-S_E[x,\dot{x}]}}{\int \mathcal{D}[x]\ \mathrm{e}^{-S_E[x,\dot{x}]}}. \tag{2.34}$$

It has to be stressed that in (2.34) the time integration in the action goes over all values from $-\infty$ to ∞, in contradistinction to the PI representation of the transition amplitude from the previous chapter. Thus, we integrate over all paths starting and ending at arbitrary points at time $-\infty$ and ∞, respectively.

The r.h.s. of (2.34) is reminiscent of a statistical ensemble average with a Boltzmann distribution given by $\exp\left(-S_E\,[x,\dot{x}]\right)$. Therefore, we refer to the denominator of the r.h.s. of (2.34) as partition function Z and to the l.h.s.,

$$\langle x(t_1)\dots x(t_l)\rangle = \frac{1}{Z}\int \mathcal{D}[x]\, x(t_1)\dots x(t_l)\, \mathrm{e}^{-S_E[x,\dot{x}]}, \tag{2.35}$$

as correlation function, to underline the similarity to a statistical system. It is this similarity to correlation functions which will be very essential for the remainder of this work; it is due to this correspondence that we can use numerical methods well known from statistical mechanics to calculate n-point functions in quantum field theories.

Chapter 3

Lattice Field Theory

This chapter is exclusively dedicated to the discretization of fields. We will start by considering the quantum mechanical harmonic oscillator (HO) as a – rather simple – field theory, afterwards we generalize the attained results to relativistic scalar fields. Subsequently we discuss fermionic fields on the lattice and the associated problem of fermion doubling in detail. In conclusion we present the link variables as lattice definition of gauge fields and finally summarize by formulating QCD on the lattice.

3.1 Harmonic oscillator as a 0+1 dimensional lattice field theory

As an instructive example on how to calculate n-point functions via the PI approach numerically, we consider the well–known quantum mechanical HO. The Hamiltonian is given by

$$H = \frac{p^2}{2m} + \frac{m\omega^2 x^2}{2}. \tag{3.1}$$

Later on we will calculate the quark propagator, which is the fermionic two-point function in SU(3) Yang-Mills theory. The analog in our setting would be the two-point function

$$\langle x(t)\, x(t')\rangle = \frac{1}{Z}\int \mathcal{D}[x]\, x(t)\, x(t')\, \mathrm{e}^{-S_E[x,\dot{x}]}, \quad t \geq t', \tag{3.2}$$

in accordance with (2.35). In this specific example, the Euclidean action is given by

$$S_E[x,\dot{x}] = \int_{-\infty}^{\infty} \mathrm{d}t \left(\frac{m\dot{x}^2}{2} + \frac{m\omega^2 x^2}{2} \right) \tag{3.3a}$$

$$= \int_{-\infty}^{\infty} \mathrm{d}t \left(-\frac{mx\ddot{x}}{2} + \frac{m\omega^2 x^2}{2} \right), \tag{3.3b}$$

where we integrated by parts and used the fact that $x(t)$ can be chosen to be zero at $\pm\infty$ to obtain (3.3b).

How can the vacuum expectation value (3.2) be interpreted? To discuss that, consider the coordinate operator in terms of creation and annihilation operators, $x = \sqrt{1/(2m\omega)} \left(a + a^\dagger\right)$, and use the fact that the annihilation operator destroys the vacuum, $a|0\rangle = 0$, in this way,

$$\begin{aligned} \langle x(t)\, x(t')\rangle =& \frac{1}{2m\omega} \langle 0| \, \mathrm{e}^{Ht} \left(a + a^\dagger\right) \mathrm{e}^{-H(t-t')} \left(a + a^\dagger\right) \mathrm{e}^{-Ht'} \, |0\rangle \\ =& \frac{1}{2m\omega} \, \mathrm{e}^{E_0(t-t')} \langle 0| \, aU(t,t')a^\dagger \, |0\rangle \\ =& \frac{1}{2m\omega} \, \mathrm{e}^{E_0(t-t')} \langle 1| \, U(t,t') \, |1\rangle \, . \end{aligned} \tag{3.4}$$

As a result we can see that the two-point function is proportional to the transition amplitude $\langle 1| \, U(t,t') \, |1\rangle$, i.e., to the probability that an excited state $|1\rangle$ at time t' evolves towards a later time t while remaining in the same state $|1\rangle$.

In the following, we will take a step backwards in the derivation of the PI. Since our goal is to calculate the two-point function (3.2) numerically, we now undo the continuum time limit which we performed in (2.33) and thus introduce a temporal lattice

$$\Lambda_t = \{n \,|\, n = 0, \ldots, N_t - 1\} \tag{3.5}$$

and replace $t = na$, where a is the step of the lattice Λ_t. Then, the "fields" $x(t)$ are to be evaluated on the lattice sites $x(n_t a) \equiv x_n$. For convenience, we will adopt periodical boundary conditions $x_N = x_0$. We remark that N_t has to be chosen large enough so that contributions from higher energy states in comparison to the vacuum are sufficiently suppressed.

The discrete version of the action (3.3b) reads

$$S_E[x] = a \sum_{n=0}^{N_t-1} \left(-\frac{mx_n}{2} \left[\frac{x_{n+1} + x_{n-1} - 2x_n}{a^2} \right] + \frac{m\omega^2 x_n^2}{2} \right). \tag{3.6}$$

We have chosen to approximate the derivative in (3.6) with the centered finite difference scheme which has errors $\mathcal{O}(a^3)$. We equivalently could have chosen a more accurate approximation

by, for example, also using next to nearest neighbor points, for details see ,e.g., [23]. In this sense is $S_E[x]$ not unique. The overall factor a in (3.6) has to be included so that the action is dimensionless in units of $\hbar$ (cf. Appendix A.1). We next want to express the action (3.6) in terms of dimensionless variables only. When we denote the dimension of length with ℓ, the dimensions of the variables in the action are

$$[a] = \ell, \quad [m] = \ell^{-1}, \quad [x] = \ell, \quad [\omega] = \ell^{-1}. \tag{3.7}$$

Consequently, we scale all variables according to their dimension with a and thus define the dimensionless quantities

$$\hat{m} = ma, \quad \hat{x} = \frac{x}{a}, \quad \hat{\omega} = \omega a. \tag{3.8}$$

Then the action can be written in terms of these dimensionless variables as

$$S_E[x] = -\frac{1}{2}\sum_{n=0}^{N_t-1} \hat{m}\hat{x}_n \left(\hat{x}_{n+1} + \hat{x}_{n-1} - 2\hat{x}_n - \hat{\omega}^2\hat{x}_n\right) \tag{3.9}$$

and on that account the *discrete* two-point function is given by

$$\langle \hat{x}_n\, \hat{x}_m \rangle = \frac{1}{Z}\int \mathcal{D}\hat{x}\, \hat{x}_n\, \hat{x}_m\, \mathrm{e}^{-S_E[\hat{x}]}, \quad n \geq m, \tag{3.10}$$

with $x_m \equiv x(n_{t'}a)$ and the integration measure defined by

$$\int \mathcal{D}\hat{x} = \left(\frac{\hat{m}}{2\pi}\right)^{\frac{N_t+1}{2}} \int \prod_{i=0}^{N_t-1} \mathrm{d}\hat{x}_i\,. \tag{3.11}$$

We want to highlight that (3.10) is well defined in contrast to the formal PI representation in the continuum. On every lattice site n, $\hat{x}_n$ has to be integrated from $-\infty$ towards ∞, whereas the main contributions to the integral come from values of $\hat{x}_n$ for which the discrete action (3.9) is close to its minimum. The weighting factor $\exp(-S_E[\hat{x}])$ suppresses contributions for very large positive and negative values of $\hat{x}_n$ due to the quadratic appearance of $\hat{x}_n$ in S_E (3.9), this renders the integral finite.

Within this simple example it is straightforward to calculate the two-point function (3.10) analytically, therefore we define the matrix

$$K_{ij} \equiv -\hat{m}\left(\delta_{i,j-1} + \delta_{i,j+1} - 2\delta_{ij} - \hat{\omega}^2\delta_{ij}\right). \tag{3.12}$$

Note that K_{ij} is positive definite and thence invertible. Using this matrix we can write the

discrete action in Gaussian form

$$S_E[x] = \frac{1}{2}\sum_{i,j=0}^{N_t-1} \hat{x}_i K_{ij} \hat{x}_j \tag{3.13}$$

and thus we can solve the multidimensional Gaussian integral, now appearing in the two-point function, to acquire

$$\langle \hat{x}_n\, \hat{x}_m \rangle = \frac{\int \mathcal{D}\hat{x}\ \hat{x}_n\, \hat{x}_m \exp\left(-\frac{1}{2}\sum_{i,j} \hat{x}_i K_{ij} \hat{x_j}\right)}{\int \mathcal{D}\hat{x}\ \exp\left(-\frac{1}{2}\sum_{i,j} \hat{x}_i K_{ij} \hat{x}_j\right)} = K^{-1}_{nm}. \tag{3.14}$$

Here we attained a very important result: equation (3.14) states that the HO two-point function is simply given by the inverse of the kernel appearing in the action. Put another way, the two-point function is the Green's function of the operator K_{nm},

$$\sum_l K_{nl} \langle \hat{x}_l\, \hat{x}_m \rangle = \delta_{nm}. \tag{3.15}$$

This is the origin why one usually refers to the vacuum expectation values as Green's n-point functions. It has to be perceived that the above Green's functions are not related to the Green function to Schrödinger's equation which we encountered in Chap. 2, that equals the propagator of wave mechanics.

In order to invert the matrix K_{nm}, we introduce the momentum space delta function[1]

$$\delta_{nm} = \int_{-\pi}^{\pi} \frac{\mathrm{d}\hat{p}}{2\pi}\, \mathrm{e}^{i\hat{p}(n-m)}\,. \tag{3.16}$$

Therewith we have

$$\begin{aligned} K_{nm} &= \hat{m} \int_{-\pi}^{\pi} \frac{\mathrm{d}\hat{p}}{2\pi} \left(-\,\mathrm{e}^{i\hat{p}} - \mathrm{e}^{-i\hat{p}} + 2 + \hat{\omega}^2\right) \mathrm{e}^{i\hat{p}(n-m)} \\ &= \hat{m} \int_{-\pi}^{\pi} \frac{\mathrm{d}\hat{p}}{2\pi} \left(-2\cos\hat{p} + 2 + \hat{\omega}^2\right) \mathrm{e}^{i\hat{p}(n-m)} \end{aligned} \tag{3.17}$$

and using $1 - \cos x = 2\sin^2 x/2$ this yields

$$K_{nm} = \int_{-\pi}^{\pi} \frac{\mathrm{d}\hat{p}}{2\pi} K(\hat{p})\, \mathrm{e}^{i\hat{p}(n-m)}\,. \tag{3.18}$$

1 Note that here and in the following, the above integral is meant symbolically: what we actually mean is $\int_{-\pi}^{\pi} \frac{\mathrm{d}\hat{p}}{2\pi} \to \sum_{\hat{p}\in(-\pi,\pi]} \frac{1}{N_t}$ since the momenta are obviously discrete as well.

In the last equation, we defined

$$K(\hat{p}) = 4\hat{m}\sin^2\frac{\hat{p}}{2} + \hat{m}\hat{\omega}. \tag{3.19}$$

Then, the two-point function is easily found to be

$$\langle \hat{x}_n\, \hat{x}_m \rangle = \int_{-\pi}^{\pi} \frac{\mathrm{d}\hat{p}}{2\pi} \frac{\mathrm{e}^{i\hat{p}(n-m)}}{4\hat{m}\sin^2 \hat{p}/2 + \hat{m}\hat{\omega}}. \tag{3.20}$$

Although we just calculated the two-point function of the HO analytically, we now briefly present how one can calculate Green's n-point functions numerically, because we will need it later when we discuss more involved field theories where an analytic solution cannot be found. Therefore, we take a closer look at (3.10) again. Since, in more general lattice field theories, one has to discretize not only time but also 3-dimensional space, one is confronted with the huge amount of $N_i^3 \times N_t$ lattice sites. In order to get a handle on the integral over all field configurations, one draws back on methods known from statistical mechanics. Monte Carlo integration with importance sampling is the method which has emerged as standard in lattice field theories. There, one approximates the integral (3.10) by an average over a statistical ensemble of N field configurations $\hat{x}(na)$, $n \in \Lambda_t$,

$$\langle \hat{x}_n\, \hat{x}_m \rangle = \frac{1}{N}\sum_{i=1}^{N} \hat{x}_n\, \hat{x}_m, \quad n \geq n'. \tag{3.21}$$

These field configurations, in turn, are generated with a Boltzmann distribution given by $\exp(-S_E\,[\hat{x}])$. The major advantage of Monte Carlo integration opposed to non-statistical integration methods is that its error is of order $\mathcal{O}(N^{-1/2})$, *independently* of the dimension of the field's domain.

3.2 Generalizing to 3+1 dimensions: the free scalar field

As already mentioned above, the preceding analysis of n-point functions for a 0+1 dimensional field theory can be generalized to 3+1 dimensions immediately. In this section, we will give a few remarks on the free scalar field $\phi(x)$ as an example of a relativistic bosonic 3+1 dimensional field theory. In this new context, x represents the vector of all Euclidean space-time coordinates x_μ with $\mu = 1,\ldots,4$. By convention, one defines the temporal component as x_4 in the Euclidean formulation to distinguish it from the temporal component x_0 from Minkowski space.

We now give a set of rules how the HO Lagrangian[1] can formally be transformed to the Lagrangian density of a free scalar field:

1. Replace the field $x(t) \to \phi(x)$.
2. Generalize integrals and derivatives to 3+1 dimensions.
3. Cancel m in the first term of the Lagrangian.
4. Replace $m\omega^2 \to M^2$ in the second term of the Lagrangian.

The Euclidean space Lagrangian density one reaches when carrying out these simple steps reads

$$\mathscr{L}(x) = \frac{1}{2}\left(\partial_\mu \phi(x)\right)^2 + \frac{1}{2}M^2\phi^2 \tag{3.22}$$

and the action is obtained by integrating $\mathscr{L}(x)$ over 3+1 dimensional space-time. After a integration by parts,[2] as we did in (3.3b), the latter becomes

$$S_E[x] = \frac{1}{2}\int \mathrm{d}^4x\, \phi(x)\left(-\Box + M^2\right)\phi(x) \tag{3.23}$$

where $\Box \equiv \sum_\mu \partial_\mu^2$ is the d'Alembert operator. Note that the parameter M in the action (3.23) is the *bare mass* and does not coincide with the physical mass in general.

We now introduce a lattice for 3+1 dimensional space-time,

$$\Lambda = \{n \equiv (n_1, \ldots, n_4) \,|\, n_\mu = 0, \ldots, N_\mu - 1\}\,, \tag{3.24}$$

where we again adopt periodical boundary conditions. Discretizing the action can be done in exactly the same way as for the HO and in complete agreement we would reveal that the two-point function $\langle 0|\, T(\hat{\phi}_n\, \hat{\phi}_m)\, |0\rangle$ is given by the inverse of the kernel appearing in the action. We simply state here the result of the inversion of the kernel which alternatively can be obtained by applying the above mentioned rules on the corresponding HO result,

$$\langle 0|\, T(\hat{\phi}_n\, \hat{\phi}_m)\, |0\rangle = \int_{-\pi}^{\pi} \frac{\mathrm{d}^4\hat{p}}{(2\pi)^4} \frac{\mathrm{e}^{i\hat{p}\cdot(n-m)}}{4\sum_\mu \sin^2 \hat{p}_\mu/2 + \hat{M}^2}. \tag{3.25}$$

$\hat{\phi}_n$ is the field ϕ_n scaled with the lattice spacing a to make it dimensionless, $\hat{\phi}_n = a\phi(na)$.

1 Cf. the expression in parentheses in (3.3a).
2 Integration by parts in n dimensions is formally known as Green's integration formula, see Appendix A.2.

3.3 Fermions on the lattice

In this section we switch from real scalar fields to complex spinor fields. We first look at classic fields

$$\psi, \overline{\psi} : \Omega \to D, \quad x \mapsto \psi(x), \overline{\psi}(x) \tag{3.26}$$

with $\Omega \subseteq \mathbb{R}^4$ and $D \subseteq \mathbb{C}^4$. The fields $\overline{\psi}(x)$ and $\psi(x)$ are related by $\overline{\psi}(x) \equiv (\psi^T(x))^* \gamma_4$, though they are treated as independent integration variables. The 4×4 Dirac matrices γ_μ fulfill the Euclidean anti-commutation relations

$$\{\gamma_\mu, \gamma_\nu\} = 2\delta_{\mu\nu} \mathbb{1}. \tag{3.27}$$

The classic equations of motion can be deduced by minimizing the fermionic action which, in the free case, is given in Euclidean space by

$$S_F[\psi, \overline{\psi}] = \int \mathrm{d}^4 x \, \overline{\psi}(x) \left(\gamma_\mu \partial_\mu + M\right) \psi(x). \tag{3.28}$$

In the quantum formulation one has to take additional contributions from configurations with non-minimal action values into account. Furthermore, the complex valued fields ψ and $\overline{\psi}$ have to be replaced by operators that anti-commute, in order to satisfy Fermi-Dirac statistics. The fermionic two-point function, i.e., the fermion propagator, which is of particular interest to this work, is related to the following formal PI expression in analogy to (2.34),

$$\left\langle \psi_\alpha(x) \, \overline{\psi}_\beta(x') \right\rangle = \frac{\int \mathcal{D}\psi \, \mathcal{D}\overline{\psi} \; \psi_\alpha(x) \, \overline{\psi}_\beta(x') \; \mathrm{e}^{-S_F[\psi, \overline{\psi}]}}{\int \mathcal{D}\psi \, \mathcal{D}\overline{\psi} \; \mathrm{e}^{-S_F[\psi, \overline{\psi}]}}. \tag{3.29}$$

The indices α, β label the different components of the spinor fields. It has to be stressed that, while on the l.h.s. of (3.29) the field components represent operators, the field components on the r.h.s. are not simply numbers, as in (2.34), instead they are anti-commuting variables,

$$\left\{ \psi_\alpha(x), \overline{\psi}_\beta(x') \right\} = 0, \tag{3.30}$$

and hence are members of the so called Grassmann algebra, for details see ,e.g., [20].

We are now ready to discretize the Dirac field. To this effect we replace continuous space-time by a discrete lattice Λ, cf. (3.24), and the discrete fermionic action then reads, in terms of dimensionless quantities only,

$$S_F[\psi, \overline{\psi}] = \sum_{n,m} \sum_{\alpha,\beta} \overline{\psi}_\alpha(n) D_{\alpha\beta}(n,m) \psi_\beta(m), \tag{3.31a}$$

with

$$D_{\alpha\beta}(n,m) \equiv \frac{1}{2}\sum_{\mu}(\gamma_\mu)_{\alpha\beta}\left[\delta_{n,m-\hat{\mu}} - \delta_{n,m+\hat{\mu}}\right] + \hat{M}\delta_{nm}\delta_{\alpha\beta}. \tag{3.31b}$$

Note that from now on we will neglect the hat on the fields ψ and $\overline{\psi}$ to simplify notations, nevertheless it will be obvious whether $\psi, \overline{\psi}$ are dimensionless or dimensionful variables in each expression. The kernel of the fermionic action, $D_{\alpha\beta}(n,m)$, is usually referred to as Dirac operator and $\hat{\mu}$ denotes the unit vector $\hat{e}_\mu$ in the direction μ. In conjunction with discretization of space-time, the formally defined PI (3.29) becomes finite and thence the discrete fermion propagator is given by

$$\left\langle \psi_\alpha(n)\,\overline{\psi}_\beta(m)\right\rangle = \frac{1}{Z}\int \mathcal{D}\psi\,\mathcal{D}\overline{\psi}\;\psi_\alpha(n)\,\overline{\psi}_\beta(m)\;\mathrm{e}^{-S_F}\,, \tag{3.32a}$$

with the partition function

$$Z = \int \mathcal{D}\psi\,\mathcal{D}\overline{\psi}\;\mathrm{e}^{-S_F} \tag{3.32b}$$

and the integration measure defined by

$$\mathcal{D}\psi\,\mathcal{D}\overline{\psi} \;=\; \prod_{n,m}\prod_{\alpha,\beta}\mathrm{d}\overline{\psi}_\alpha(n)\,\mathrm{d}\psi_\beta(m)\,. \tag{3.33}$$

We are now ready to perform the integral in (3.32a). Remark that, contrary to the Gaussian integral in (3.14), where we had to integrate over conventional numbers, we are here confronted with an integral over Grassmann numbers. For details of Grassmann integration we refer to [20] and summarize the results relevant to our analysis:

$$\int \mathcal{D}\psi\,\mathcal{D}\overline{\psi}\;\;\mathrm{e}^{-\sum_{n,m}\overline{\psi}_\alpha(n)D_{\alpha\beta}(n,m)\psi_\beta(m)} \;=\; \det\left[D\right], \tag{3.34a}$$

and, moreover,

$$\int \mathcal{D}\psi\,\mathcal{D}\overline{\psi}\,\psi_\alpha(n)\,\overline{\psi}_\beta(m)\;\mathrm{e}^{-\sum_{n,m}\overline{\psi}_\alpha(n)D_{\alpha\beta}(n,m)\psi_\beta(m)} \;=\; \det\left[D\right]D^{-1}_{\alpha\beta}(n,m). \tag{3.34b}$$

Since we deal with the ratio of these two integrals, the factors $\det\left[D\right]$ cancel and we are left with the result analog to the free scalar field: the free fermion propagator is given by the inverse of the Dirac operator,

$$\left\langle \psi_\alpha(n)\,\overline{\psi}_\beta(m)\right\rangle = D^{-1}_{\alpha\beta}(n,m). \tag{3.35}$$

The inversion of the Dirac operator, to obtain the fermion propagator, can be done in the same way as the inversion of the corresponding kernel in Sect. 3.1, where we used the momentum

space delta function, and thus we acquire for the lattice fermion propagator

$$\left\langle \psi_\alpha(n)\,\overline{\psi}_\beta(m)\right\rangle = \int_{-\pi}^{\pi} \frac{\mathrm{d}^4\hat{p}}{(2\pi)^4} \frac{-i\,(\gamma_\mu)_{\alpha\beta}\,\hat{k}_\mu + \hat{M}\delta_{\alpha\beta}}{\hat{k}^2 + \hat{M}^2}\, \mathrm{e}^{i\hat{p}\cdot(n-m)}, \tag{3.36}$$

where we have defined the dimensionless "lattice fermion momenta"

$$\hat{k}_\mu \equiv \sin\hat{p}_\mu \iff k_\mu \equiv {}^1\!/_a \sin\left(p_\mu a\right). \tag{3.37}$$

From (3.36) we can immediately read of the free momentum space fermion propagator, that we will denote with $S_{\alpha\beta}(\hat{p})$,

$$S_{\alpha\beta}(\hat{p}) = \frac{-i\,(\gamma_\mu)_{\alpha\beta}\,\hat{k}_\mu + \hat{M}\delta_{\alpha\beta}}{\hat{k}^2 + \hat{M}^2}. \tag{3.38}$$

Its inverse, the free momentum space Dirac operator, is then given by

$$S^{-1}_{\alpha\beta}(\hat{p}) \equiv D_{\alpha\beta}(\hat{p}) = i\,(\gamma_\mu)_{\alpha\beta}\,\hat{k}_\mu + \hat{M}\delta_{\alpha\beta}. \tag{3.39}$$

Of particular concern is the difference between the just introduced lattice fermion momenta and the momenta of the free scalar field, (3.25), which we found to be $2\sin\hat{p}_\mu/2$. It turns out that the differing factor of one half in the argument of the sine is very crucial to the existence of the correct continuum limit. While in the case of lattice fermions the sine is integrated over the whole Brillouine zone (BZ) $(-\pi, \pi]$, the sine in the propagator of the free scalar field takes only values within half of the BZ, cf. Fig. 4.29. The correct naive continuum limit[1] of the free scalar field is ensured by the bijective character of its lattice momentum.

In the massless case, the free lattice fermion propagator (3.38) has not only a single pole for $p_\mu = 0$, $\mu = 1, \ldots, 4$, as in the continuum, but it has additional poles whenever all p_μ equal either zero or ${}^\pi\!/_a$. Hence the propagator has $2^4 = 16$ poles, the number of poles gets doubled for each dimension d. Thus, the naive discretization of the Dirac field describes 16 degenerate flavors of fermions, i.e., 16 fermions of mass M. This phenomenon is referred to as "fermion doubling" and one problem encountered therewith is that QCD only has asymptotic freedom for the number of flavors being less than ${}^{33}\!/_2$ and 16 is rather close to this transition. Another problem is the loss of axial anomaly on the lattice due to fermion doubling, for details on the latter see ,e.g., [24].

In the following we will introduce two possibilities how to circumvent the problem of fermion doubling. We will present Wilson's approach as well as the approach by Kogut and Susskind to get rid of, or at least to drastically reduce, the number of the doublers.

1 Scale all quantities with powers of a, according to their canonical dimensions and let $a \to 0$.

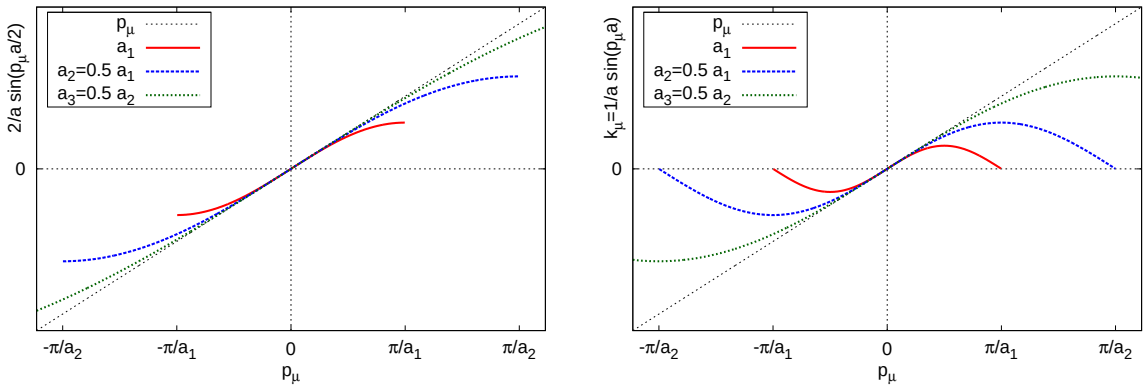

(a) Free scalar field **(b)** Free Dirac field

Figure 3.1: Lattice momenta for different values of the lattice spacing a.

3.3.1 Wilson fermions

The idea of Wilson to eliminate the doublers is to give them an additional mass which depends on the lattice spacing a and becomes infinite in the limit $a \to 0$. To this effect, consider the replacement

$$M \to M + \frac{r}{a} \sum_{\mu} \left(1 - \cos\left(p_\mu a\right)\right) \tag{3.40}$$

for M in the expression for the free momentum space Dirac operator, (3.39). The parameter r is arbitrary but in practical calculations usually set to one, for ease of notation we will neglect it in the remainder of this work. Note that we deal with dimensionful quantities in this passage, in order to make the a dependence of the rightmost term in (3.40), the so called Wilson term, explicit. The Wilson term has no influence on the physical pole $p = (0, \ldots, 0)$ of (3.38) and it lifts the mass of the doublers towards infinity in the continuum limit, thus, at least in the limit $a \to 0$, the doublers decouple from the theory due to this additional mass term.

In the following, we prove that the Wilson term is simply the Fourier transform of the kernel of the discrete Laplace operator. To show this, we plug the momentum space delta function

(3.16) into the discrete Laplace kernel and that leads to

$$-\sum_{\mu}\left(\frac{\delta_{n,m-\hat{\mu}}+\delta_{n,m+\hat{\mu}}-2\delta_{nm}}{2a}\right) \tag{3.41a}$$

$$=\int_{-\pi}^{\pi}\frac{\mathrm{d}^4\hat{p}}{(2\pi)^4}\sum_{\mu}\frac{1}{2a}\left(-\mathrm{e}^{i\hat{p}\cdot(n-m+\hat{\mu})}-\mathrm{e}^{i\hat{p}\cdot(n-m-\hat{\mu})}+2\,\mathrm{e}^{i\hat{p}\cdot(n-m)}\right) \tag{3.41b}$$

$$=\int_{-\pi}^{\pi}\frac{\mathrm{d}^4\hat{p}}{(2\pi)^4}\frac{1}{a}\sum_{\mu}(1-\cos\hat{p}_\mu)\,\mathrm{e}^{i\hat{p}\cdot(n-m)}\,. \tag{3.41c}$$

Having gained the Wilson term in coordinate space, we are now in the position to write down the free coordinate space "Wilson Dirac operator" which is the sum of (3.31b) and (3.41a),

$$D^{(\mathrm{W})}_{\alpha\beta}(n,m)=\frac{1}{2}\sum_{\mu}\left[(\gamma_\mu-\mathbb{1})_{\alpha\beta}\,\delta_{n,m-\hat{\mu}}-(\gamma_\mu+\mathbb{1})_{\alpha\beta}\,\delta_{n,m+\hat{\mu}}\right]+\left(\hat{M}+4\right)\delta_{nm}\delta_{\alpha\beta}. \tag{3.42}$$

As we have seen, Wilson fermions offer a clear and transparent way to eliminate the doublers. On the other hand, though, the most significant downside of Wilson fermions is that the Wilson term explicitly breaks chiral symmetry,[1] even for non-vanishing mass. Obviously, this flaw makes Wilson fermions inappropriate for studying effects of chiral symmetry breaking on the lattice. Below we discuss another approach how to gain control of the doubling problem which retains a residual chiral symmetry.

3.3.2 Staggered fermions

Before we introduce the ansatz by Kogut and Susskind [25], let us shortly specify how momenta are represented on the lattice. As already mentioned above, we restrict the lattice momenta $\hat{p}_\mu$ to the first BZ $(-\pi,\pi]$. Thus, we let

$$\hat{p}_\mu=\frac{2\pi}{N_\mu}\left(n_\mu+1-{}^{N_\mu}\!/_2\right),\quad n_\mu=0,\ldots,N_\mu-1. \tag{3.43}$$

Notice that the problem of fermion doubling is only apparent for momenta $\hat{p}_\mu > {}^{\pi}\!/_2$ or $\hat{p}_\mu \leq -{}^{\pi}\!/_2$. These momenta belong to lattice sites contained in the set

$$K_\mu\equiv\left\{n_\mu\,|\,n_\mu\leq\left({}^{N_\mu}\!/_4\right)\vee n_\mu>\left({}^{3N_\mu}\!/_4\right)\right\}, \tag{3.44a}$$

whereas the set

$$M_\mu\equiv\left\{n_\mu\,|\,\left({}^{N_\mu}\!/_4\right)<n_\mu\leq\left({}^{3N_\mu}\!/_4\right)\right\} \tag{3.44b}$$

1 For a short revision of chiral symmetry see Appendix A.3.

contains lattice points that do not contribute to the problem of fermion doubling since $\sin(\hat{p})$, restricted to $(-\pi/2, \pi/2]$, is bijective. Obviously, the cardinality of both sets equals $N_\mu/2$ and we could define a one-to-one mapping between the sets M_μ and K_μ for fixed μ. Taking into account that our lattice is four dimensional, $\mu = 1, \ldots, 4$, we may correspondingly connect every point in $M \equiv \{n \mid n_\mu \in M_\mu \; \forall \mu\}$ uniquely with $2^4 - 1 = 15$ points lying in $K \equiv \{n \mid \exists \mu : n_\mu \in K_\mu\}$. Remember that we adopted periodical boundary conditions, therefore, we can write the discrete momentum $\hat{p}$ as

$$\hat{p}_\mu = \hat{q}_\mu + \rho_\mu \pi, \quad \hat{q}_\mu \in M_\mu, \quad \rho_\mu = \{0, 1\}. \tag{3.45}$$

The essential step in the construction of the Kogut–Susskind fermions is that one uses each of the clusters of 16 connected lattice sites[1] to host a new fermionic field of a fixed momentum $\hat{q} \in M$ and 16 components $\rho = (\rho_1, \ldots, \rho_4), \rho_\mu = 0, 1$ which we may denote by $\chi_\rho(\hat{q})$. Interpreted another way, the field χ is a *scalar* (Grassmann valued) field of the initial momentum $\hat{p}$, thus

$$\chi_\rho(\hat{q}) = \chi(\hat{q} + \rho\pi) = \chi(\hat{p}). \tag{3.46}$$

Despite we do not know yet how to interpret this new field $\chi_\rho(\hat{q})$, it is remarkable that it is solely defined to live on the "good" lattice sites M which are not affected by the problem of fermion doubling. One might already guess that since we reduced the fermionic degree of freedom per lattice site from four to one, we contingently reduced in correspondence the number of fermions in our theory from sixteen to four which indeed turns out to be true. For a derivation of the fact that the number of flavors[2] described by the staggered fermion formulation is four, see ,e.g., [24].

Having shown this rather descriptive and motivating outline for the construction of the *staggered* fermions, we now come to the technical derivation: we define the so called staggered transformation as

$$\overline{\psi}(n) = \overline{\psi}'(n)\gamma_4^{n_4}\gamma_3^{n_3}\gamma_2^{n_2}\gamma_1^{n_1}, \quad \psi(n) = \gamma_1^{n_1}\gamma_2^{n_2}\gamma_3^{n_3}\gamma_4^{n_4}\psi'(n), \tag{3.47}$$

where $n = (n_1, \ldots, n_4)$ is a lattice site in coordinate space. Clearly, the mass term of the fermionic action (3.31a), $\overline{\psi}(n)M\psi(n)$, is invariant under this transformation because $\gamma_\mu^2 = \mathbb{1}$ for all μ. Next we consider the kinetic term of the fermionic action,

$$\frac{1}{2}\sum_{n,m}\sum_{\mu}\gamma_\mu\overline{\psi}(n)\left[\psi(n+\hat{\mu}) - \psi(n-\hat{\mu})\right]. \tag{3.48}$$

1 These clusters build hypercubes of length π in momentum space.
2 When referring to the different flavors of the staggered fields one usually speaks of *taste* instead of flavor.

As we readily see, the lattice coordinates n of $\overline{\psi}$ and ψ differ by one unit in direction of $\hat{\mu}$; as a consequence, when performing the staggered transformation (3.47), all $\gamma_\nu^{n_\nu}$ cancel, except for $\nu = \mu$. This remaining γ_μ, on the other hand, gets canceled by the one which is already apparent in the Dirac operator and we are left with only an eventual sign change due to the anti-commutativity of the gamma matrices and the need to swap them in order to cancel them.

In this way we get rid of the Dirac structure of the action; we cancel all γ-matrices and the resulting action is diagonal in Dirac space. Hence, all four Dirac components of the fields $\overline{\psi}'(n)$ and $\psi'(n)$ are equivalent and we will only keep one of them which we call $\overline{\chi}(n)$ and $\chi(n)$, respectively. The free fermionic action, in terms of the Kogut–Susskind fields, then reads

$$S_F[\chi,\overline{\chi}] = \sum_{n,m} \overline{\chi}(n) D^{(\mathrm{KS})}(n,m) \chi(m), \tag{3.49a}$$

$$D^{(\mathrm{KS})}(n,m) \equiv \frac{1}{2} \sum_\mu \eta_\mu(n) \left[\delta_{n,m-\hat{\mu}} - \delta_{n,m+\hat{\mu}}\right] + \hat{M}\delta_{nm}, \tag{3.49b}$$

where we defined the staggered sign function

$$\eta_\mu(n) \equiv (-1)^{\sum_{\nu<\mu} n_\nu}. \tag{3.50}$$

As a remark, we now give the coordinate space interpretation which corresponds to the one we adopted in our motivation in momentum space: interpret the field $\chi(n)$ as a field with 16 components $\chi_\rho(h)$ living on a lattice with double lattice spacing,[1] $h = n/2$, and spread the 16 field components among the hypercubes of length a,

$$\chi(n) = \chi(h+\rho) = \chi_\rho(h), \quad \rho_\mu \in \{0,1\}. \tag{3.51}$$

For the later analysis of the fermion propagator we need the Kogut–Susskind Dirac operator in momentum space. From the above discussion it is evident that

$$\chi(n) = \int_{-\pi}^{\pi} \frac{\mathrm{d}^4\hat{p}}{(2\pi)^4} \, \mathrm{e}^{i\hat{p}\cdot n} \, \chi(\hat{p}) = \int_{-\pi/2}^{\pi/2} \frac{\mathrm{d}^4\hat{q}}{(2\pi)^4} \sum_{\rho_\mu=0}^{1} \mathrm{e}^{i(\hat{q}+\rho\pi)\cdot n} \, \chi_\rho(\hat{q}), \tag{3.52}$$

with $\chi_\rho(\hat{q})$ given by (3.46). When plugging (3.52) and the momentum space delta function into (3.49) one obtains, see [13],

$$S_F[\chi,\overline{\chi}] = \int_{-\pi/2}^{\pi/2} \frac{\mathrm{d}^4\hat{q}}{(2\pi)^4} \sum_{\alpha,\beta} \overline{\chi}_\alpha(\hat{q}) \left[i \sum_\mu (\overline{\gamma}_\mu)_{\alpha\beta} \sin(\hat{q}_\mu) + \hat{M}\overline{\delta}_{\alpha\beta} \right] \chi_\beta(\hat{q}). \tag{3.53}$$

1 This corresponds to restricting the momenta to the inner half of the BZ.

Note that here, α, β are not Dirac indices but staggered multi-indices. The staggered momentum space Dirac operator stands within brackets and can directly be read off. In (3.53) we defined

$$(\overline{\gamma}_\mu)_{\alpha\beta} \equiv (-1)^{\alpha_\mu} \overline{\delta}_{\alpha+\theta(\mu),\beta} \tag{3.54a}$$

with

$$\overline{\delta}_{\alpha\beta} \equiv \delta_{\alpha_\mu \beta_\mu | \mathrm{mod}\ 2} \tag{3.54b}$$

and

$$\theta_\nu(\mu) = \begin{cases} 1 & \text{if } \nu < \mu, \\ 0 & \text{else.} \end{cases} \tag{3.54c}$$

The $(\overline{\gamma}_\mu)_{\alpha\beta}$ form a staggered Dirac algebra

$$\left\{\overline{\gamma}_\mu, \overline{\gamma}_\nu\right\}_{\alpha\beta} = 2\delta_{\mu\nu}\overline{\delta}_{\alpha\beta}. \tag{3.55}$$

We close this section by recalling the main advantage of staggered fermions over Wilson fermions: we show that the former feature a residual chiral symmetry. The equivalent of γ_5 for staggered fermions is found to be

$$\eta_5(n) = (-1)^{\sum_{\nu=1}^{4} n_\nu}. \tag{3.56}$$

Therewith consider the staggered chiral transformation

$$\overline{\chi}(n) \to \overline{\chi}(n)\, \mathrm{e}^{i\alpha\eta_5(n)}, \quad \chi(n) \to \mathrm{e}^{i\alpha\eta_5(n)}\, \chi(n) \tag{3.57}$$

under which the staggered action (3.49), in the limit of vanishing mass M, is invariant since $\gamma_5(n \pm \hat{\mu})$ has a relative minus sign in comparison to $\gamma_5(n)$ and thus the exponentials cancel.

3.3.3 Improved staggered fermions: the Asqtad action

The errors of the Kogut–Susskind action are of order $\mathcal{O}(a^2)$ and we now shortly present an improved staggered action which eliminates all errors of order a^2. The Asqtad[1] action [26] was mainly constructed with the aim of reducing taste symmetry breaking of the four staggered quark tastes but beside achieving the latter it also exhibits good rotational symmetry properties.

Taste changing can be minimized by replacing the nearest neighbor terms in the action by an average over paths connecting the corresponding points. The Asqtad action uses three-link, five-link and seven-link paths or *staples*. When referring to this procedure one speaks of

1 The name Asqtad action is a shorthand for a-squared tadpole improved action.

"fattening" the links. Additionally, the Asqtad action contains the Naik term [27] to improve the dispersion relation and a planar five-link Lepage term [28] to correct the infrared. All terms are tadpole improved [29] and as the tadpole u_0 we will use the forth root of the average plaquette.

The free momentum space Dirac operator, using this action, has the form

$$D_{\alpha\beta}(q) = iu_0 \sum_{\mu} (\overline{\gamma}_\mu)_{\alpha\beta} \sin(\hat{q}_\mu) \left(1 + 1/6 \sin^2(\hat{q}_\mu)\right) + \hat{M}\overline{\delta}_{\alpha\beta}. \tag{3.58}$$

3.4 The need for gauge fields

The fundamental fields of nature are believed to be Dirac fields which describe matter, i.e., fermions like electrons and quarks, and gauge fields which describe the fundamental forces, i.e., bosons like photons and gluons. The last section was dedicated to fermionic fields. It now remains to introduce gauge fields in order to describe fundamental field theories like Quantum Electrodynamics (QED) or Quantum Chromodynamics (QCD). To get started, we shortly review the introduction of gauge fields in the continuum before we introduce them on the lattice.

3.4.1 Gauge fields in the continuum

Once again, have a look at the fermionic (continuum) action in Euclidean space

$$S_F[\psi,\overline{\psi}] = \int \mathrm{d}^4x\, \overline{\psi}(x) \left(\gamma_\mu \partial_\mu + M\right) \psi(x), \tag{3.59}$$

notice that we use matrix/vector notation in Dirac space here. This action is invariant under a global gauge symmetry

$$\overline{\psi}(x) \to \overline{\psi}(x) G^{-1}, \quad \psi(x) \to G\psi(x) \tag{3.60}$$

where G is an element of the underlying gauge group, U(1) in the case of QED and, as we will see in the next chapter, SU(3) for QCD. For the moment one may think of G as an element of U(1), i.e., $G = \mathrm{e}^{i\Lambda}$ with $\Lambda \in \mathbb{R}$.

When we demand this symmetry to be local instead of global, we have to introduce a vector valued field

$$A : \Omega \to D, \quad x \mapsto A(x) \tag{3.61}$$

where $\Omega \subseteq \mathbb{R}^4$ and $D \subseteq \mathbb{R}^4$. We include this vector field into the action by replacing the derivative ∂_μ by the covariant derivative $D_\mu = \partial_\mu + iA_\mu$. Then the action (3.60), with ∂_μ

replaced by D_μ, becomes invariant under following local transformations

$$\overline{\psi}(x) \to \overline{\psi}(x)G^{-1}(x) \tag{3.62a}$$
$$\psi(x) \to G(x)\psi(x) \tag{3.62b}$$
$$A_\mu(x) \to G(x)A_\mu(x)G^{-1}(x) + i\left(\partial_\mu G(x)\right)G^{-1}(x). \tag{3.62c}$$

Note that for QED $A_\mu(x)$ and $G(x)$ commute and thus (3.62c) reduces to $A_\mu(x) \to A_\mu(x) - i\partial_\mu \Lambda(x)$. Hence, in order to ensure local gauge invariance of the fermionic fields, we have to introduce an additional field $A_\mu(x)$ which is therefore referred to as *gauge field*.

3.4.2 Gauge fields on the lattice

Now we perform the analog steps on the lattice, consequently, we demand the fermionic lattice action,[1]

$$S_F[\psi,\overline{\psi}] = a^4 \sum_{n\in\Lambda} \overline{\psi}(n)\left[\sum_{\mu=1}^{4} \frac{\psi(n+\hat{\mu}) - \psi(n-\hat{\mu})}{2a} + M\psi(n)\right], \tag{3.63}$$

to be invariant under local gauge transformations. The mass term is already invariant and for this reason we focus on the kinetic term, i.e., we require $\overline{\psi}(n)\psi(n\pm\hat{\mu})$ to be invariant under

$$\overline{\psi}(n) \to \overline{\psi}(n)G^{-1}(n), \quad \psi(n) \to G(n)\psi(n). \tag{3.64}$$

It is easy to see that we can achieve invariance when we introduce a oriented field $U_{\pm\mu}(n)$ which transforms under gauge transformations as

$$U_{\pm\mu}(n) \to G(n)U_{\pm\mu}(n)G^{-1}(n\pm\hat{\mu}). \tag{3.65}$$

Then the first part of the kinetic term transforms as+

$$\begin{aligned}\overline{\psi}(n)U_\mu(n)\psi(n+\hat{\mu}) \longrightarrow &\overline{\psi}(n)G^{-1}(n)G(n)U_\mu(n)G^{-1}(n+\hat{\mu})G(n+\hat{\mu})\psi(n+\hat{\mu}) \\ &= \overline{\psi}(n)U_\mu(n)\psi(n+\hat{\mu})\end{aligned} \tag{3.66}$$

and, equivalently, the second part

$$\begin{aligned}\overline{\psi}(n)U_{-\mu}(n)\psi(n-\hat{\mu}) \longrightarrow &\overline{\psi}(n)G^{-1}(n)G(n)U_{-\mu}(n)G^{-1}(n-\hat{\mu})G(n-\hat{\mu})\psi(n-\hat{\mu}) \\ &= \overline{\psi}(n)U_{-\mu}(n)\psi(n-\hat{\mu}).\end{aligned} \tag{3.67}$$

1 For this analysis it suffices to consider the naive fermion action which exhibits doublers.

We see that the field $U_\mu(n)$ links neighboring lattice sites n and $n \pm \hat{\mu}$, therefore, the $U_\mu(n)$ are called link variables. When we invert (3.67) and shift all sites $n \to n + \hat{\mu}$ we can identify

$$U_{-\mu}(n) = U_\mu^{-1}(n - \hat{\mu}), \tag{3.68}$$

that means the link variable in negative direction $-\hat{\mu}$ is given by the inverse link variable from the site $n - \hat{\mu}$ in positive direction $\hat{\mu}$, see Fig. 3.2. One may compare the link variables with the

Figure 3.2: Link variables

path ordered continuum gauge transporter to find a connection between the link variables and the continuum gauge field A_μ, see [20, 24],

$$U_\mu(n) = \mathrm{e}^{iaA_\mu(n)}\,. \tag{3.69}$$

3.5 Lattice Quantum Chromodynamics

We finally have all ingredients together to describe QCD on a discrete space-time lattice. QCD is the theory of the strong interaction which is responsible for the hadron spectrum, hadrons are the fundamental building blocks of matter and are themselves built up from two or three quarks. The quarks carry, besides the electromagnetic charge, a so called color charge[1] from which there are three types, thus the corresponding gauge group is SU(3). Usually one refers to these color charges as red, green and blue plus their counterparts anti-red, anti-green and anti-blue as charges of the anti-quarks. As a matter of fact, hadrons exist in nature only as color-neutral composites of these quarks, i.e., they are either build up from three (anti-)quarks with color charges (anti-)red, (anti-)green and (anti-)blue, resulting in a color neutral composite called baryon, or from two quarks, i.e., a quark and an anti-quark, making up a meson. This phenomenon is known as color confinement.

Moreover, we nowadays know about six different types of quarks. To distinguish them, one speaks of different flavors of quarks which are named up, down, charm, strange, top and bottom and they differ above all in their masses. They also differ in their electric charge but this will

1 Hence the name *Chromo*dynamics

not be of interest to us since we do not take QED effects into account.

The second sort of particles in QCD are the gluons and there are eight different types of them, according to the eight generators of the group SU(3). The gluons act as the force transmitters of the strong nuclear force in the same way the photons transmit the electromagnetic force, i.e., the quarks exchange gluons and thus feel a force between them. But there is a vital difference between photons and gluons, the latter carry themselves a color charge and as a result gluons interact with the like. This difference cannot be overemphasized since it is believed to be the origin of color confinement and makes QCD a highly non-trivial theory. The origin of the gluonic self-interaction lies in the non-commutativity of the underlying gauge group SU(3). Non-commutative groups, or non-Abelian groups, as gauge groups, were suggested by Yang and Mills [30] and accordingly the corresponding theories are referred to as Yang-Mills theories.

The quarks, being fermions, have to be described by Dirac fields

$$\psi^{(f)}(n)^a_\alpha, \quad \overline{\psi}^{(f)}(n)^a_\alpha \tag{3.70}$$

where $\alpha = 1, \ldots, 4$ is the Dirac index as before and $a = 1, 2, 3$ is the newly introduced color index, f is the flavor index which we will neglect most often. To obtain the quark action – the free fermionic lattice action – either Wilson type or staggered type, with which we became acquainted in the previous section, have only to be modified to include a sum over the additional indices of color and flavor.

To incorporate the gluonic fields, we couple the gauge group valued link variables

$$U^{ab}_\mu(n) \tag{3.71}$$

to the quark fields. Here again, the Roman letters $a, b = 1, 2, 3$ represent color. On that account, for fixed μ, $U^{ab}_\mu(n)$ is an element of the non-Abelian group SU(3) and its inverse is given by $U^{ab}_\mu(n)^\dagger$.

Then the full fermionic lattice action of QCD, with Wilson fermions, in its most explicit form reads

$$\begin{aligned} S_F[\psi,\overline{\psi},U] = \sum_{f=1}^{6} a^4 \sum_{n,m\in\Lambda} \overline{\psi}^{(f)}(n)^a_\alpha \Bigg(\frac{1}{2a} \sum_{\mu=1}^{4} \Big[(\gamma_\mu - \mathbb{1})_{\alpha\beta} U^{ab}_\mu(n) \delta_{n,m-\hat{\mu}} \\ - (\gamma_\mu + \mathbb{1})_{\alpha\beta} U^{ab}_\mu(n)^\dagger \delta_{n,m+\hat{\mu}} \Big] + \left(M^{(f)} + 4/a \right) \delta_{nm} \delta_{\alpha\beta} \delta_{ab} \Bigg) \psi^{(f)}(m)^b_\beta \end{aligned} \tag{3.72}$$

where a sum over α, β and a, b is understood. The expression in parentheses is the Wilson Dirac

operator, thence

$$S_F[\psi,\overline{\psi},U] = \sum_{f=1}^{6} a^4 \sum_{n,m\in\Lambda} \overline{\psi}^{(f)}(n)^a_\alpha \, D^{(\mathrm{W})}[U](n,m)^{ab}_{\alpha\beta} \, \psi^{(f)}(m)^b_\beta, \tag{3.73}$$

where we made the gauge field dependence of $D^{(\mathrm{W})}[U]$ explicit. For sake of readability we will adopt matrix/vector notation in Dirac and color space in the remainder of this work where appropriate.

The fermionic term is just the first part of the complete QCD action. What is still missing is the kinetic term of the gluons, that we will discuss now. Therefore, we initially convince ourselves that the trace of a closed loop of N link variables

$$\mathrm{tr}\left[U_{\mu_1}(n_1)U_{\mu_2}(n_2)\dots U_{\mu_N}(n_1)\right] \tag{3.74}$$

is a gauge invariant object. This can be seen when taking into account the transformation property (3.65) of the link variables and the cyclic permutation property of the trace: all gauge group elements $G(n) \in \mathrm{SU}(3)$ between two link variables cancel $G^\dagger(n_i+\hat{\mu}_i)G(n_i+\hat{\mu}_i) = \mathbb{1}$ and the leftovers to the left of the path, $G(n_1)$, and the right of the path, $G^\dagger(n_1)$, cancel as well since we may cyclic permute under the trace so that $G(n_1)$ and $G^\dagger(n_1)$ stand next to each other. The shortest such closed loop on the lattice is called plaquette and is defined by

$$U_{\mu\nu}(n) = U_\mu(n)U_\nu(n+\hat{\mu})U^\dagger_\mu(n+\hat{\nu})U^\dagger_\nu(n), \tag{3.75}$$

where we used (3.68) for the links in negative $\hat{\mu},\hat{\nu}$ direction, cf. Fig. 3.3.

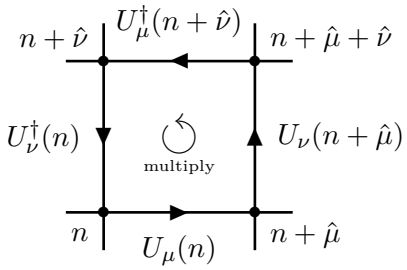

Figure 3.3: The gauge invariant plaquette

Wilsons gauge action [31] is constructed by summing over all possible plaquettes subtracted from the identity matrix and taking the real part of the trace therefrom,

$$S_G[U] = \frac{2}{g^2} \sum_{n\in\Lambda} \sum_{\mu<\nu} \mathfrak{Re}\ \mathrm{tr}\left[\mathbb{1} - U_{\mu\nu}(n)\right]. \tag{3.76}$$

When taking the naive continuum limit this expression converts into the familiar continuum expression, see ,e.g., [24],

$$S_G[A] = \frac{1}{2g^2} \int \mathrm{d}^4x \ \mathrm{tr}\left[F_{\mu\nu}(x)F_{\mu\nu}(x)\right], \tag{3.77}$$

where $F_{\mu\nu}$ is the field strength tensor

$$F_{\mu\nu}(x) = \partial_\mu A_\nu(x) - \partial_\nu A_\mu(x) + i[A_\mu(x), A_\nu(x)]. \tag{3.78}$$

We are now ready with the construction of a lattice formulation of QCD. The full lattice QCD action is then given by

$$S_{QCD}[\psi,\overline{\psi},U] = S_F[\psi,\overline{\psi},U] + S_G[U], \tag{3.79}$$

with $S_G[U]$ being Wilson's gauge action, (3.76), and with $S_F[\psi,\overline{\psi},U]$ given either by (3.73) or by the corresponding expression for staggered fermions (3.49), where one still has to add color and flavor indices.

Chapter 4

Quark Propagator from the Lattice

In this chapter we discuss the numerical calculation of the fermionic two-point function of QCD on a space-time lattice. To this effect we analyze the peculiarities of gauge fixing on the lattice, present the methods we use for fixing the Coulomb gauge as well as the residual gauge and for the inversion of the Dirac operator. Moreover, we introduce the dressing functions of the interacting propagator and show how these can be extracted, once the lattice propagator is on hand, for the case of Wilson's fermions and staggered fermions. At the end of this chapter we show the skeleton of a computer program which actually calculates the fermionic Green's function.

4.1 Path integral representation of the quark propagator

From what we discussed in the previous two chapters, we are now able to write down the PI formulation of the fermionic two-point function of QCD, the quark propagator,

$$S(n,m) \equiv \left\langle \psi(n)\,\overline{\psi}(m) \right\rangle = \frac{\int \mathcal{D}U\,\mathcal{D}\psi\,\mathcal{D}\overline{\psi}\,\psi(n)\,\overline{\psi}(m)\;\mathrm{e}^{-S_F\left[\psi,\overline{\psi},U\right]-S_G[U]}}{\int \mathcal{D}U\,\mathcal{D}\psi\,\mathcal{D}\overline{\psi}\;\mathrm{e}^{-S_F\left[\psi,\overline{\psi},U\right]-S_G[U]}}, \tag{4.1}$$

where the fermionic action S_F is given by (3.49) or (3.73) and the gauge action S_G by (3.76). Note that $S(n,m)$ is a matrix in color and Dirac space and thus has $N_c^2 \cdot 4^2 = 9 \cdot 16 = 144$ components for each combination of n and m. Naturally, we also integrate over all possible gauge field configurations in (4.1) where, again, those configurations which are close to the classical minimum give the main contributions. The integration measures for the quark fields are defined as in (3.33) with additional color indices and the integration measure for the gluon

fields is given by

$$\mathcal{D}U = \prod_n \prod_\mu \mathrm{d}U_\mu(n)\,, \tag{4.2}$$

where each integration measure $\mathrm{d}U_\mu(n)$ for fixed n, μ is a gauge invariant measure over the continuous compact group SU(3), known as Haar measure. It is normalized to

$$\int \mathrm{d}U_\mu(n) = 1, \quad n \in \Lambda, \mu = 1, \ldots, 4. \tag{4.3}$$

The explicit form of the Haar measure is given, e.g., in [24] but is not relevant to us since we will utilize Monte Carlo integration to calculate the quark propagator numerically on the lattice. Observe that we cannot simply calculate an ensemble average over Grassmann variables opposed to the case of the 0+1 dimensional scalar field in Sect. 3.1 eq. (3.21), where we dealt with conventional numbers. Fortunately, though, we can explicitly integrate out the quark field dependence of (4.1), to this effect use (3.34) to obtain

$$S(n,m) = \frac{\int \mathcal{D}U\; D^{-1}\,[U]\,(n,m)\; \mathrm{e}^{-\ln\,\det[D[U]] - S_G[U]}}{\int \mathcal{D}U\; \mathrm{e}^{-\ln\,\det[D[U]] - S_G[U]}}. \tag{4.4}$$

Note that unlike in (3.34), here the *fermion determinant* $\det[D]$ does not cancel because the Dirac operator $D[U](n,m)$ depends on the link variables U_μ – which stems from the coupling of the link variables to the quark fields – and we integrate over all U_μ. Nevertheless, it is remarkable that the PI expression for the quark propagator (4.4) does not include quark field configurations anymore but solely contains (non-local) expressions depending on the link variables.

Now, having got rid of the propagator's quark field dependence, we can calculate the propagator numerically by generating N gauge field configurations $U_\mu(n)^{(i)}, i = 1, \ldots, N$, with a Boltzmann distribution given by the *effective action*

$$\mathrm{e}^{-\ln\,\det[D] - S_G[U]} \tag{4.5}$$

and then inverting the Dirac operator on these configurations. Finally we average over the results from all configurations,

$$S(n,m) = \frac{1}{N} \sum_{i=1}^{N} D^{-1}[U^{(i)}](n,m). \tag{4.6}$$

4.1.1 Quenched approximation

It has to be remarked that since the Dirac operator, $D^{ab}_{\alpha\beta}[U](n,m)$, for fixed color and Dirac indices, is a huge matrix in n,m with number of entries of the order $\mathcal{O}\left((L^3 \times T)^2\right) = \mathcal{O}(10^{11})$, it is incredibly expensive, in terms of computation time, to calculate the fermion determinant. For this reason we will adopt the so called quenched approximation on those configurations which we generate on our own. Within this approximation, one sets the fermion determinant equal to one and therefore the PI expression for the quark propagator simplifies to

$$S(n,m) = \frac{\int \mathcal{D}U \; D^{-1}[U](n,m) \; \mathrm{e}^{-S_G[U]}}{\int \mathcal{D}U \; \mathrm{e}^{-S_G[U]}}. \tag{4.7}$$

The quenched approximation corresponds to neglecting the effects of closed quark loops as can be deduced in the hopping expansion for the Dirac operator. There, one writes the Dirac operator as, cf. (3.72),

$$D[U] = (M + {}^4\!/_a)\,(\mathbb{1} - \kappa H[U]) \tag{4.8}$$

and expands it for small $\kappa = {}^1\!/_{(2Ma+8)}$, i.e., for large mass. κ is referred to as *hopping parameter* and H is the so called *hopping matrix*,

$$H[U](n,m) = \sum_{\mu=1}^{4} \left[(\mathbb{1} - \gamma_\mu)\, U_\mu(n) \delta_{n,m-\hat{\mu}} - (\mathbb{1} + \gamma_\mu)\, U_\mu(n) \delta_{n,m+\hat{\mu}}\right]. \tag{4.9}$$

Put another way, in the quenched approximation one increases the mass of the sea quarks[1] towards infinity and thus no quark/anti-quark pairs can be created and annihilated out of the vacuum. On the other hand, when one does take the fermion determinant in the effective action into account, with an arbitrary number of dynamic quark flavors, one speaks correspondingly of a simulation with dynamic quarks or a dynamic simulation.

Gauge field configurations with a Boltzmann distribution given solely by $\exp(-S_G[U])$, i.e., in the aforementioned quenched approximation, can be generated with, e.g., the heat bath algorithm [32]. Creutz introduced in [32] the heat bath algorithm for SU(2) gauge theories and Cabibbo and Marinari [33] showed how to update general SU(N) gauge configurations applying the heat bath algorithm on SU(2) subgroups of SU(N).

1 One distinguishes between the propagating quarks (*valence quarks*) and the quarks which are dynamically created and annihilated out of the vacuum. To the latter one refers as *sea quarks* following Dirac's picture of the sea of particles and anti-particles.

4.1.2 Dynamical simulations

In addition to the gauge field configurations in quenched approximation which we generate on our own with the heat bath algorithm, we will make use of configurations containing dynamical quarks, provided by the MILC Collaboration [34] via the Gauge Connection.[1]

4.2 Gauge fixing

In the continuum, gauge fixing is necessary to make the theory well-defined.[2] In comparison, on the lattice, gauge fixing is not a prerequisite in principle; all gauge invariant PI are well-defined and computable. Nevertheless, one has to fix the gauge on the lattice as well to compute non-gauge invariant quantities. Assume a non-gauge invariant quantity $O[U]$, for its vacuum expectation value yields under arbitrary gauge transformations $U \to U'$,

$$\langle O[U'] \rangle = \frac{1}{Z} \int \mathcal{D}U'\, O[U']\, \mathrm{e}^{-S_G[U']} = \frac{1}{Z} \int \mathcal{D}U\, O[U']\, \mathrm{e}^{-S_G[U]}, \tag{4.10}$$

since the action and the gauge measure are gauge invariant. Because any desired gauge transformation in (4.10) may be chosen, we equivalently could average over the whole gauge group. Thus the vacuum expectation value of a non-gauge invariant quantity equals its average over the gauge group and vanishes. Based on this observation, Elitzur [35] proved that spontaneous breaking of local symmetries is impossible.

Whereas physical quantities are gauge invariant and the fermionic action, i.e., the combination of the quark fields and the Dirac operator,

$$S_F[\psi,\overline{\psi},U] = a^4 \sum_{n,m} \overline{\psi}(n)\, D[U](n,m)\, \psi(m) \tag{4.11}$$

is per construction of the gauge links invariant under gauge transformations (3.65), the Dirac operator alone

$$D[U](n,m) = \frac{1}{2a} \sum_{\mu} \left[\gamma_\mu U_\mu(n) \delta_{n,m-\hat{\mu}} - \gamma_\mu U_\mu(n) \delta_{n,m+\hat{\mu}}\right] + \mathbb{1} M \delta_{nm}, \tag{4.12}$$

here in its naive discretization, is not gauge invariant. Thus the quark propagator, being the inverse of the Dirac operator, is neither gauge invariant and we have to choose a particular gauge before we invert the Dirac operator on each gauge field configuration.

1 http://qcd.nersc.gov/

2 Fixing the gauge in the continuum removes zero modes of the inverse gluon propagator which give rise to singularities in the gluon propagator.

4.2.1 Coulomb gauge

We will gauge-rotate all gauge links in such a way that they fulfill the Coulomb gauge condition, which in the continuum reads $\partial_i A_i(x) = 0$, where the Roman index i runs only over the spatial components, $i = 1, 2, 3$. As we show in Appendix A.4, this is equivalent to maximizing the following gauge functional with respect to gauge transformations $G(x) \in \mathrm{SU}(3)$ for all x_4,

$$\tilde{F}_G[A](x_4) = \sum_{i=1}^{3} \int \mathrm{d}^3\boldsymbol{x} \ \mathrm{tr}\left[\Big(G(x)A_i(x)G^\dagger(x)\Big)^2\right]. \tag{4.13}$$

On the lattice, an equivalent extremization prescription can be formulated by, for instance, maximizing

$$F_G[U](n_4) = a^2 \sum_{i=1}^{3} \sum_{n_1,n_2,n_3} \mathrm{tr}\left[G(n)U_i(n)G^\dagger(n+\hat{i}) + G(n+\hat{i})U_i^\dagger(n)G^\dagger(n)\right] \tag{4.14}$$

for each n_4 with respect to $G(n) \in \mathrm{SU}(3)$, see (A.20).

Note that (4.14) has number of degrees of freedom of the order $\mathcal{O}(L^3 \times T \times (N_c^2 - 1)) = \mathcal{O}(10^7)$ and moreover has very many local maxima, the so-called Gribov copies [4]. Therefore, maximizing (4.14) is a highly non-trivial task. Two algorithms which have proven to be adequate to attack this problem are *simulated annealing* [36], which is a global optimizer, and *overrelaxation*, [37] which is a local optimizer, and especially the combination of these two. Nonetheless, these algorithms cannot ensure either that the unique global extremum of (4.14) will be reached. For the quark propagator, though, we will show that the remaining arbitrariness due to Gribov copies is of negligible influence. Studies, as for example [16], where the Landau gauge quark propagator is compared to the Gribov copy free Laplacian gauge quark propagator, point towards the same assertion. We will choose the termination criterion for fixing the Coulomb gauge as

$$\frac{1}{2VN_c} \sum_{i,n} \mathfrak{Re}\left\{\mathrm{tr}\left[U_i(n) - U_i(n-\hat{i})\right]\right\} < \varepsilon, \tag{4.15}$$

where ε we be specified below.

4.2.2 Residual gauge freedom

Once a maximum of (4.14) is found, hence the gauge is fixed to the Coulomb gauge, we are left with a residual gauge freedom with respect to space independent gauge transformations $G(x_4) \in \mathrm{SU}(3)$, as we prove in Appendix A.4. In the following we present two possible procedures how to fix this residual gauge as well.

Integrated Polyakov gauge

One possible choice to fix the residual gauge freedom in the continuum is to require

$$\int \mathrm{d}^3x\, \partial_\mu A_\mu(x) = 0 \iff \partial_4 \int \mathrm{d}^3x\, A_4(x) = 0. \tag{4.16}$$

The lattice version thereof, cf. [11], is to seek a gauge $G(n_4)$ such that

$$\hat{u}(n_4) \equiv \frac{1}{L^3} \sum_{\boldsymbol{n}} U_4(n) \stackrel{!}{\to} \text{const}, \tag{4.17}$$

where $L^3 = \prod_i N_i$ is the amount of lattice sites per time-slice. Such a gauge would manifestly be space independent since we average on every time-slice over all spatial degrees of freedom. Note that $\hat{u}(n_4)$, as defined in (4.17) as a sum of SU(3) elements, is itself not an SU(3) element. With the intent to project $\hat{u}(n_4)$ onto a group element $u(n_4)$ of SU(3), we utilize Cabibbo–Marinari cooling [33] and find $u(n_4)$ as the maximum

$$\max_{u(n_4)} \mathfrak{Re}\ \mathrm{tr}\left[u(n_4)\hat{u}^\dagger(n_4)\right]. \tag{4.18}$$

One should acknowledge that the above projection is much easier in the case of the group SU(2) since the sum of SU(2) matrices is proportional to another SU(2) element and thus one would simply have to divide $\hat{u}(n_4)$ by $\sqrt{\det\left[\hat{u}(n_4)\right]}$.

Next we define the integrated Polyakov loop [38] by

$$P \equiv \mathrm{tr}\left[\prod_{n_4} u(n_4)\right], \tag{4.19}$$

which, as a closed loop, is a gauge invariant object as we have shown in (3.74). Explicitly, for P holds under gauge transformations

$$P \to P' = \mathrm{tr}\left[\prod_{n_4} G(n_4)u(n_4)G^\dagger(n_4+1)\right] = P. \tag{4.20}$$

Then it is totally legitimate to choose $G(n_4)$ such that for all n_4,

$$G(n_4)u(n_4)G^\dagger(n_4+1) = P^{1/T}, \tag{4.21}$$

where $P^{1/T}$ is the T-th root of P, $T = N_4$ being the number of lattice points in the temporal direction. For a review of algorithms to find the matrix p-th root we refer to [39]. Hence, if we choose, without loss of generality, $G(0) = \mathbb{1}$, we may find all $G(n_4)$ recursively by solving (4.21)

for $G^\dagger(n_4+1)$,

$$G^\dagger(n_4+1) = u^\dagger(n_4) G^\dagger(n_4) P^{1/T}. \tag{4.22}$$

Once this recursion is executed, we gauge all $U_\mu(n)$ via

$$U_4'(n) = G(n_4) U_4(n) G^\dagger(n_4+1) \tag{4.23a}$$

or

$$U_i'(n) = G(n_4) U_i(n) G^\dagger(n_4), \tag{4.23b}$$

respectively, to eliminate the residual gauge freedom.

Integrated maximal trees

Hereafter, we suggest another possibility how the residual gauge freedom can be fixed that, in comparison to the previous scheme, has the advantage of lacking the need of calculating matrix p-th roots and moreover is related to the maximal-tree gauge which is a peculiarity of the lattice. Define $\hat{u}(n_4)$ as in (4.17) and project it to SU(3) as in (4.18). Then simply set

$$\begin{aligned} G(0) &= \mathbb{1}, \\ G(1) &= u(0), \\ G(2) &= u(0)u(1), \\ &\vdots \\ G(T-1) &= u(0)u(1)u(2)\dots u(T-2), \end{aligned} \tag{4.24}$$

to get a set of space independent gauge transformations $G(n_4)$. In the limit of a single spatial lattice site, i.e., a temporal line, this gauge would transform into a maximal-tree gauge. That means it would gauge all but one of the temporal links, $U_4(n)$, to the identity. In this sense, this gauge is reminiscent of the *temporal gauge* where all $A_\mu(n)$ are set to 0 and thus all $U_\mu(n) = \mathbb{1}$.[1] In the limit of a single spatial lattice site $u(n_4) = U_4(n_4)$ holds and thus we would obtain, when gauging with (4.24),

$$\begin{array}{rcrcrl} U_4(0) & \to & G(0)U_4(0)G^\dagger(1) & = & U_4(0)U_4^\dagger(0) & = \mathbb{1}, \\ U_4(1) & \to & G(1)U_4(1)G^\dagger(2) & = & U_4(0)U_4(1)U_4^\dagger(1)U_4^\dagger(0) & = \mathbb{1}, \\ & \vdots & & \vdots & & \vdots \\ U_4(T-1) & \to & G(T-1)U_4(T-1)G^\dagger(0) & = & U_4(0)U_4(1)\dots U_4(T-1) & \neq \mathbb{1}. \end{array} \tag{4.25}$$

1 We cannot gauge *all* $U_\mu(n)$ to the identity on a lattice with periodic boundary conditions since the Polyakov loop is conserved.

4.3 Calculating the propagator

After we removed the gauge freedom on a per-configuration basis, the next step in the construction of the momentum space quark propagator is to invert the Dirac operator, on each configuration, and subsequently Fourier transform it to momentum space.

4.3.1 Inverting the Dirac operator

In every step of the Monte Carlo–Markov chain we have to invert the Dirac operator, $D^{ab}_{\alpha\beta}[U](n,m)$, for all combinations of the color indices a,b and Dirac indices α,β. The Dirac operator is translationally invariant on a periodic lattice,

$$D[U](n,m) = D[U](n+\ell,m+\ell), \quad \ell = (\ell_1,\ldots,\ell_4). \tag{4.26}$$

Therefore, inverting the Dirac operator for all combinations of n,m results in a lot of redundant information.[1] Taking this and the fact that inverting the huge matrix of the Dirac operator is quite expensive into account, we choose to calculate the propagator not for all combinations of n,m but fix m to an arbitrary site, let us choose $m = 0$.

Consequently, for a given *point-source* $(0,\overline{\alpha},\overline{a})$, we have to solve

$$\sum_{m,\beta,b} D^{ab}_{\alpha\beta}(n,m) S^{b\overline{a}}_{\beta\overline{\alpha}}(m,0) = \delta(n)\delta_{a\overline{a}}\delta_{\alpha\overline{\alpha}} \qquad \forall\,\overline{\alpha},\overline{a}, \tag{4.27}$$

for $S^{b\overline{a}}_{\beta\overline{\alpha}}(m,0)$ to obtain the coordinate space quark propagator.

We used and tested a variety of algorithms to perform this inversion, e.g., MinRes, BiCGStab and UML [40].

4.3.2 Momentum space quark propagator

Once the coordinate space propagator $S(m,0)$ is obtained, it remains to Fourier transform it to momentum space,

$$S(p) = \sum_m \mathrm{e}^{-ip\cdot m}\, S(m,0), \tag{4.28}$$

1 Though it would increase statistics.

where the discrete momenta are given by

$$\begin{aligned} p_i &= \frac{2\pi}{N_i a}\left(n_i + 1 - \frac{N_i}{2}\right), \quad n_i = 0, \ldots, N_i - 1, \\ p_4 &= \frac{2\pi}{N_4 a}\left(n_4 + \frac{1}{2} - \frac{N_4}{2}\right), \quad n_4 = 0, \ldots, N_4 - 1. \end{aligned} \tag{4.29}$$

The difference of $1/2$ between the spatial momenta p_i and the energy p_4 stems from the anti-periodic boundary conditions in the temporal direction. We use anti-periodic boundary conditions in the temporal direction, as appropriate for fermions, to ensure the reconstruction of the Minkowski type Hilbert space [22].

4.4 Dressing functions

In the aforegoing sections we discussed in detail how the interacting momentum space quark propagator can be obtained on the lattice and we are now in the position to study its properties.

From (3.38) we know that the momentum space quark propagator at tree-level[1] is of the form

$$S^{(0)}(p)^{ab}_{\alpha\beta} = \frac{-i(\gamma_i)_{\alpha\beta}\hat{k}_i - i(\gamma_4)_{\alpha\beta}\hat{k}_4 + \hat{M}\delta_{\alpha\beta}}{\hat{\boldsymbol{k}}^2 + \hat{k}_4^2 + \hat{M}^2}\,\delta_{ab}, \tag{4.30}$$

with the lattice fermion momenta $\hat{k}_\mu \equiv \sin \hat{p}_\mu$ which we introduced in (3.37). In expression (4.30) the superscript 0 shall remind as that we are confronted with the free propagator. Since we study the propagator in Coulomb gauge, which distinguishes spatial from temporal degrees of freedom, we separated $\gamma_\mu k_\mu$ into its spatial and temporal parts. Using matrix/vector notation in Dirac space and omitting color indices, this yields

$$S^{(0)}(p) = a^{-1}\frac{-i\gamma_i k_i - i\gamma_4 k_4 + M\mathbb{1}}{\boldsymbol{k}^2 + k_4^2 + M^2} \tag{4.31a}$$

$$= a\left(i\gamma_i k_i + i\gamma_4 k_4 + M\mathbb{1}\right)^{-1}, \tag{4.31b}$$

where we made the implicit a-dependence explicit. The last equation can be verified by multiplying both sides with the inverse tree-level quark propagator, i.e., the free momentum space Dirac operator,

$$S^{(0)}(p)^{-1} = i\gamma_i k_i a + i\gamma_4 k_4 a + Ma\mathbb{1}. \tag{4.32}$$

Our interest lies in how the free propagator changes when the interactions with the gluon fields are turned on. We expect the full propagator to be of similar form to its tree-level

1 This means having set all gauge links to $\mathbb{1}$ and thereby turned off the interaction with the gluons.

counterpart, thus we may write for the full inverse propagator

$$S^{-1}(p) = i\gamma_i k_i a A_s(p) + i\gamma_4 k_4 a A_t(p) + i\gamma_i k_i \gamma_4 k_4 a^2 A_d(p) + B_m(p)\mathbb{1}. \tag{4.33}$$

In (4.33) we introduced dimensionless real scalar functions $A_s(p), A_t(p), A_d(p)$ and $B_m(p)$ to which we will refer to as the spatial, temporal, a potential mixed and the massive component, respectively. These functions must clearly depend on the momentum and due to asymptotic freedom we expect the full propagator to merge into its tree-level expression for large momenta. Regarding the extraction of these scalar functions from the lattice quark propagator, we have to distinguish between Wilson type and Kogut–Susskind type fermions.

4.4.1 Wilson fermions

Remember that the only difference between Wilson's formulation of the momentum space Dirac operator and its naive discretization is the additional Wilson term, cf. (3.40). Hence, formally we simply may write $M(p)$ instead of M, where $M(p)$ stands for the r.h.s. of (3.40), to account for the Wilson term, then $M(p)$ coincides with $B_m(p)$ at tree-level.

With the aim of extracting the dressing functions $A_s(p), A_t(p), A_d(p)$ and $B_m(p)$, we multiply the inverse lattice quark propagator (4.33) with $\gamma_i k_i, \gamma_4 k_4, \gamma_i k_i \gamma_4 k_4$ or $\mathbb{1}$, respectively, take the trace with respect to Dirac and color indices and use

$$\begin{aligned} \operatorname{tr}\left[\gamma_\mu\right] &= 0, \\ \operatorname{tr}\left[\gamma_\mu\gamma_\nu\right] &= 4\delta_{\mu\nu}, \\ \operatorname{tr}\left[\gamma_\mu\gamma_\nu\gamma_\rho\right] &= 0, \\ \operatorname{tr}\left[\gamma_\mu\gamma_\nu\gamma_\rho\gamma_\sigma\right] &= 4\left(\delta_{\mu\nu}\delta_{\rho\sigma} - \delta_{\mu\rho}\delta_{\nu\sigma} + \delta_{\mu\sigma}\delta_{\nu\rho}\right). \end{aligned} \tag{4.34}$$

From the last-mentioned set of equations follows in particular

$$\begin{aligned} \operatorname{tr}\left[(\gamma_i k_i a)^2\right] &= 4\sum_{i=1}^{3} k_i^2 a^2, \\ \operatorname{tr}\left[(\gamma_i k_i a \gamma_4 k_4 a)^2\right] &= -4\sum_{i=1}^{3} k_i^2 a^2 k_4^2 a^2 \end{aligned} \tag{4.35}$$

and in this way we attain the following expressions for the dressing functions

$$A_s(p) = \frac{-i}{4N_c \sum_i k_i^2 a} \operatorname{tr}\left[\gamma_i k_i S^{-1}(p)\right], \tag{4.36a}$$

$$A_t(p) = \frac{-i}{4N_c k_4^2 a} \operatorname{tr}\left[\gamma_4 k_4 S^{-1}(p)\right], \tag{4.36b}$$

$$A_d(p) = \frac{-i}{4N_c \sum_i k_i^2 k_4^2 a^2} \operatorname{tr}\left[\gamma_4 k_4 \gamma_i k_i S^{-1}(p)\right], \tag{4.36c}$$

$$B_m(p) = \frac{1}{4N_c} \operatorname{tr}\left[S^{-1}(p)\right]. \tag{4.36d}$$

The factor of $4N_c$ results from taking the trace over Dirac and color indices.

Now we know how to obtain the dressing functions from the Dirac operator $S^{-1}(p)$. It is the inverse Dirac operator, though, which coincides with the fermionic two-point function. Such being the case, consider the quark propagator (4.31a) dressed with the same functions,

$$S(p) = \frac{-i\gamma_i k_i a A_s(p) - i\gamma_4 k_4 a A_t(p) - i\gamma_i k_i \gamma_4 k_4 a^2 A_d(p) + B_m(p)\mathbb{1}}{D^2(p)}, \tag{4.37}$$

where we defined in the denominator as

$$D^2(p) \equiv \sum_i k_i^2 a^2 A_s^2(p) + k_4^2 a^2 A_t^2(p) + k_4^2 \sum_i k_i^2 a^4 A_d^2(p) + B_m^2(p). \tag{4.38}$$

Thence we can calculate, in the same manner as before, the dressing functions of the quark propagator as:

$$\mathcal{A}_s(p) \equiv \frac{A_s(p)}{D^2(p)} = \frac{i}{4N_c \sum_i k_i^2 a} \operatorname{tr}\left[\gamma_i k_i S(p)\right], \tag{4.39a}$$

$$\mathcal{A}_t(p) \equiv \frac{A_t(p)}{D^2(p)} = \frac{i}{4N_c k_4^2 a} \operatorname{tr}\left[\gamma_4 k_4 S(p)\right], \tag{4.39b}$$

$$\mathcal{A}_d(p) \equiv \frac{A_d(p)}{D^2(p)} = \frac{i}{4N_c \sum_i k_i^2 k_4^2 a^2} \operatorname{tr}\left[\gamma_i k_i \gamma_4 k_4 S(p)\right], \tag{4.39c}$$

$$\mathcal{B}_m(p) \equiv \frac{B_m(p)}{D^2(p)} = \frac{1}{4N_c} \operatorname{tr}\left[S(p)\right]. \tag{4.39d}$$

In Appendix A.5 we show the equivalence

$$\mathcal{A}_t(p) = \frac{A_t(p)}{D^2(p)} \;\wedge\; \mathcal{A}_s(p) = \frac{A_s(p)}{D^2(p)} \wedge \mathcal{A}_d(p) = \frac{A_d(p)}{D^2(p)} \;\wedge\; \mathcal{B}_m(p) = \frac{B_m(p)}{D^2(p)} \tag{4.40a}$$

$$\iff A_t(p) = \frac{\mathcal{A}_t(p)}{\mathcal{D}^2(p)} \;\wedge\; A_s(p) = \frac{\mathcal{A}_s(p)}{\mathcal{D}^2(p)} \wedge A_d(p) = \frac{\mathcal{A}_d(p)}{\mathcal{D}^2(p)} \;\wedge\; B_m(p) = \frac{\mathcal{B}_m(p)}{\mathcal{D}^2(p)}, \tag{4.40b}$$

with

$$\mathcal{D}^2(p) \equiv \sum_i k_i^2 a^2 \mathcal{A}_s^2(p) + k_4^2 a^2 \mathcal{A}_t^2(p) + k_4^2 \sum_i k_i^2 a^4 \mathcal{A}_d^2(p) + \mathcal{B}_m^2(p). \tag{4.41}$$

In consequence, we may first calculate the functions $\mathcal{A}_s(p), \mathcal{A}_t(p), \mathcal{A}_d(p)$ and $\mathcal{B}_m(p)$ from the lattice quark propagator as depicted in (4.39) and then ultimately acquire the dressing functions $A_s(p), A_t(p), A_d(p)$ and $B_m(p)$ by (4.40b).

It is also worth mentioning that by proceeding in the same manner we are able to extract the fermion lattice momenta k_μ directly from the tree-level quark propagator. Consider the tree-level Dirac operator (4.32) rewritten as

$$S^{(0)}(p)^{-1} = i\gamma_\mu C_\mu(p) + M(p)a\mathbb{1}. \tag{4.42}$$

If we want to extract the functions $C_\mu(p)$, which we expect to coincide with the fermion lattice momentum $k_\mu a$, we find

$$\mathcal{C}_\mu(p) = \frac{i}{4N_c} \operatorname{tr}\left[\gamma_\mu S^{(0)}(p)\right] \tag{4.43a}$$

and

$$C_\mu(p) = \frac{\mathcal{C}_\mu(p)}{\mathcal{C}_\mu^2(p) + \hat{M}^2(p)}. \tag{4.43b}$$

An analog decomposition of the lattice quark propagator in Landau gauge, where there are only two dressing functions, was done in [12].

4.4.2 Staggered fermions

In (3.53) we casted the free staggered momentum space Dirac operator into a form reminiscent of the Wilson or naive discretization case,

$$S_{\alpha\beta}^{(0)}(q)^{-1} = i\sum_\mu (\overline{\gamma}_\mu)_{\alpha\beta} \sin(\hat{q}_\mu) + \hat{M}\overline{\delta}_{\alpha\beta}. \tag{4.44}$$

Here we suppressed color indices and α,β are not Dirac- but staggered multi-indices $\alpha = (\alpha_1, \ldots, \alpha_4), \alpha_\mu = 0, 1$. Remember that the discrete momentum $\hat{q}_\mu$ is restricted to the inner BZ, $\hat{q}_\mu \in (-\pi/2, \pi/2]$, for staggered fermions. We will also make use of the shorthand for the fermion lattice momenta, as before, thus in the context of staggered fermions we set $\hat{k}_\mu \equiv \sin \hat{q}_\mu$.

We first sum over one of the propagator's multi-indices, $\sum_\beta = \sum_{\beta_1,\ldots,\beta_4=0}^{1}$, and define

$$G_\alpha(q) \equiv \sum_\beta S_{\alpha\beta}^{(0)}(q) = \sum_\beta \frac{-i(\overline{\gamma}_\mu)_{\alpha\beta}\hat{k}_\mu + \hat{M}\overline{\delta}_{\alpha\beta}}{\hat{k}^2 + \hat{M}^2}. \tag{4.45}$$

In order to evaluate the r.h.s. of (4.45), we realize that

$$\sum_\beta (\overline{\gamma}_\mu)_{\alpha\beta} \equiv \sum_\beta (-1)^{\alpha_\mu} \overline{\delta}_{\alpha+\theta(\mu),\beta} = (-1)^{\alpha_\mu} \tag{4.46}$$

and therefore we can write the dressed staggered Coulomb gauge propagator as

$$G_\alpha(q) = \frac{-i(-1)^{\alpha_i} k_i a A_s(q) - i(-1)^{\alpha_4} k_4 a A_t(q) - i(-1)^{\alpha_i+\alpha_4} k_i k_4 a^2 A_d(q) + B_m(q)}{D^2(q)} \tag{4.47}$$

with $D^2(q)$ defined in analogy to the case of Wilson's fermions. Then we multiply by $(-1)^{\alpha_i}$, $(-1)^{\alpha_4}$, $(-1)^{\alpha_i+\alpha_4}$ or 1, respectively, sum over α and use

$$\sum_\alpha (-1)^{\alpha_\mu+\alpha_\nu} = 16\,\delta_{\mu\nu}. \tag{4.48}$$

Subsequently we take the trace with respect to color indices and obtain for the staggered propagator's dressing functions

$$\mathcal{A}_s(q) \equiv \frac{A_s(q)}{D^2(q)} = \frac{i}{16 N_c \sum_i k_i^2 a} \sum_i \sum_\alpha (-1)^{\alpha_i} k_i \,\mathrm{tr}\,[G_\alpha(q)]\,, \tag{4.49a}$$

$$\mathcal{A}_t(q) \equiv \frac{A_t(q)}{D^2(q)} = \frac{i}{16 N_c k_4^2 a} \sum_\alpha (-1)^{\alpha_4} k_4 \,\mathrm{tr}\,[G_\alpha(q)]\,, \tag{4.49b}$$

$$\mathcal{A}_d(q) \equiv \frac{A_d(q)}{D^2(q)} = \frac{i}{16 N_c \sum_i k_i^2 k_4^2 a^2} \sum_i \sum_\alpha (-1)^{\alpha_i+\alpha_4} k_i k_4 \,\mathrm{tr}\,[G_\alpha(q)]\,, \tag{4.49c}$$

$$\mathcal{B}_m(q) \equiv \frac{B_m(q)}{D^2(q)} = \frac{1}{16 N_c} \sum_\alpha \,\mathrm{tr}\,[G_\alpha(q)]\,. \tag{4.49d}$$

An equivalent decomposition of the staggered quark propagator in Landau gauge was performed in [14].

4.5 Summary and pseudocode

As a summary of the present chapter we review the construction of the Coulomb gauge quark propagator on the lattice, in quenched approximation, within a short program in pseudocode, see Algorithm 4.1. It is clear that these few lines of code only represent the very basic steps and are not comparable to a complete computer program. Therefore, Algorithm 4.1 exclusively serves as an overview and repetition of the main steps in the calculation, in particular, all subroutines and parallelization issues are passed over.

Algorithm 4.1 Calculating the dressing functions of the quark propagator

read parameters from file
define and initialize a lattice, gauge field, random number generator etc.
define lattice momenta $\hat{p}_\mu$, cf. (4.29)

for all n, μ **do**
  set $U_\mu = \mathbb{1}$ {gluon interaction off}
end for

invert Dirac operator to obtain tree-level quark propagator
Fourier transform tree-level quark propagator
extract fermion lattice momenta $\hat{k}_\mu(p)$

for $i = 1$ to $N_{\text{equilibrate}}$ **do**
  heat bath pass on gauge fields {bring configuration into equilibrium}
end for

{Monte Carlo integration}
for $n = 1$ to number of Monte Carlo steps **do**
  for $i = 1$ to $N_{\text{discarded}}$ **do**
    heat bath pass on gauge fields {update config.}
  end for
  {Fix the Coulomb gauge}
  for $T = T_{\text{start}}$ to T_{end} **do**
    simulated annealing {cool config. with respect to gauge functional value F_G}
  end for
  while Coulomb gauge not satisfactory reached **do**
    overrelaxation
  end while
  fix residual gauge
  invert Dirac operator to obtain quark propagator
  Fourier transform quark propagator
  extract dressing functions
end for
do statistics, i.e., average over results and calculate Jackknife errors [41]
print results

Chapter 5

Results

In this chapter we will present our findings for the Coulomb gauge lattice quark propagator. We will start by comparing the outcomes from the propagator with Wilson fermions to the propagator using staggered Fermions with Kogut–Susskind (KS) and Asqtad action. After shortly discussing the sensitivity of the propagator on Gribov copies, we will investigate renormalization of the propagator and prove that the static Coulomb gauge quark propagator is renormalizable. Finally, we will introduce dynamical quarks into our simulation and analyze the effects they have on the quark propagator. In between we detect that our results seem not to be strongly affected by finite volume and finite lattice spacing effects.

Throughout this work we use the C++ library FermiQCD by Fermilab [40] which is a toolbox containing classes, functions and algorithms for lattice quantum field theory computations. FermiQCD is set on top of Matrix Distributed Processing (MDP) [42] which, on the other hand, provides an interface to the Message Passing Interface (MPI) in order to enable the user to write parallel code.

5.1 Quenched approximation

We generated three different sets of gauge configurations using Cabibbo–Marinari's pseudo heat bath algorithm [33] with the gauge action (3.76),

$$S_G[U] = \frac{\beta}{N_c} \sum_{n\in\Lambda} \sum_{\mu<\nu} \mathfrak{Re}\ \mathrm{tr}\left[\mathbb{1} - U_{\mu\nu}(n)\right], \tag{5.1}$$

where we introduced a common shorthand, the *inverse coupling* $\beta = {}^{2N_c}/_{g^2}$. In QCD, the number of color charges is $N_c = 3$ and thus $\beta = {}^{6}/_{g^2}$. We chose three different values for

the inverse coupling β which is accompanied by three different lattice spacings a; in order to obtain the same physics at different coupling strengths one has to adapt the lattice spacing: this connection is described by the renormalization group equations [43]. For a given value of the inverse coupling, one has to set the scale, i.e., determine the lattice spacing, by making contact to physical observables. This can be done, for instance, with the static quark potential and in particular the *Sommer parameter* [44]. We set the scale for our values of β using the parametrization of $a(\beta)$, $5.7 \leq \beta \leq 6.92$, by Sommer and Necco [45]. The parameters of our gauge configurations are summarized in Tab. 5.1, there, N_{config} denotes the number of configurations we generated, hence the number of samples in the Monte Carlo integration.

β	N_{config}	$L^3 \times T$	a	La	Ta
5.7	94	$16^3 \times 32$	0.170 fm	2.72 fm	5.44 fm
6.0	108	$16^3 \times 32$	0.093 fm	1.49 fm	2.98 fm
6.5	131	$16^3 \times 32$	0.045 fm	0.72 fm	1.44 fm

Table 5.1: Parameters of the configurations in quenched approximation.

We start our simulation with a cold start, i.e., we set all gauge links to the identity. Subsequently, we perform 2500 equilibrating sweeps, cf. $N_{\text{equilibrate}}$ in Algorithm 4.1, and thereafter we apply $N_{\text{discarded}} = 250$ updating sweeps before picking the first configuration, followed by, again, 250 updating sweeps before picking the next configuration. After picking a configuration, we fix it to the Coulomb gauge with an accuracy of $\varepsilon = 10^{-12}$, see (4.15), and thereafter fix the residual gauge by either the integrated Polyakov scheme or the integrated maximal tree scheme that we introduced in Sect. 4.2.2.

5.1.1 Wilson fermions

We begin studying the quark propagator using Wilson fermions on the set of gauge configurations for which $\beta = 6.0$, see Tab. 5.1, and fix the residual gauge using integrated maximal trees. We set the hopping parameter κ to 0.124 to be sure not to get conflicted with *exceptional configurations*.[1] When one wants to determine the corresponding dimensionless bare mass $\hat{m} \equiv ma$, one may be lead to simply solve κ for $\hat{M}$, cf. (4.8), but the parameter $\hat{M}$ does not directly correspond to a bare mass for Wilson fermions. The origin thereof lies in the fact that the Wilson term explicitly breaks chiral symmetry. The pion is believed to be the Goldstone boson [46] of chiral symmetry breaking and hence its mass $\hat{M}_\pi$ should vanish for zero bare

1 Certain fluctuations of the gauge fields may lead to small eigenvalues of the Dirac operator and thereby make the numerical inversion problematic. It can be shown that for $\kappa < 1/8$ there are no exceptional configurations [20, 24].

quark mass $\hat{m}$. This will happen for a certain value of κ, called critical value,

$$\kappa_c = \frac{1}{2\hat{M}_c + 8}. \tag{5.2}$$

Therefore, a possible definition for the bare quark mass arises as $\hat{m} = \hat{M} - \hat{M}_c$, or equivalently

$$\hat{m} = \frac{1}{2}\left(\frac{1}{\kappa} - \frac{1}{\kappa_c}\right). \tag{5.3}$$

The value of κ_c clearly depends on the inverse coupling β. For our gauge configurations with $\beta = 6.0$, κ_c is approximately 0.1352 [47] and thus the bare mass $\hat{m} = 0.334$. In physical units this corresponds to $m \approx 707\,\text{MeV}$, see (A.5).

Tree-level

To get started, we investigate the quark propagator at tree-level. We extract the functions $C_\mu(p)$, that we expect to coincide with the lattice fermion momenta, from the tree-level propagator as depicted in Sect. 4.4.1. They are plotted against the discrete momenta pa in Fig. 5.1. As can

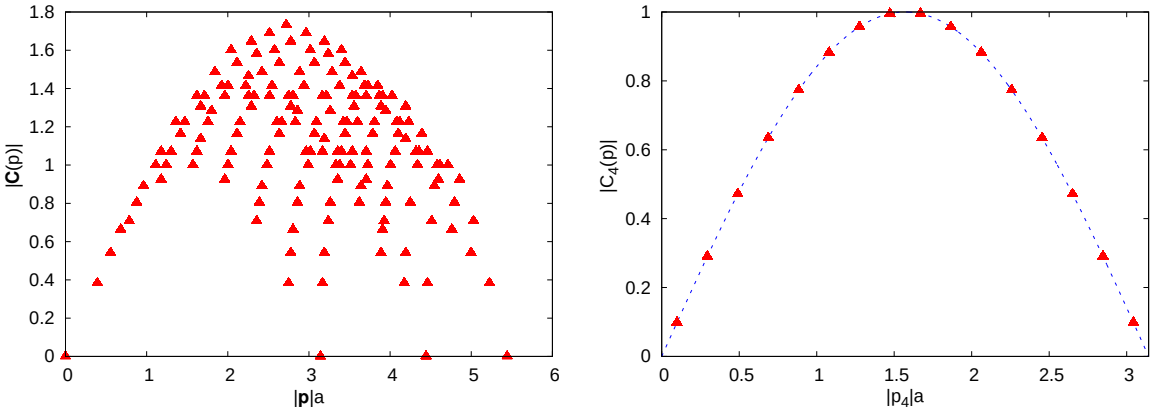

Figure 5.1: Lattice momenta extracted from the tree-level propagator using Wilson fermions.

be seen, the data for $C_4(p)$ perfectly agrees with the fermion lattice momentum $k_4 a \equiv \sin(p_4 a)$, what serves as a consistency check. The data for $|\boldsymbol{C}(p)| \equiv \sqrt{\sum_i C_i^2(p)}$ does not show the same smoothness, this is very natural, though, since the x-axis combines three momenta, $|\boldsymbol{p}|a \equiv \sqrt{\sum_i p_i}a$, and obviously, these artifacts will vanish when we separate out such three-momenta for which the magnitude of the various components differs greatly. Momenta for which all components are of the same magnitude lie close to the diagonal of momentum space. We will only take such momenta into account and hence we perform a so-called *cylinder cut* on our data and thereby take only these momenta into account which lie within a certain distance

to the diagonal in 4-dimensional momentum space. In addition, the cylinder cut is expected to minimize finite lattice spacing artifacts, cf. [15, 48]. We define the distance to the diagonal as

$$\Delta p = |p| \sin\theta(p), \tag{5.4}$$

where $\theta(p)$ is the angle between the diagonal and p, i.e.,

$$\cos\theta(p) = \frac{p}{|p|} \cdot \hat{n}, \quad \hat{n} = \frac{1}{2}(1,1,1,1). \tag{5.5}$$

We will select those momenta which lie within a cylinder of radius equal to one unit of spatial momentum, i.e., those momenta for which $\Delta p a \leq 2\pi/L$. The effect of this cut on the fermion lattice momenta functions can be seen in Fig. 5.2. As expected, this cut clearly removes the artifacts for $|\boldsymbol{C}(p)|$ while the data for $C_4(p)$ remains unchanged.

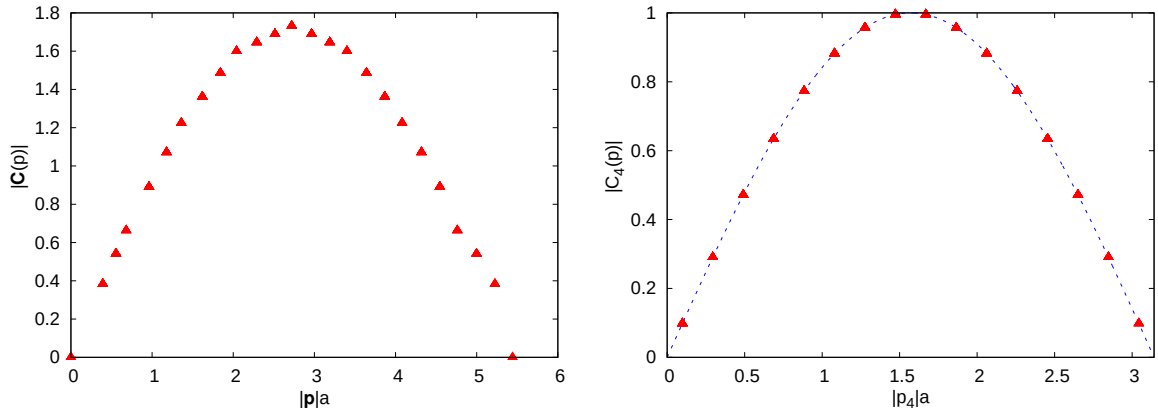

Figure 5.2: Cylinder cut lattice momenta from Wilson fermions.

As a further consistency check, we extract and plot the dressing functions $A_s^{(0)}(p)$, $A_t^{(0)}(p)$, $A_d^{(0)}(p)$ and $B_m^{(0)}(p)$ at tree-level, they are shown in Fig. 5.3. We see that the spatial and the temporal components are simply one for all momenta, as is manifest from the tree-level propagator (4.30). Unsurprisingly, the mixed component equals zero throughout the momentum range, up to a few artifacts in the deep infrared (IR) and ultraviolet (UV).[1] The plot for the massive component $B_m^{(0)}(p)$ is more interesting, it nicely shows the shape of the Wilson term $M(p)$ (3.40) to which it equals at tree-level. Therefore, everything is consistent and exactly as expected at tree-level and we are ready to continue investigating the quark propagator under the influence of the gluon fields.

1 IR/UV because small/large momenta are equivalent to long/short wave-lengths.

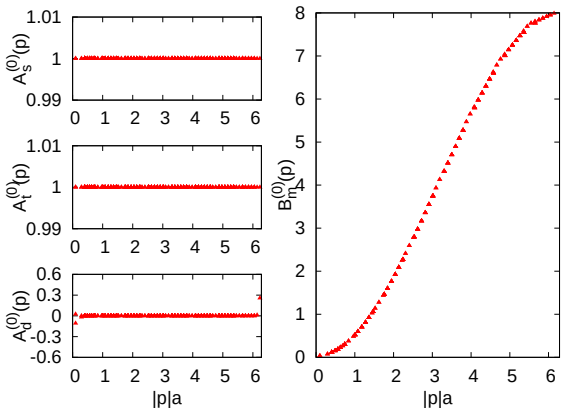

Figure 5.3: Dressing functions of the Wilson type quark propagator at tree-level.

Beyond tree-level

We now turn on the interactions with the gluons and study the derivation of the dressing functions from their tree-level forms. In Fig. 5.4 we show all four dressing functions, with the same parameters as before, calculated from the interacting propagator via Monte Carlo integration. The errors throughout this work are of Jackknife type [40, 41]. We see that the scalar function $A_s(p)$ shows non-trivial behavior when we couple gluons to the quark fields, although the derivation from one is relatively small, whereas $A_t(p)$ now lies at around 0.3 and therewith much lower than at tree-level. The Monte Carlo integration result for the mixed component $A_d(p)$ points towards a striking observation, the speculative term $i\gamma_i k_i \gamma_4 k_4 a^2 A_d(p)$ seems not to exist even beyond tree-level. $A_d(p)$ shows quite some noise in the IR and the UV, though we already saw artifacts in this region at tree-level.[1] The massive component exhibited a non-trivial shape already at tree-level, due to the Wilson term, and since we are interested in the derivation from tree-level, we divide $B_m(p)$ by its tree-level form. The result of this *tree-level correction* is depicted with open circles (blue) in Fig. 5.4. This correction nicely reveals the (non-perturbative) effect of mass generation in the IR. In the UV, on the contrary, the scalar function $B_m(p)$ goes asymptotically to one due to the asymptotic freedom of QCD.

In the following we investigate the discrete symmetries of the propagator in order to average over these to increase statistics. First, note that QCD and thus the propagator are invariant under parity transformations, $S(-p) = S(p)$, which is valid for all four-momenta components and thus results in a 2^4 degeneracy. Furthermore, we expect the lattice propagator to be subject to a residual rotational symmetry inherited from its continuum counterpart. The rotational symmetry, on a lattice with $L \neq T$, reduces to the cubic point group. This symmetry manifests

1 We considered this term without the factor i as well, it is zero, too.

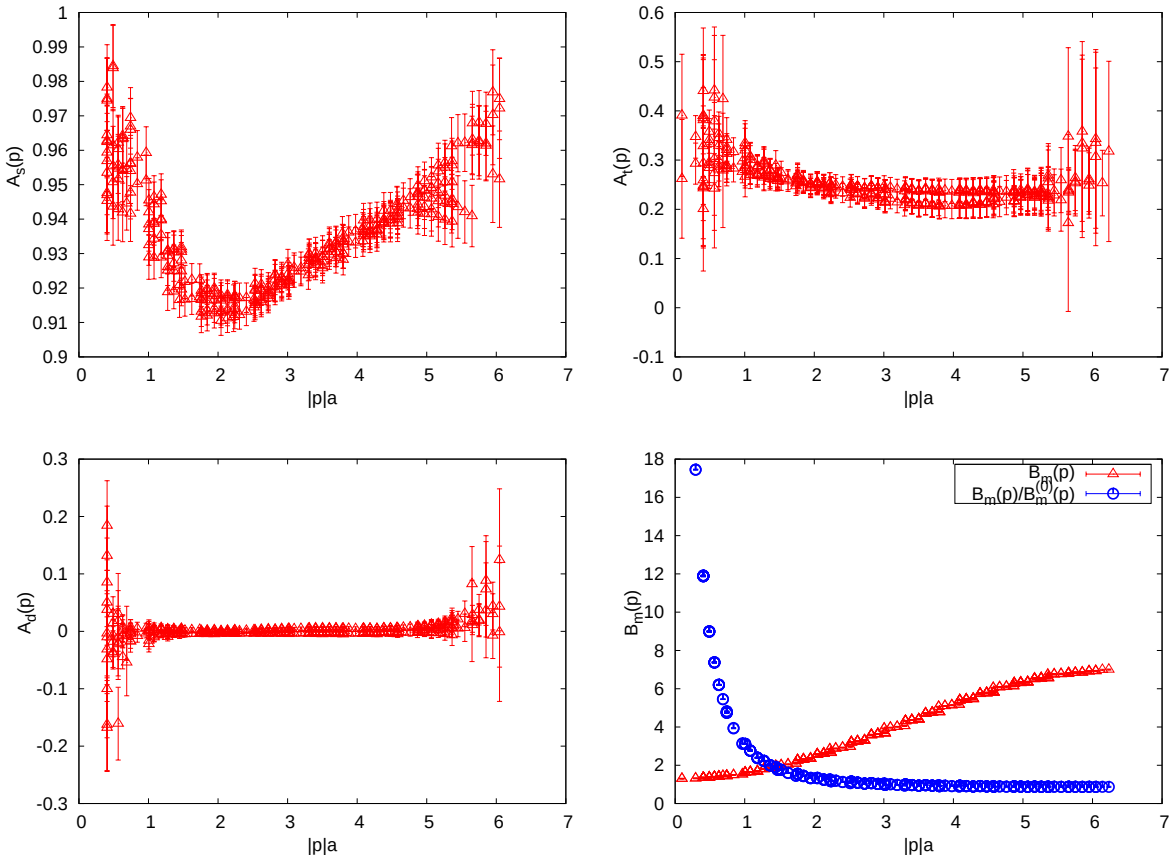

Figure 5.4: Dressing functions.

itself for the propagator as

$$S(p_1,p_2,p_3,p_4) = S(p_i,p_j,p_k,p_4), \tag{5.6}$$

where i,j,k is one arbitrary permutation of $1,2,3$ out of the 3! possibilities. Following these lines of argument, for a given discrete momentum $\overline{p}$, we average the dressing functions evaluated at all $2^4 \cdot 3! = 96$ momenta which are related through parity and cubic symmetries to $\overline{p}$. Fig. 5.5 clearly shows that this procedure reduces the errors from statistical uncertainty.

5.1.2 Staggered fermions

We proceed to the study of the quark propagator using staggered fermions, on the same set of gauge configurations ($\beta = 6.0$) with the same residual gauge fixing scheme. For staggered fermions one can tune the bare mass parameter itself while for Wilson fermions we had to set up the parameter κ and therewith determined the value of the bare mass. We set the mass parameter to $\hat{m} = 0.334$ and therewith we put on the same bare mass as we did for Wilson

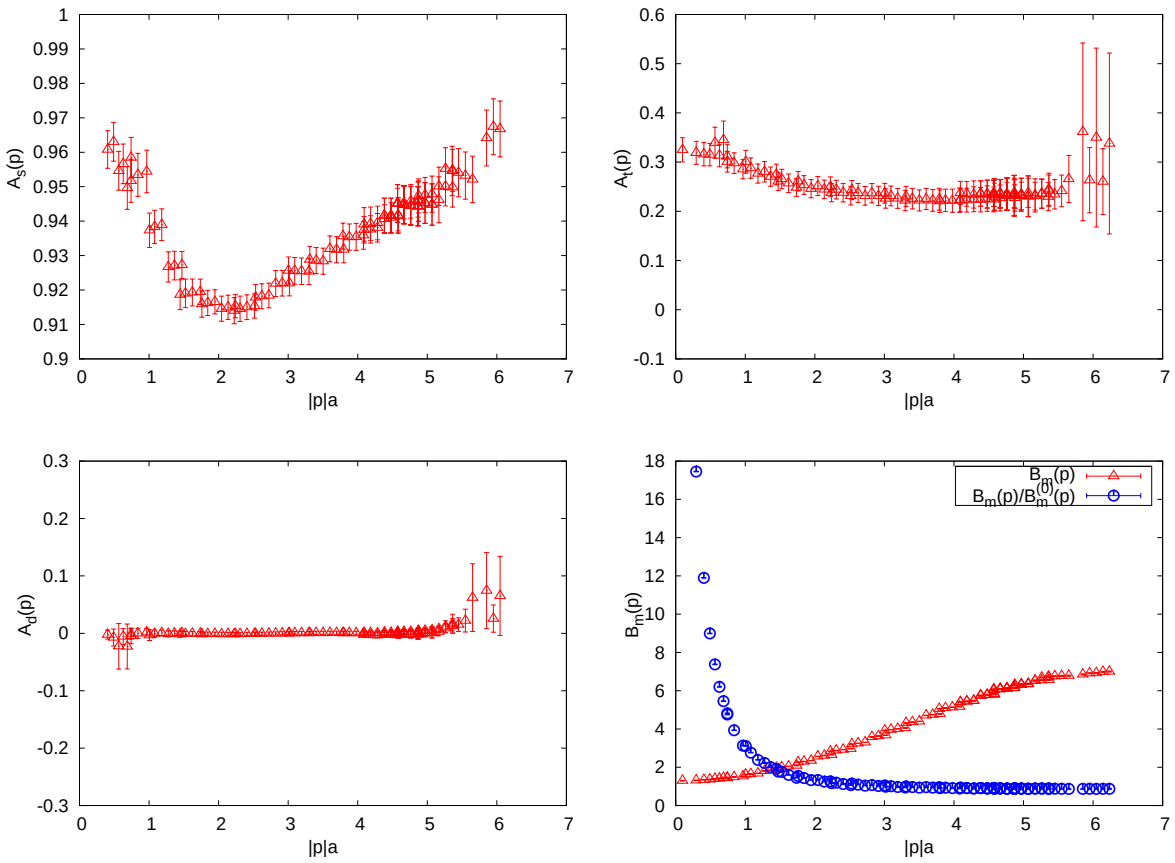

Figure 5.5: Dressing functions with cubic and parity symmetry averaging.

fermions. Nevertheless, comparison of these two different approaches to lattice fermions have to be considered with care: as we discussed in Chap. 3, the ansatz by Kogut and Susskind describes four degenerate tastes of fermions whereas the problem of fermion doubling for Wilson fermions is only resolved in the continuum limit. As we did for Wilson fermions, we first check our code and our analysis for consistency by considering the tree-level quark propagator. In Fig. 5.6a we show the fermion lattice momenta of the KS action extracted from tree-level. The difference to the case of Wilson fermions is obvious, the momenta range is smaller since staggered fermions take only momentum values within the inner half of the BZ which, by construction, circumvents the problem of fermion doubling. The fermion lattice momenta of staggered fermions are bijective, thus we may use the more adequate fermion lattice momenta $k_\mu a$ itself on the abscissa and plot the dressing functions against the latter. At tree-level, the spatial component of the dressing functions is one for staggered fermions as well, up to a few slight artifacts of the order 0.05 in the IR. The temporal component equals one perfectly

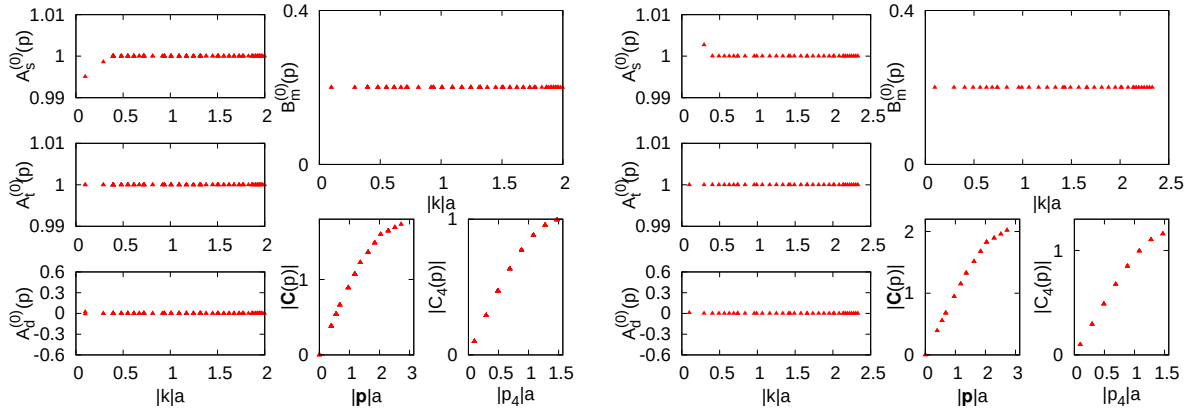

(a) KS action **(b)** Asqtad action

Figure 5.6: Staggered fermions: tree-level behavior.

while the mixed component is exactly zero. The massive component is constant at a value of *two-times* the bare mass $\hat{m}$ which stems from the fact that KS fermions have an effective lattice spacing of $2a$ as we encountered in the construction of staggered fermions in Sect. 3.3.2. In consequence, we will have to divide the massive component by $2a$ when adopting physical units.

Moving on to the study beyond tree-level, we first show the results of the scalar functions without any cut but with cubic and parity averaging, see Fig. 5.7. This may be compared to Fig. 5.8, which is exactly the same data but with an additional cylinder cut to show once more the effect of taking only those values of pa into account which lie close to the diagonal in momentum space. When we compare these data plots to the previous plots for Wilson fermions, we detect, first of all, that the spatial component $A_s(p)$ is greater than one for low to medium momenta and asymptotically goes to one in the UV. This seems to be much more reasonable since we expect the propagator to show non-trivial behavior in the low to medium momentum region and due to asymptotic freedom we expect it to merge into its tree-level form for large enough momenta. The function $A_t(p)$ lies even lower than for Wilson fermions and is almost constant. The massive function $B_m(p)$, for staggered fermions, has a very similar shape as $A_s(p)$. In comparison to Wilson fermions it increases about ten times less in the IR which seems to be more accurate. From staggered fermions, it is even more obvious that the speculative mixed component does not exist. The larger errors for $A_d(p)$ with cylinder cut opposed to without cylinder cut originate from the fact that we average over less cubic and parity symmetric data points when applying a cylinder cut. Since it is manifest that $A_d(p)$ vanishes, we will not further consider it in this work. Note that the sets of data points in Fig. 5.7 which lie (approximately) on parallel straight lines with positive slope for $A_s(p)$ and $B_m(p)$ belong to momenta with the same energy p_4. Hence the slope of these lines is coupled

to the time dependence of the scalar functions.

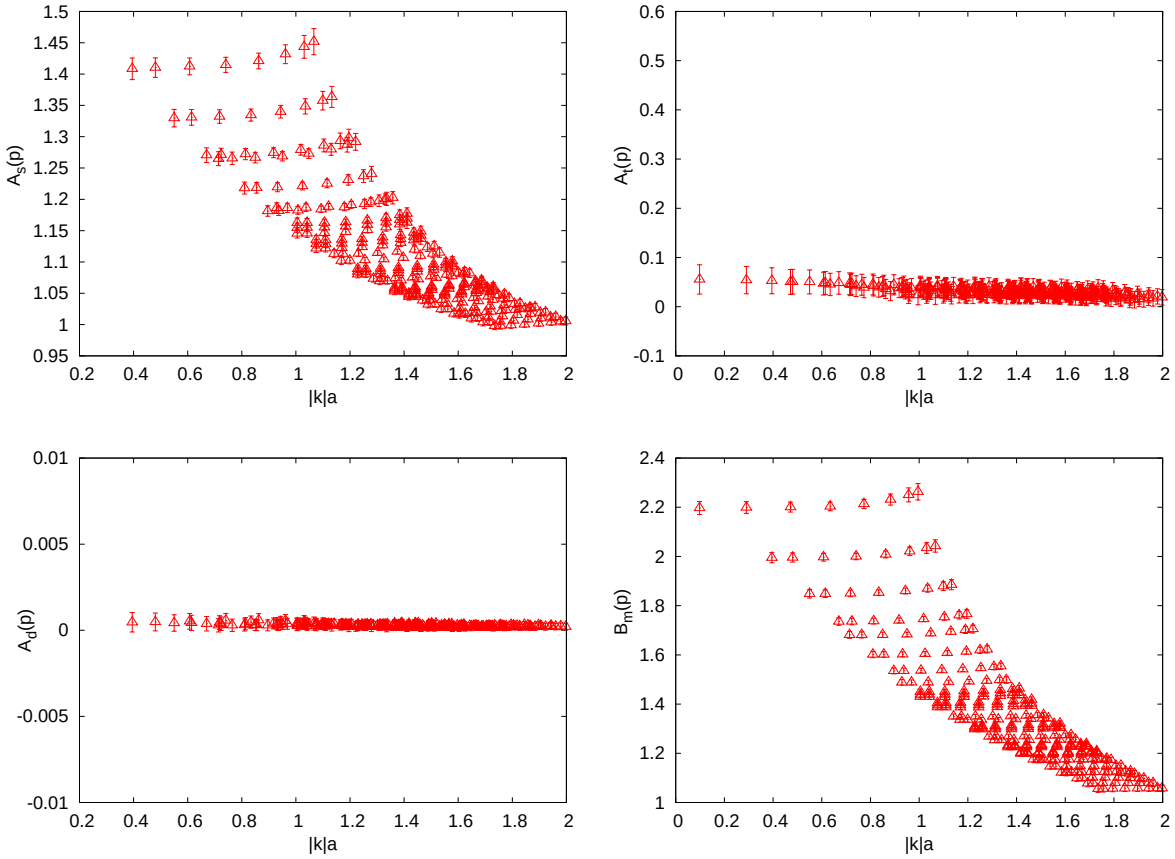

Figure 5.7: Dressing functions from staggered fermions with cubic and parity averaging.

5.1.3 Improved staggered fermions

So far, we have shown the dressing functions from the staggered quark propagator obtained from the KS action (3.49) which we now contrast to the dressing functions from the Asqtad action for which the Dirac operator is given in (3.58). At tree-level, see Fig. 5.6b, the only difference opposed to KS fermions is the fermion lattice momentum which, for the Asqtad action, is given by

$$\hat{k}_\mu \equiv \sin(\hat{q}_\mu)\left(1+\frac{1}{6}\sin^2(\hat{q}_\mu)\right). \tag{5.7}$$

We will use this momentum, extracted from tree-level, on the abscissa for plots of the scalar functions. Note that lattice fermion momentum from the Asqtad action stretches further into the UV: whereas the maximal momenta for the KS action is $2/a$, with the Asqtad action one reaches $7/6a$.

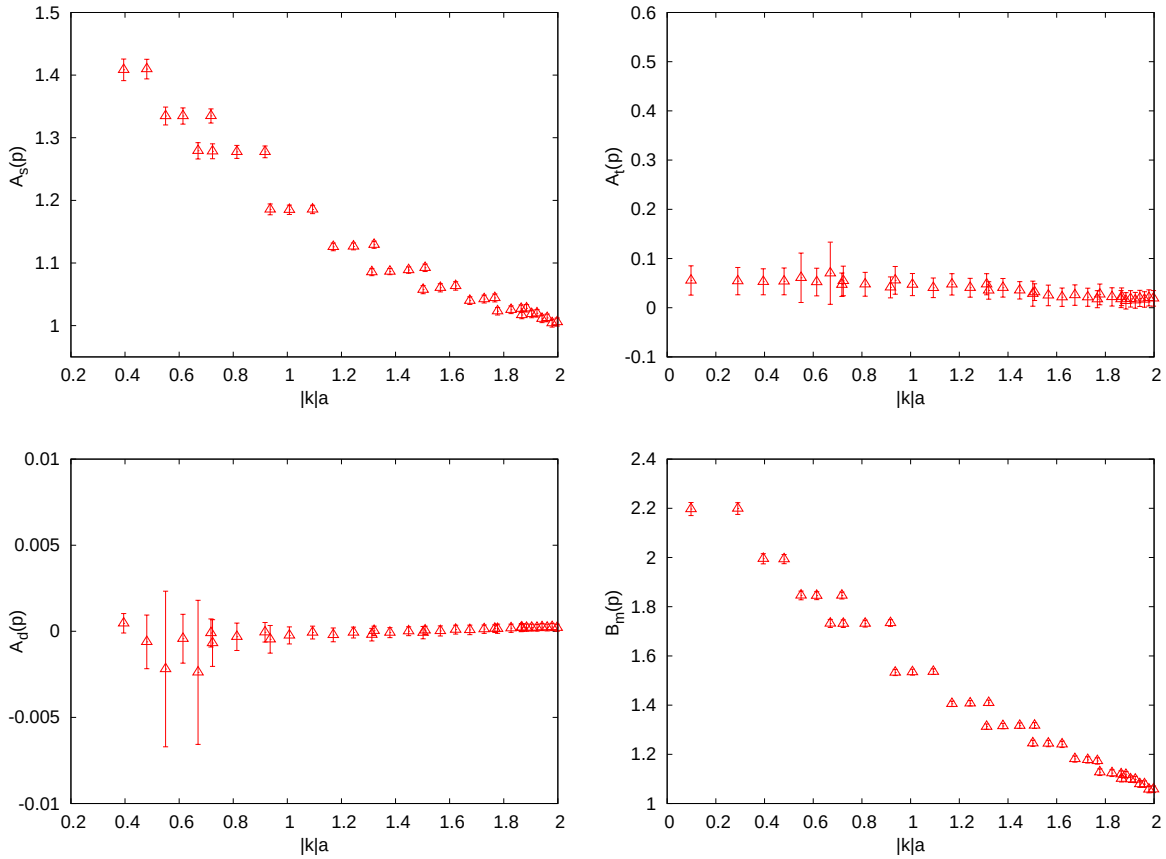

Figure 5.8: Cylinder cut dressing functions from staggered fermions with cubic and parity averaging.

A comparison of the scalar functions obtained from the KS action opposed to the Asqtad action is given in Fig. 5.9. For both actions we used the same set of gauge configurations ($\beta = 6.0$) and the same residual gauge fixing scheme (maximal trees), the bare mass was set to $ma = 0.1$, for both actions, which corresponds to 212 MeV. We observe that the function $A_s(p)$ from the Asqtad action lies slightly above the one from the KS action whereas for the massive component, $B_m(p)$, it is the other way round. It is remarkable that for both actions, the function $A_t(p)$ lies higher and has a significantly steeper slope as in Fig. 5.8 where the mass was chosen to be 707 MeV. The main advantages for the propagator when switching to the Asqtad action are improved rotational symmetry and better asymptotic behavior for the renormalization function as was found in [16] in Landau gauge. The improvement of rotational symmetry is not crucial to us since we average over cubic symmetry but we will benefit from the enhanced asymptotic behavior when studying renormalization.

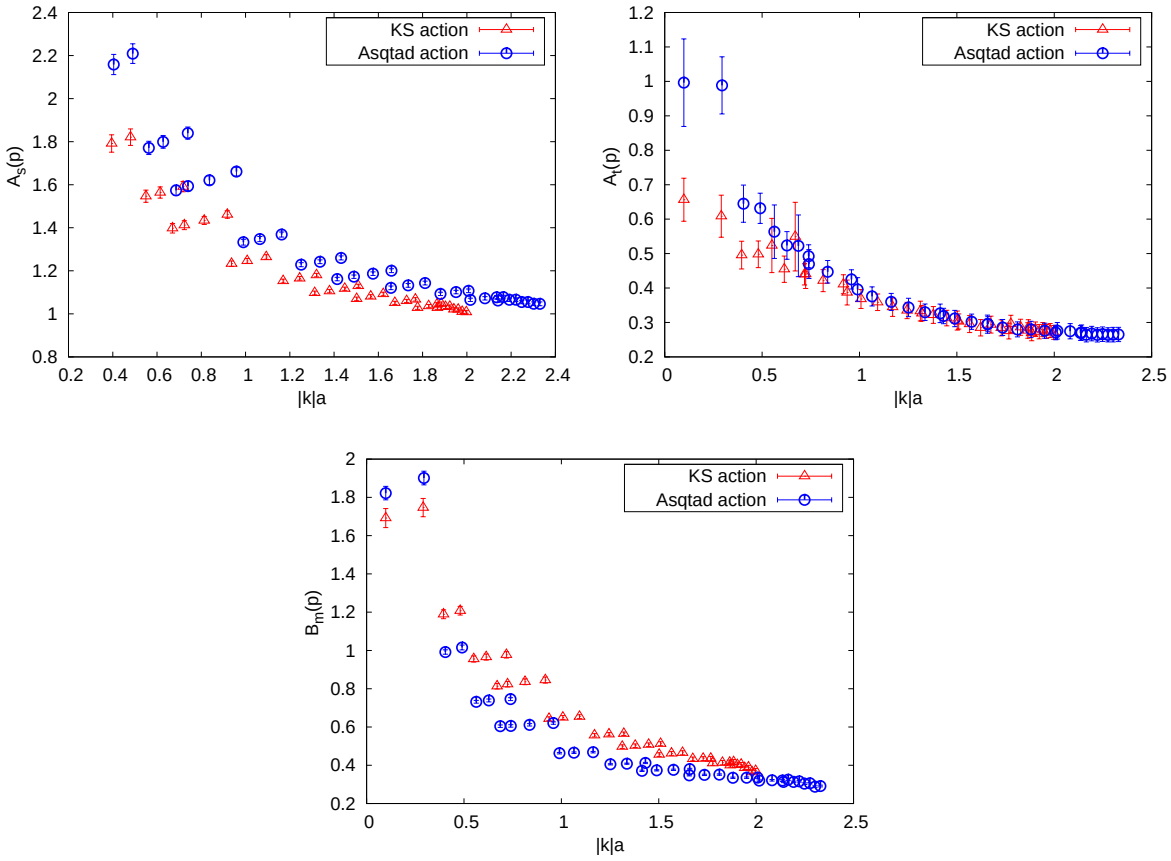

Figure 5.9: Comparison of the KS and the Asqtad action.

5.1.4 Gribov copies

We close this section by giving a few remarks on the dependence of the quark propagator on the arbitrariness in the gauge fixing process on the lattice. Remember that the gauge functional (4.14) has many local maxima called Gribov copies and therefore the requirement to fix the gauge in such a way that (4.14) gets maximized, is not unique. In order to study the effects of the Gribov copies on the propagator, we consider a set of SU(2) gauge configurations consisting of one hundred $12^3 \times 24$ samples, each generated with the inverse coupling being $\beta = 2.5$. We made 25 copies of each configuration and fixed all of them to the Coulomb gauge, then we compared the functional value (4.14) of all copies for each configuration and kept only the one which achieved the highest score. In another run we fixed each configuration to the Coulomb gauge and accepted it immediately, for comparison, since this is the way we ordinarily fix the gauge. We use the gauge group SU(2) for this analysis since it is much cheaper for SU(2) to fix the gauge in comparison to SU(3).

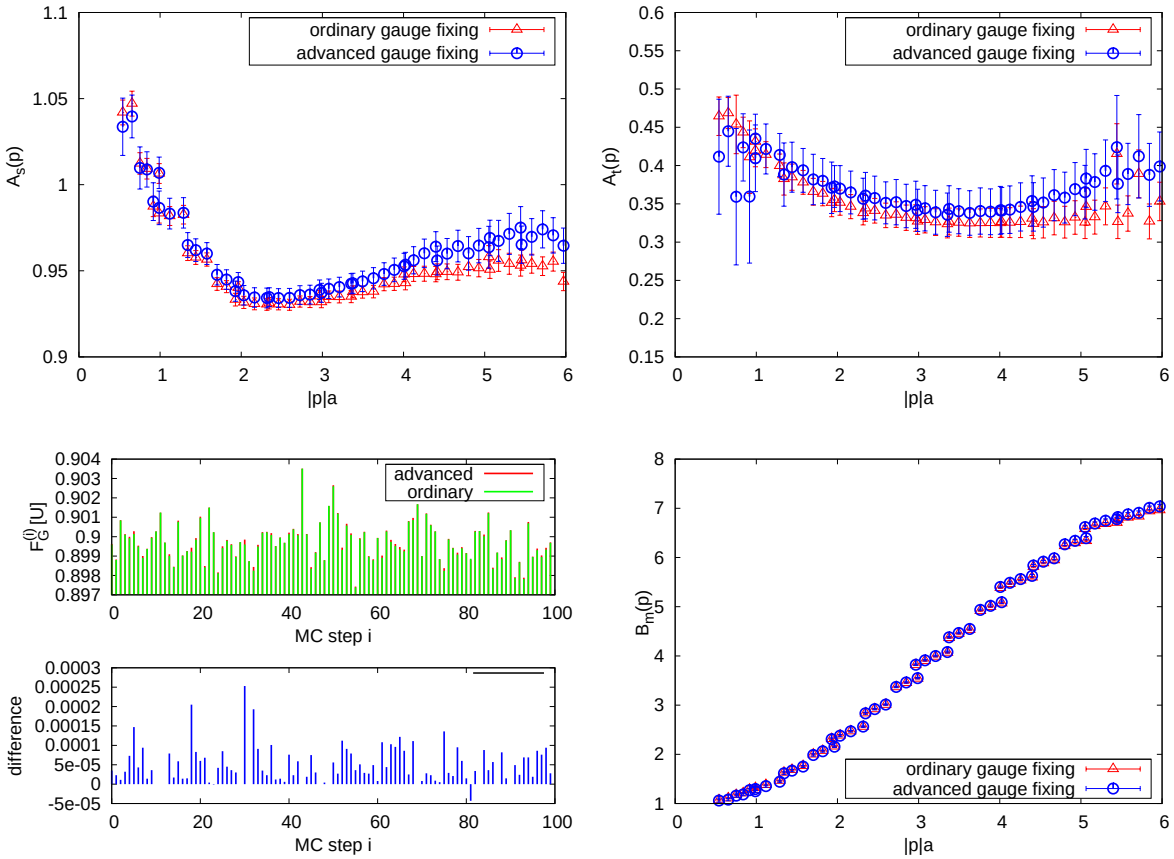

Figure 5.10: Gribov copy sensitivity of the dressing functions.

In Fig. 5.10 we compare the dressing functions of the Wilson type fermionic two-point function which we obtained from this "advanced gauge fixing scheme" to the ones which we encountered with our ordinary procedure. Moreover, a bar chart is shown in Fig. 5.10, there we compare the functional values we reached, for each step i of the Monte Carlo integration, with these two different gauge fixing procedures. As can be seen, for the massive component there is no difference at all, for the temporal part the two functions differ slightly within the error bars and for the spatial function there is a small discrepancy in the UV. The bottom line is that we do not expect our data to be seriously affected by Gribov copies.

5.2 Renormalization

The aim of this section is to check the renormalizability of the Coulomb gauge lattice quark propagator. The introduction of a space-time lattice to a quantum field theory serves as an UV

cutoff: the largest available momentum on the lattice is π/a. Thus the lattice is a regulator of the theory – it renders all path integrals finite – and the lattice quark propagator is the regularized propagator $S^{\mathrm{reg}}(a;p)$. The Landau gauge lattice quark propagator *is* renormalizable within the standard momentum subtraction scheme (MOM) [12] and hence is related to the renormalized quark propagator $S(\mu;p)$ through the quark wave-function renormalization constant Z_2 which depends on the cutoff a and on the renormalization point μ,

$$S^{\mathrm{reg}}(a;p) = Z_2(\mu;a)S(\mu;p). \tag{5.8}$$

In a renormalizable theory like QCD, when performing the continuum limit, $a \to 0$,[1] the renormalized quantities become independent of the cutoff a.

5.2.1 The dynamic propagator

To investigate renormalizability of the Coulomb gauge quark propagator, we make the following ansatz for the renormalized propagator

$$S(\mu;p) \equiv (i\gamma_i k_i a A_s(\mu;p) + i\gamma_4 k_4 a A_t(\mu;p) + B_m(\mu;p))^{-1} \tag{5.9a}$$

$$= Z(\mu;p)\,(i\gamma_i k_i a + i\gamma_4 k_4 a\alpha(p) + aM(p))^{-1}\,, \tag{5.9b}$$

thence

$$Z(\mu;p) = A_s^{-1}(\mu;p), \quad \alpha(p) = \frac{A_t(\mu;p)}{A_s(\mu;p)}, \quad M(p) = \frac{B_m(\mu;p)}{A_s(\mu;p)a}, \tag{5.10}$$

where $Z(\mu;p)$ and $\alpha(p)$ are dimensionless and $M(p)$ has dimension of mass. The MOM scheme has the renormalization point boundary conditions

$$Z(\mu;\mu) = 1, \quad \alpha(\mu) = c(\mu), \quad M(\mu) = m(\mu), \tag{5.11}$$

where in an asymptotically free theory like QCD, for a large enough renormalization point μ, $m(\mu)$ becomes the running quark mass and $c(\mu)$ is expected to go to one. The l.h.s. of (5.8) is independent of the renormalization point, thus the r.h.s. must be equal for different renormalization points μ and μ' and in consequence

$$\frac{Z_2(\mu;a)}{Z_2(\mu';a)} = \frac{Z(\mu';p)}{Z(\mu;p)}. \tag{5.12}$$

1 One actually lets $\beta \to \infty$ when performing the continuum limit.

Eq. (5.12) states that a change of renormalization point is just an overall rescaling of the renormalization function $Z(\mu; p)$, while $\alpha(p)$ and $M(p)$ must be renormalization point independent. In the following we will write $Z(p)$ instead of $Z(\mu; p)$ for ease of notation, nevertheless the renormalization point dependence of the renormalization function has to be understood. We

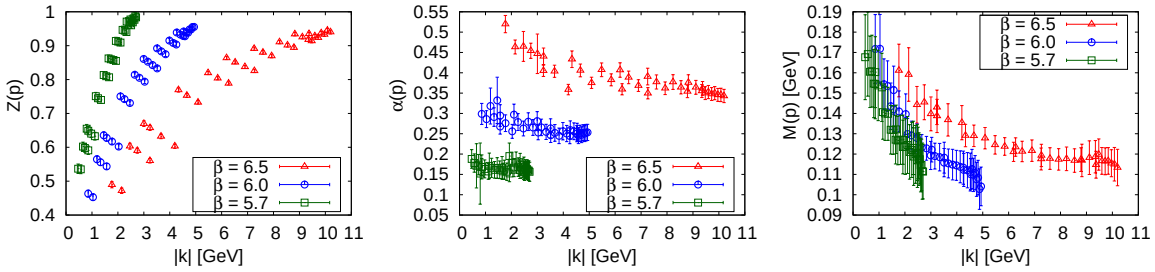

Figure 5.11: Scalar functions for different β using integrated maximal trees.

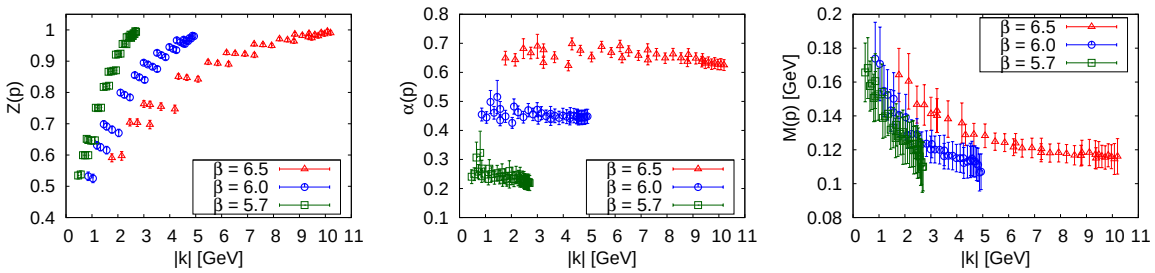

Figure 5.12: Scalar functions for different β using the integrated Polyakov gauge.

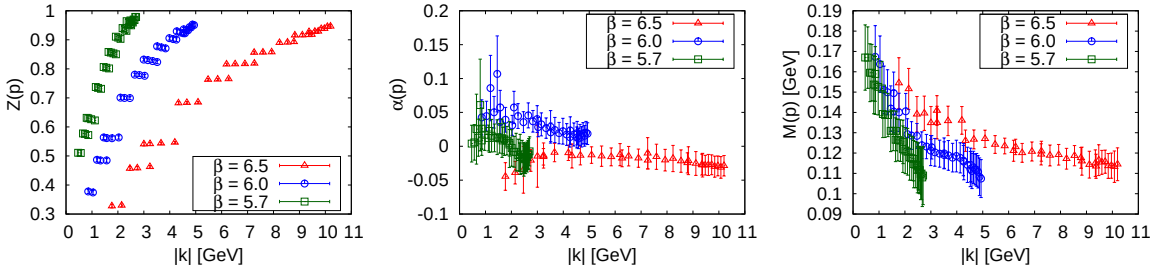

Figure 5.13: Scalar functions for different β without fixing the residual gauge.

compare the functions $Z(p)$, $\alpha(p)$ and $M(p)$ for different values of β, thus for different cutoffs a. We tuned each dimensionless bare mass so that the physical mass matches for all β, see Tab. 5.2. We make this comparison for the two different residual gauge fixing schemes since we expect the residual gauge fixing scheme to influence the time dependence of the propagator. In

β	a	ma	m
5.7	0.170 fm	0.1827	212 MeV
6.0	0.093 fm	0.1	212 MeV
6.5	0.045 fm	0.0484	212 MeV

Table 5.2: Masses for the various β.

Fig. 5.11 we show the three scalar functions with the residual gauge fixed by the integrated maximal tree scheme. In Fig. 5.12 the same functions are shown for the integrated Polyakov scheme and in Fig. 5.13 we show, in addition, the results of a run where we left the residual gauge unfixed.

When looking at the renormalization functions $Z(p)$ for the three different ways how we fixed the residual gauge freedom, it becomes apparent that the sets of data points which lie (approximately) on parallel straight lines have different slopes for the different residual gauges. Especially, in the case of no residual gauge fixing, the slope vanishes which indicates that time-dependence of the Coulomb gauge quark propagator vanishes when one leaves the residual gauge unfixed.

Without further investigating the functions $Z(p)$ and $M(p)$ we want to foreground the behavior of $\alpha(p)$: for the integrated maximal tree gauge Fig. 5.11 and for the integrated Polyakov gauge, for all β seems $\alpha(p)$ be either independent of the momentum or slightly fall down for higher momenta. Without having fixed the residual gauge freedom, see Fig. 5.13, $\alpha(p)$ is close to zero for $\beta = 5.7$ and $\beta = 6.0$ whereas for $\beta = 6.5$ it is even less than zero which gives rise to that $\alpha(p)$ indeed equals the average over the gauge group and thus is zero when leaving the gauge freedom with respect to time-dependent gauge transformations unfixed.

The very crucial observation of this section is that $\alpha(p)$ is clearly *not* independent of the renormalization point and therefore the Coulomb gauge quark propagator, as it stands, is not renormalizable. We continue by exploring the static Coulomb gauge quark propagator.

5.2.2 The static propagator

Remember that we decomposed the inverse propagator into a spatial and a temporal component and dressed it with scalar functions according to

$$S^{-1}(p) = i\gamma_i k_i a A_s(p) + i\gamma_4 k_4 a A_t(p) + B_m(p) \tag{5.13}$$

$$= i\gamma_i k_i a \frac{\mathcal{A}_s(p)}{\mathcal{D}^2(p)} + i\gamma_4 k_4 a \frac{\mathcal{A}_t(p)}{\mathcal{D}^2(p)} + \frac{\mathcal{B}_m(p)}{\mathcal{D}^2(p)} \tag{5.14}$$

or equivalently

$$S(p) = -i\gamma_i k_i a \mathcal{A}_s(p) - i\gamma_4 k_4 a \mathcal{A}_t(p) + \mathcal{B}_m(p) \tag{5.15}$$

$$= -i\gamma_i k_i a \frac{A_s(p)}{D^2(p)} - i\gamma_4 k_4 a \frac{A_t(p)}{D^2(p)} + \frac{B_m(p)}{D^2(p)}, \tag{5.16}$$

where we defined the denominators as

$$D^2(p) \equiv \boldsymbol{k}^2 a^2 A_s^2(p) + k_4^2 a^2 A_t^2(p) + B_m^2(p), \tag{5.17}$$

$$\mathcal{D}^2(p) \equiv \boldsymbol{k}^2 a^2 \mathcal{A}_s^2(p) + k_4^2 a^2 \mathcal{A}_t^2(p) + \mathcal{B}_m^2(p). \tag{5.18}$$

Now we integrate over the energy $\hat{k}_4$ to obtain the *static propagator*. In analogy to Chap. 3, we will write $\int_{-\pi}^{\pi} \frac{\mathrm{d}\hat{p}_4}{2\pi}$ to indicate integration over $\hat{k}_4$, despite that on the lattice, integration is actually performed by averaging over k_4, i.e., $1/T \sum_{\hat{k}_4}$ for all $\boldsymbol{k}a$. When we denote the static propagator with $\overline{S}(\boldsymbol{p})$, we obtain

$$\overline{S}^{-1}(\boldsymbol{p}) = i\gamma_i k_i a \int_{-\pi}^{\pi} \frac{\mathrm{d}\hat{p}_4}{2\pi} A_s(p) + \int_{-\pi}^{\pi} \frac{\mathrm{d}\hat{p}_4}{2\pi} B_m(p) \tag{5.19}$$

$$= i\gamma_i k_i a \int_{-\pi}^{\pi} \frac{\mathrm{d}\hat{p}_4}{2\pi} \frac{\mathcal{A}_s(p)}{\mathcal{D}^2(p)} + \int_{-\pi}^{\pi} \frac{\mathrm{d}\hat{p}_4}{2\pi} \frac{\mathcal{B}_m(p)}{\mathcal{D}^2(p)} \tag{5.20}$$

and

$$\overline{S}(\boldsymbol{p}) = -i\gamma_i k_i a \int_{-\pi}^{\pi} \frac{\mathrm{d}\hat{p}_4}{2\pi} \mathcal{A}_s(p) + \int_{-\pi}^{\pi} \frac{\mathrm{d}\hat{p}_4}{2\pi} \mathcal{B}_m(p) \tag{5.21}$$

$$= -i\gamma_i k_i a \int_{-\pi}^{\pi} \frac{\mathrm{d}\hat{p}_4}{2\pi} \frac{A_s(p)}{D^2(p)} + \int_{-\pi}^{\pi} \frac{\mathrm{d}\hat{p}_4}{2\pi} \frac{B_m(p)}{D^2(p)}. \tag{5.22}$$

Note that the temporal function $A_t(p)$ is even and thus the product $\hat{k}_4 A_t(p)$, integrated from $-\pi$ to π, vanishes.

From the static propagator we extract the static renormalization function $Z(\boldsymbol{p})$ and the static mass function $M(\boldsymbol{p})$,

$$Z(\boldsymbol{p}) = \left(\int_{-\pi}^{\pi} \frac{\mathrm{d}\hat{p}_4}{2\pi} A_s(p) \right)^{-1}, \quad M(\boldsymbol{p}) = \frac{\int_{-\pi}^{\pi} \frac{\mathrm{d}\hat{p}_4}{2\pi} B_m(p)}{\int_{-\pi}^{\pi} \frac{\mathrm{d}\hat{p}_4}{2\pi} A_s(p)}. \tag{5.23}$$

Details of the extraction of static functions $Z(\boldsymbol{p})$ and $M(\boldsymbol{p})$ from the static propagator are given in Appendix A.6.

The outcome for the static functions $Z(\boldsymbol{p})$ and $M(\boldsymbol{p})$ for different β and different residual gauge fixing procedures are given in Fig. 5.14 – Fig. 5.16. It has to be pointed out that a cylinder cut is not necessary for the data extracted from the static propagator. We performed a cone cut, though, on the data for $Z(\boldsymbol{p})$: the cone cut eliminates points in the IR which are

β	a	μ	$1/Z_2(a;\mu)$		
			Integrated maximal tree gauge	Integrated Polyakov gauge	Residual gauge unfixed
5.7	0.170 fm	-	0.65	0.75	0.615
6.0	0.093 fm	-	0.825	0.886	0.805
6.5	0.045 fm	8 GeV	1.062	1.018	1.086

Table 5.3: Renormalization constants $Z_2(a;\mu)$.

not reliable on lattices with small physical volumes [48]. The function $M(\boldsymbol{p})$ is uncut. As the renormalization point of $Z(\boldsymbol{p})$ we choose a momentum value of 8 GeV, for all three residual gauge fixing schemes, which determines the renormalization constant $Z_2(a;\mu)$ for $\beta = 6.5$. For β equal to 6.0 and 5.7 we precede the other way round; we choose a renormalization constant $Z_2(a;\mu)$ in such a way that $Z(a;p)$ transitions as smoothly as possible from one β to the next. The best result obtained in this way is for the integrated Polyakov gauge, where the different $Z(a;p)$ merge into a single smooth curve. The renormalization constants $Z_2(a;\mu)$ for all curves are summarized in Tab. 5.3.

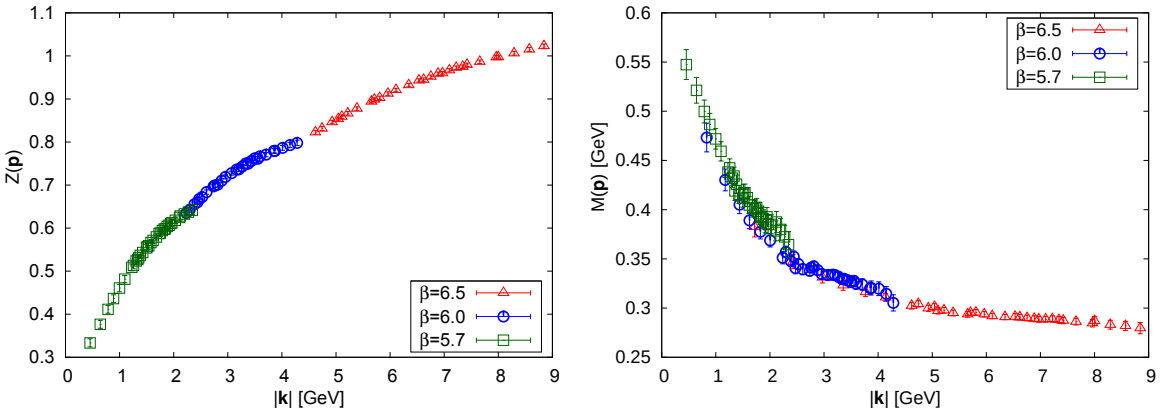

Figure 5.14: Functions from the static propagator, residual gauge freedom fixed using integrated maximal trees.

We find that the mass function $M(\boldsymbol{p})$ of the Coulomb gauge lattice quark propagator is renormalization point independent. $M(\boldsymbol{p})$ nicely shows a dynamical mass generation in the IR and the slope increases strongly at around 3.5 GeV. To summarize, we find that the static Coulomb gauge lattice quark propagator is multiplicative renormalizable whereas the dynamic propagator is not.

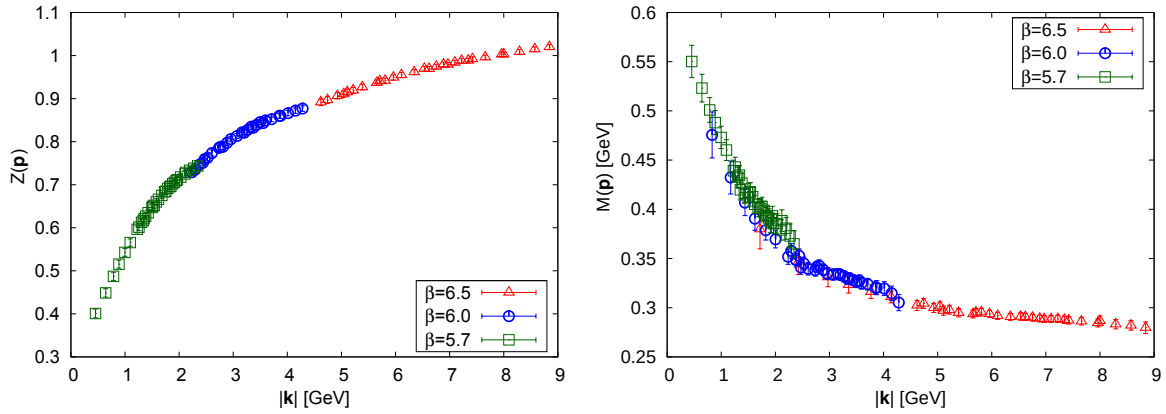

Figure 5.15: Functions from the static propagator, residual gauge freedom fixed using the integrated Polyakov gauge.

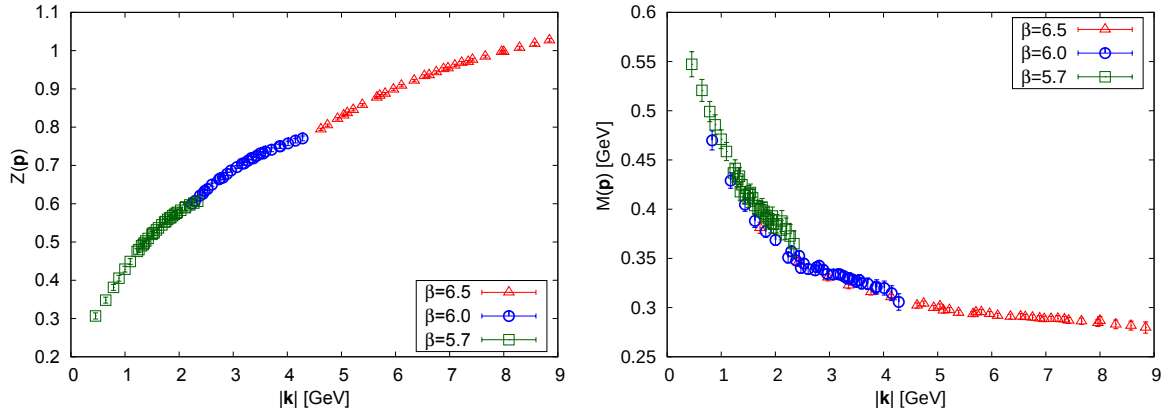

Figure 5.16: Functions from the static propagator, residual gauge freedom not fixed.

5.3 Unquenching

We downloaded two sets of gauge field configurations provided by the MILC Collaboration [34] via the Gauge Connection.[1] Both sets are of equal size and lattice spacing. The only difference between them is that one includes $N_f = 2 + 1$ flavors of dynamical quarks: two degenerate light quarks of mass 11 MeV and a strange quark of mass 79 MeV [49]. These configurations were generated using a tadpole and Symanzik improved gauge action and, to incorporate the dynamical fermions, the Asqtad action, for details see [34]. The parameters of

1 http://qcd.nersc.gov/

both configurations are summarized in Tab. 5.4. We gauged both configurations to the Coulomb gauge with a precision of $\varepsilon = 10^{-6}$ and left the residual gauge unfixed.

N_f	N_{config}	$L^3 \times T$	a	$m_{u/d}\, a$	$m_{u/d}$	$m_s\, a$	m_s	La	Ta
quenched	79	$20^3 \times 64$	0.125 fm	∞	∞	∞	∞	2.5 fm	8 fm
2+1	88	$20^3 \times 64$	0.125 fm	0.007	11 MeV	0.05	79 MeV	2.5 fm	8 fm

Table 5.4: Parameters of the configurations by the MILC Collaboration.

5.3.1 Finite volume effects

Before we begin studying the effects due to the sea quarks, we use the quenched set from the MILC Collaboration to investigate sensitivity of the propagator on the finite size of the lattice. We want to compare the mass function obtained from the quenched MILC configurations with the mass function from one of our $16^3 \times 32$ lattices. To this effect, we take the set of gauge configurations with $\beta = 6.0$ and tune the mass parameters on both sets so that they match within physical units. In Tab. 5.5, we list details of the physical volumes of the two lattices under investigation and the bare mass parameters.

$L^3 \times T$	a	La	Ta	ma	m
$20^3 \times 64$	0.125 fm	2.5 fm	8.0 fm	0.04	63 MeV
$16^3 \times 32$	0.093 fm	1.49 fm	2.98 fm	0.0298	63 MeV

Table 5.5: Details of the analysis of finite volume effects.

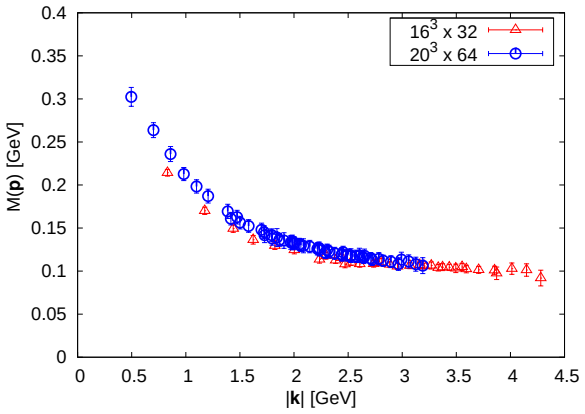

Figure 5.17: Mass function $M(\boldsymbol{p})$ from different lattices.

We observe, see Fig. 5.17, that the momentum range of these two lattices overlaps in the range from about 0.8 GeV to approximately 3.2 GeV. Whereas the mass functions differ only slightly in the lower region of the overlapping range. Seen as a whole, the two functions nicely

merge into a single smooth curve. Thus, we are lead to conclude that finite volume effects, as well as finite lattice spacing effects, are of negligible influence. Additionally, the agreement of the two mass functions shows that fixing the Coulomb gauge with a precision of $\varepsilon = 10^{-6}$, which is the best we could achieve for the MILC configurations, suffices.

5.3.2 Effects of dynamical quarks

We computed the static Coulomb gauge quark propagator on both gauge field configuration sets form the MILC Collaboration with the same five bare quark masses, ranging from 14–95 MeV. A list of all bare masses we used, in lattice units and in physical units, is given in Tab. 5.6.

ma	0.06	0.04	0.02	0.01	0.0087
m [MeV]	95	63	32	16	14

Table 5.6: Various bare masses for the analysis of unquenching.

The mass function $M(\boldsymbol{p})$ from both, the quenched approximation and full QCD, for the various bare masses is shown in Fig. 5.18 and the corresponding renormalization function $Z(\boldsymbol{p})$ is given in Fig. 5.19. Furthermore, we show a direct comparison of the two scalar functions from the

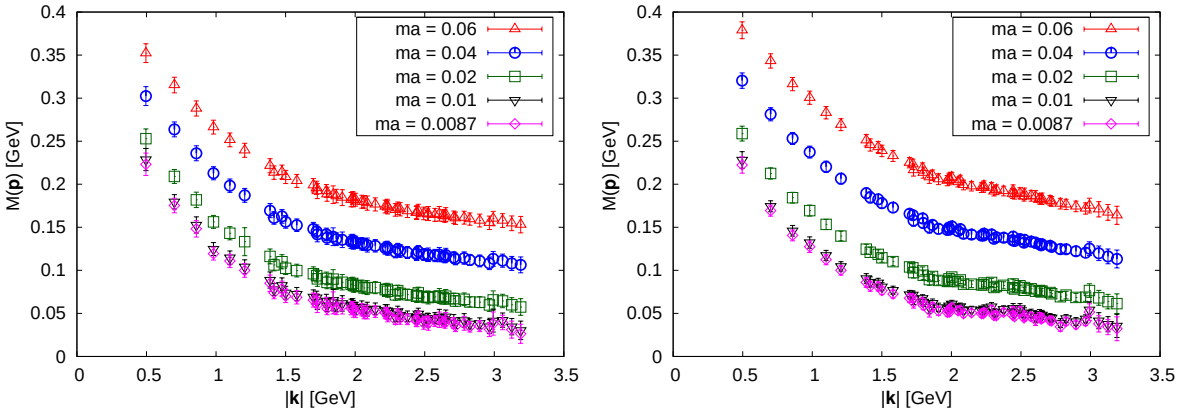

(a) Quenched approximation. **(b)** Full QCD.

Figure 5.18: Mass function $M(\boldsymbol{p})$ for various masses ma.

quenched sets versus the unquenched sets in Fig. 5.20. There, we chose the bare mass for the quenched configurations as $ma = 0.01$ and for the configurations with dynamical quarks as $ma = 0.0087$, so that the physical running mass[1] matches, approximately. As we will reveal

1 The running mass is obtained for very large momenta, when, due to asymptotic freedom, the coupling strength goes to zero. The running quark mass, or also called current quark mass – or dressed mass – is the mass which is obtained in experiments.

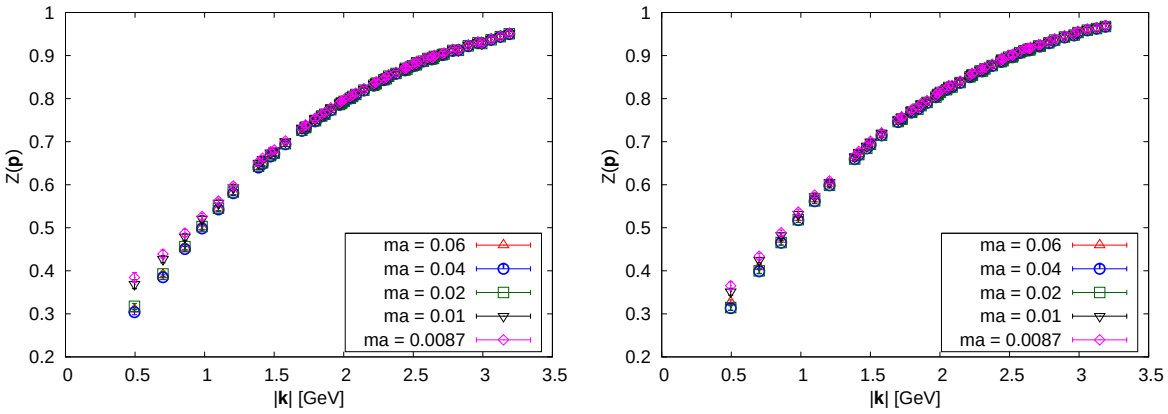

(a) Quenched approximation. **(b)** Full QCD.

Figure 5.19: Renormalization function $Z(\boldsymbol{p})$ for various bare masses ma.

below, in full QCD, a bare mass results in a larger running mass, opposed to the same bare mass within the quenched approximation. It should be stressed again that the only difference between these two sets of configurations is that one has $2 + 1$ flavors of dynamical quarks and the other has not. The first observation we make is that the renormalization function

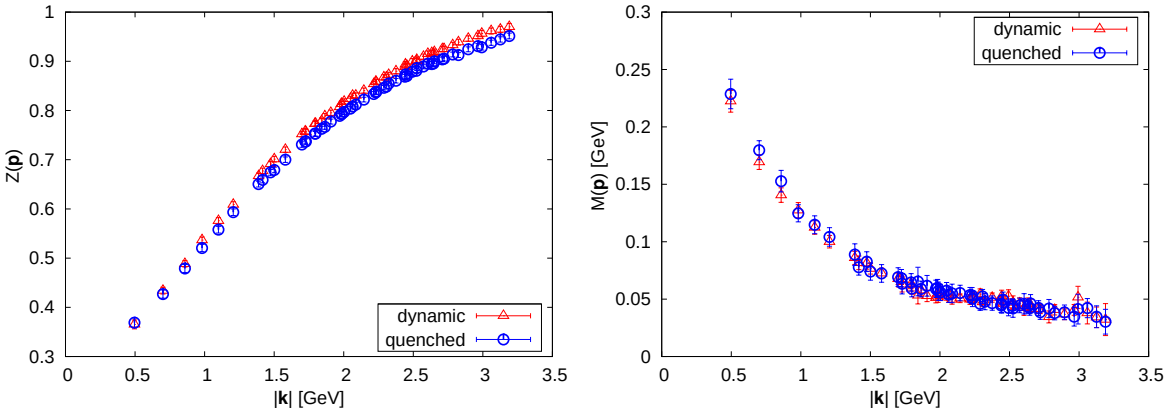

(a) Quenched approximation. **(b)** Full QCD.

Figure 5.20: The effects of unquenching.

agrees well for all bare masses and has a very similar shape for quenched and unquenched configurations. Comparing the mass function from full QCD to the one from the quenched approximation, we cannot detect a significant difference with the naked eye. It seems, that more mass is dynamically generated when sea quarks are available, this will be further investigated below.

5.3.3 The chiral limit

We want to extrapolate the mass function towards zero bare mass, this limit is usually referred to as *chiral limit*, since the Dirac operator becomes chirally symmetric for vanishing bare quark mass, for details see Appendix A.3. We use a simple linear extrapolation: for all $\boldsymbol{p}$, we fit the data of the mass function, which we assume to be linear in m, with the ansatz

$$M_{\boldsymbol{p}}(m) = \alpha m + \beta. \tag{5.24}$$

The extrapolation point $M_{\boldsymbol{p}}(m=0) = \beta$ corresponds to the chiral limit for the corresponding value of $\boldsymbol{p}$. See Fig. 5.22a, for the chiral limit of $M(\boldsymbol{p})$ in the quenched approximation and for full QCD. The chiral extrapolation of the mass function stays clearly above zero for the momentum scale we consider. Although the shape of the function gives rise to an asymptotic behavior towards zero.

5.3.4 Fitting the mass function

Our goal is to extract the running mass and the constituent quark mass,[1] as a function of the bare mass, from the quark propagator's mass function. Consider following model function,

$$M(\boldsymbol{p},m) = \frac{m_\chi(m)}{1 + b\frac{\boldsymbol{k}^2}{\Lambda^2}\log\left(\mathrm{e} + \frac{\boldsymbol{k}^2}{\Lambda^2}\right)^{-\gamma}} + \frac{m_r(m)}{\log\left(\mathrm{e} + \frac{\boldsymbol{k}^2}{\Lambda^2}\right)^{\gamma}}, \tag{5.25}$$

where $m_r(m)$ is the running mass, which obviously depends on the bare mass m. The constituent quark mass can be found by considering the mass function for zero momentum,

$$M(0,m) = m_\chi(m) + m_r(m). \tag{5.26}$$

We fitted the model function $M(\boldsymbol{p},m)$ to our data, whereby $m_r(0) = 0$ was set as a constraint. The result thereof is given in Fig. 5.21, for the quenched and the unquenched propagator. In Fig. 5.22b, we compare the chiral limit for quenched and unquenched configurations including the fitting function. The corresponding fit parameters are given in Tab. 5.7 and Tab. 5.8. The scale Λ of the fit coincides well with the scale Λ_{QCD}, as expected. What immediately attracts the attention of the observer when looking at the fits for the mass function, with and without dynamical quarks, Fig. 5.21, is, that the constituent quark masses, for the various bare masses, tend to be closer together in full QCD than in the quenched approximation.

1 The constituent quark mass is one third of the nucleons mass, i.e., the mass that a quark adopts within the nucleon.

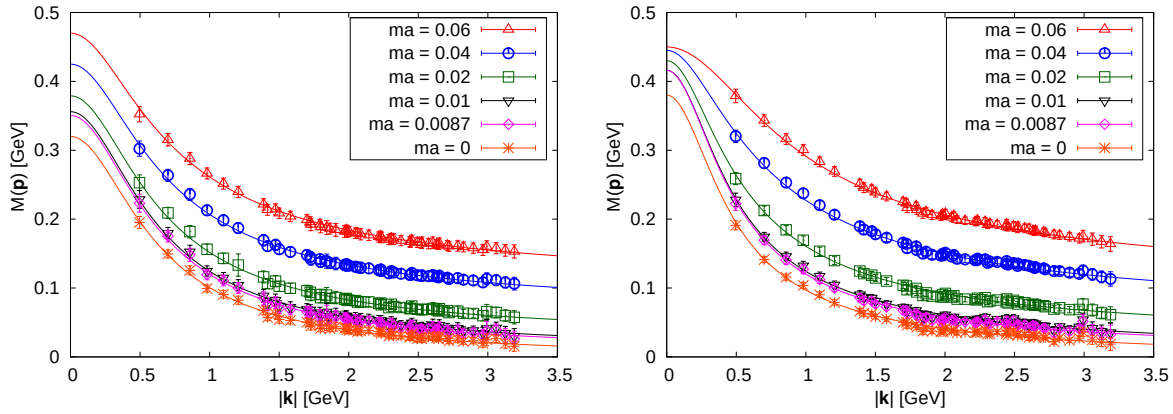

(a) Quenched approximation. **(b)** Full QCD.

Figure 5.21: Modelling the mass function.

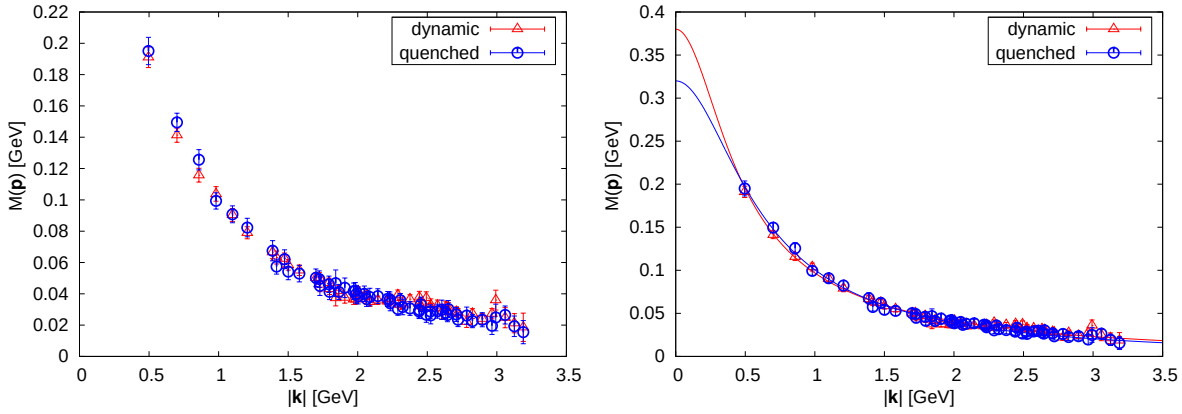

(a) **(b)**

Figure 5.22: Quenched approximation vs. full QCD: chiral limit of $M(\boldsymbol{p})$.

This can be explored in more detail when considering Fig. 5.23a, where we plotted the constituent quark mass as a function of the bare mass: while the constituent quark mass from the quenched approximation increases almost linearly with the bare quark mass, the constituent quark mass in full QCD indicates an asymptotic behavior. The latter states, that in full QCD, we are lead to assume that above a certain bare mass, or dressed mass since they are related linearly according to Fig. 5.23b, the constituent quark mass will be mainly due to the dressed mass and dynamical mass generation will play a minor role. This can be underlined with Fig. 5.23c: m_χ, being the difference between the constituent quark mass and the running mass, is a measure of how much mass is dynamically generated. As Fig. 5.23c shows, for our heaviest valence quark, dynamical mass generation vanishes. This is also in accordance with nature,

	b	Λ [GeV]	γ
dynamical	1.57(1)	0.59(1)	0.80(1)
quenched	0.98(1)	0.595(10)	0.445(10)

Table 5.7: Fit parameters b, Λ, γ.

ma	0.06	0.04	0.02	0.01	0.0087	0
m_χ [GeV] (dynamical)	0.38(2)	0.38(1)	0.37(1)	0.30(1)	0.155(10)	0.00(5)
m_χ [GeV] (quenched)	0.32(2)	0.33(1)	0.33(1)	0.31(1)	0.27(1)	0.23(1)
m_r [GeV] (dynamical)	0 (constr.)	0.036(1)	0.046(1)	0.13(1)	0.29(1)	0.45(1)
m_r [GeV] (quenched)	0 (constr.)	0.0205(10)	0.026(1)	0.069(1)	0.155(15)	0.24(1)

Table 5.8: Fit parameters $m_\chi(m)$ and $m_r(m)$.

the mass of charmonium, e.g., is not much larger than two times the mass of the charm quark. Moreover, from Fig. 5.23c, we can obtain that dynamical mass generation, as a function of the physical dressed mass, is similar for quenched and unquenched QCD.

It is also remarkable, that the constituent quark mass is indeed *approximately* one third of the mass of the proton. On third of the mass of the proton would be $\approx 310\,\text{MeV}$, thus our values of 320 MeV (quenched) and 380 MeV (unquenched) are slightly above. It has to be pointed out, though, that our light sea quarks are not as light as the physical up and down quarks. That might partly account for the difference. Another uncertainty stems from systematic errors like finite cutoff effects and the lack of a sufficient amount of data points in the deep IR.

5.3.5 Comparison to Landau gauge

In [17], a related study of unquenching effects of the lattice quark propagator was performed in Landau gauge. There, almost the same gauge field configurations from the MILC Collaboration were used. The only difference in their configurations was, that the light sea quarks were slightly heavier, $ma = 0.01$. Furthermore, the same Asqtad staggered fermions were used. Thus, this should serve as an appropriate environment for comparison.

One advantage of Landau gauge is, that since one does not integrate out the energy, one obtains more data points in the deep IR. In general, the authors of [17] found a slightly higher mass generation in the quenched case as well as unquenched in comparison to our study. Moreover, they found in particular, that mass generation is slightly screened by dynamical fermions which we cannot confirm on the basis of our work in Coulomb gauge. The investigation of this discrepancy could be the basis for further studies.

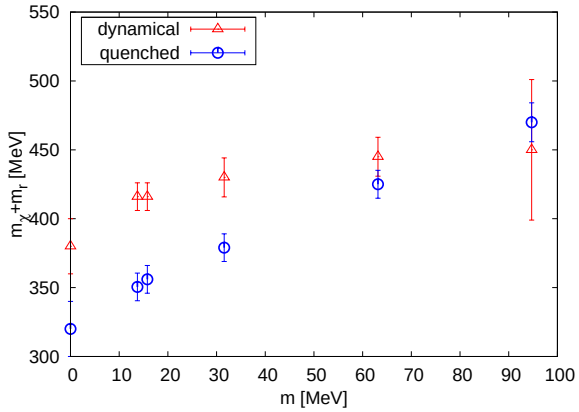

(a) Constituent quark mass as a function of the bare mass.

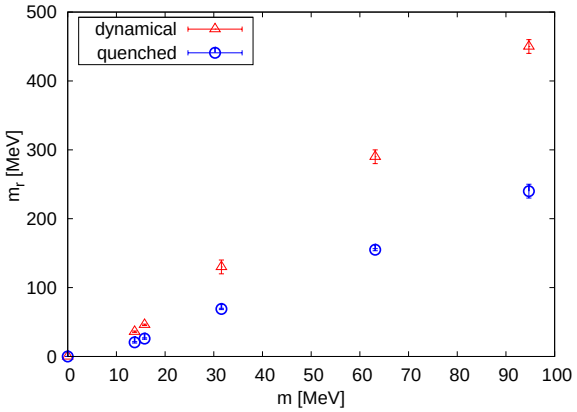

(b) Running quark mass as a function of the bare mass.

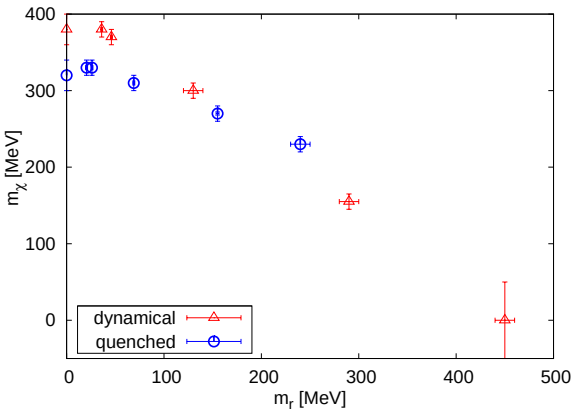

(c) Dynamical mass generation as a function of the dressed mass m_r.

Figure 5.23: Constituent and running masses as functions of the bare mass.

Chapter 6

Conclusion

In this work, we decomposed the Coulomb gauge quark propagator into a spatial, a temporal and a massive part, as well as into a speculative mixed part. We showed how the effects of the interaction of the propagator with the gluon fields can be described by scalar momentum-dependent functions, attached to the several parts of the propagator. The extraction of these functions from the lattice quark propagator for Wilson fermions and Kogut–Susskind fermions have been derived.

We found that the speculative mixed component is non-existent. For the remaining three scalar functions, staggered fermions have shown to be superior to Wilson fermions in describing dynamics beyond tree-level. The Asqtad action was found to bring further improvement thereon. We analyzed the ambiguities in the gauge fixing process due to Gribov copies and found that their influence on the quark propagator is small. Two different schemes of residual gauge fixing were compared and it was detected that their impact is only reflected in the time-dependence of the propagator. Moreover, the static propagator is insensitive to which residual gauge is chosen, even if the residual gauge is left unfixed. The renormalizability of the quark propagator was tested and was found to be given only for the static propagator. The influence of the finite lattice volume and the finite lattice spacing on the propagator was investigated and found to be small.

We explored the quark propagator on gauge field configurations containing 2+1 flavors of dynamical quarks. It was found that the quark propagator is not strongly altered by sea quark effects. We extrapolated the mass function to the chiral limit and investigated the effect of dynamical mass generation and its dependence on sea quarks. It was found that in full QCD, dynamical mass generation ceases with increasing running mass.

The natural continuation of the study of the Coulomb gauge lattice quark propagator is to

extend the computation of the mass function towards larger lattices, smaller masses of the sea quarks and various cutoff scales. Larger lattices will enable one, to further advance into the deep IR and thereby observe the flattening of the mass function. It could also be interesting to study the Coulomb gauge lattice quark propagator with finite temperature and finite chemical potential.

Bibliography

[1] Fritzsch, Gell-Mann, "Current algebra- quarks and what else?," *16. International Conference High energy physics, Cern* (1972) .
v, 1

[2] Fritzsch, Gell-Mann, Leutwyler, "Advantages of the color octet gluon picture," *Physics Letters B* **47** (1973) .
v, 1

[3] K. G. Wilson, "Confinement of quarks," *Phys. Rev. D* **10** (1974) 2445.
v, 1

[4] V. Gribov, "Quantization of non-abelian gauge theories," *Nucl. Phys. B* **139** (1978) 1.
vi, 2, 35

[5] D. Zwanziger, "Lattice Coulomb hamiltonian and static color-Coulomb field ," *Nucl. Phys. B* **485** (1997) .
vi, 2

[6] D. Zwanziger, "Renormalization in the Coulomb gauge and order parameter for confinement in QCD," *Nucl. Phys. B* **518** (1998) .
vi, 2

[7] P. Watson and H. Reinhardt, "The Coulomb gauge ghost Dyson-Schwinger equation," arXiv:1007.2583 [hep-th].
vi, 2

[8] D. R. Campagnari, H. Reinhardt, and A. Weber, "Perturbation theory in the Hamiltonian approach to Yang- Mills theory in Coulomb gauge," *Phys. Rev.* **D80** (2009) 025005, arXiv:0904.3490 [hep-th].
vi, 2

[9] P. Watson and H. Reinhardt, "Perturbation Theory of Coulomb Gauge Yang-Mills Theory Within the First Order Formalism," *Phys. Rev.* **D76** (2007) 125016, arXiv:0709.0140 [hep-th].

vi, 2

[10] M. Quandt, H. Reinhardt, and G. Burgio, "The role of center vortices in Gribov's confinement scenario," *Phys. Rev.* **D81** (2010) 065016, arXiv:1001.3699 [hep-lat].
vi, 2

[11] G. Burgio, M. Quandt, and H. Reinhardt, "Coulomb gauge gluon propagator and the Gribov formula," *Phys. Rev. Lett.* **102** (2009) 032002, arXiv:0807.3291 [hep-lat].
vi, 2, 36

[12] J. I. Skullerud and A. G. Williams, "Quark propagator in Landau gauge," *Phys. Rev.* **D63** (2001) 054508, arXiv:hep-lat/0007028.
vi, 2, 42, 57

[13] P. O. Bowman, U. M. Heller, D. B. Leinweber, A. G. Williams, and J. B. Zhang, "Quark Propagator from LQCD and Its Physical Implications," in *Lecture Notes in Physics*, vol. 663, pp. 17–63.
Springer Berlin / Heidelberg, 2005.
http://dx.doi.org/10.1007/11356462_2.
vi, 2, 23

[14] P. O. Bowman, U. M. Heller, and A. G. Williams, "Quark propagator from an improved staggered action in Laplacian and Landau gauges," *Nucl. Phys. Proc. Suppl.* **109A** (2002) 163–167, arXiv:hep-lat/0112027.
vi, 2, 43

[15] **CSSM Lattice** Collaboration, F. D. R. Bonnet, P. O. Bowman, D. B. Leinweber, A. G. Williams, and J.-b. Zhang, "Overlap quark propagator in Landau gauge," *Phys. Rev.* **D65** (2002) 114503, arXiv:hep-lat/0202003.
vi, 2, 48

[16] P. O. Bowman, U. M. Heller, and A. G. Williams, "Lattice quark propagator with staggered quarks in Landau and Laplacian gauges," *Phys. Rev.* **D66** (2002) 014505, arXiv:hep-lat/0203001.
vi, 2, 35, 54

[17] P. O. Bowman *et al.*, "Unquenched quark propagator in Landau gauge," *Phys. Rev.* **D71** (2005) 054507, arXiv:hep-lat/0501019.
vi, 2, 68

[18] F. D. R. Bonnet, D. B. Leinweber, A. G. Williams, J. M. Zanotti, and J. B. Zhang, "Quark propagator in a covariant gauge," *Nucl. Phys. Proc. Suppl.* **109A** (2002) 158–162, arXiv:hep-lat/0202011.
vi, 2

[19] J. J. Sakurai, *Modern Quantum Mechanics (Revised Edition)*.
Addison Wesley, September, 1993.
3, 5

[20] H. J. Rothe, *Lattice Gauge Theories*.
World Scientific, 3rd ed., 2005.
3, 7, 17, 18, 27, 46

[21] H. Reinhardt, "Quantum Field Theory." Lecture notes, unpublished.
3, 8

[22] J. Glimm and A. Jaffe, *Quantum Physics. A Functional Integral Point of View*.
Springer-Verlag, 2nd ed., 1987.
7, 39

[23] A. Quarteroni, R. Sacco, and F. Saleri, *Numerical Mathematics (Texts in Applied Mathematics)*.
Springer-Verlag New York, Inc., 2nd ed., 2006.
13

[24] C. Gattringer and C. B. Lang, *Quantum Chromodynamics on the Lattice: An Introductory Presentation*.
Springer, 1st ed., October, 2009.
http://www.amazon.com/exec/obidos/redirect?tag=citeulike07-20&path=ASIN/3642018491.
19, 22, 27, 30, 32, 46

[25] J. Kogut and L. Susskind, "Hamiltonian formulation of Wilson's lattice gauge theories,"*Phys. Rev. D* **11** (Jan, 1975) 395.
21

[26] **MILC** Collaboration, K. Orginos, D. Toussaint, and R. L. Sugar, "Variants of fattening and flavor symmetry restoration," *Phys. Rev.* **D60** (1999) 054503, arXiv:hep-lat/9903032.
24

[27] S. Naik, "On-shell improved lattice action for QCD with Susskind fermions and asymptotic freedom scale," *Nucl. Phys.* **B316** (1989) 238.
25

[28] G. P. Lepage, "Flavor-symmetry restoration and Symanzik improvement for staggered quarks," *Phys. Rev.* **D59** (1999) 074502, arXiv:hep-lat/9809157.
25

[29] G. P. Lepage and P. B. Mackenzie, "On the viability of lattice perturbation theory," *Phys. Rev.* **D48** (1993) 2250–2264, arXiv:hep-lat/9209022.
25

[30] C. Yang and R. Mills, "Conservation of Isotopic Spin and Isotopic Gauge Invariance," *Phys. Rev.* **96** (1954) 191.
28

[31] K. Wilson, "Confinement of quarks," *Phys. Rev. D* **10** (1974) 2445.
29

[32] M. Creutz, "Monte Carlo study of quantized SU(2) gauge theory," *Phys. Rev. D* **21** (1980) 2308.
33

[33] N. Cabibbo and E. Marinari, "A New Method for Updating SU(N) Matrices in Computer Simulations of Gauge Theories," *Phys. Lett. B* **119** (1982) 387. http://www.slac.stanford.edu/spires/find/hep/www?j=PHLTA,B119,387.
33, 36, 45

[34] C. W. Bernard *et al.*, "The QCD spectrum with three quark flavors," *Phys. Rev.* **D64** (2001) 054506, arXiv:hep-lat/0104002.
34, 62

[35] S. Elitzur, "Impossibility of Spontaneously Breaking Local Symmetries," *Phys. Rev.* **D12** (1975) 3978–3982.
34

[36] C. D. G. S. Kirkpatrick and M. P. Vecchi, "Optimization by Simulated Annealing," *Science* **220** (1983) 671.
35

[37] J. E. Mandula and M. Ogilvie, "Efficient gauge fixing via overrelaxation," *Physics Letters B* **248** (1990) no. 1-2, 156 – 158. http://www.sciencedirect.com/science/article/B6TVN-46YSKXM-CB/2/d82308fbb15e56bce446611b7efbff68.
35

[38] A. Polyakov, "Compact gauge fields and the infrared catastrophe," *Phys. Lett. B* **59** (1975) 82.
36

[39] D. A. Bini, N. J. Higham, and B. Meini, "Algorithms for the Matrix pth Root," *Numerical Algorithms* **39** (2005) no. 4, 349.
36

[40] **FermiQCD** Collaboration, M. Di Pierro *et al.*, "www.fermiqcd.net," *Nucl. Phys. Proc. Suppl.* **129** (2004) 832–834, arXiv:hep-lat/0311027.
38, 45, 49

[41] B. Efron, *The Jackknife, the Bootstrap, and Other Resampling Plans.* Society for Industrial Mathematics, 1982.
44, 49

[42] M. Di Pierro, "Parallel programming with matrix distributed processing," arXiv:hep-lat/0505005.
45

[43] J. Collins, *Renormalization.* Cambridge University Press, 1984.
46

[44] R. Sommer, "A new way to set the energy scale in lattice gauge theories and its application to the static force and [sigma]s in SU (2) Yang-Mills theory," *Nuclear Physics B* **411** (1994) no. 2-3, 839 – 854. http://www.sciencedirect.com/science/article/B6TVC-472SYSS-C7/2/1ce34f7a5993f4bb1d094ca2c74c29ac.
46

[45] S. Necco and R. Sommer, "The Nf=0 heavy quark potential from short to intermediate distances," hep-lat/0108008.
46

[46] L. H. Ryder, *Quantum Field Theory.* Cambridge University Press, 2nd ed., 1996.
46

[47] **UKQCD** Collaboration, K. C. Bowler *et al.*, "Quenched QCD with O(a) improvement. I: The spectrum of light hadrons," *Phys. Rev.* **D62** (2000) 054506, arXiv:hep-lat/9910022.
47

[48] D. B. Leinweber, J. I. Skullerud, A. G. Williams, and C. Parrinello, "Gluon propagator in the infrared region,"*Phys. Rev. D* **58** (Jul, 1998) 031501.
48, 61

[49] MILC Collaboration, "MILC Gauge Configurations." www.physics.indiana.edu/~sg/milc/lattices.pdf.
62

[50] L. C. Evans, *Partial Differential Equations.*

American Mathematical Society, 1998.
84

Lists

List of Figures

List of Tables

List of Acronyms

PI path integral
QCD Quantum Chromodynamics
QED Quantum Electrodynamics
HO harmonic oscillator
r.h.s. right-hand side
l.h.s. left-hand side
BZ Brillouine zone
MDP Matrix Distributed Processing
MPI Message Passing Interface
UV ultraviolet
IR infrared
MOM momentum subtraction scheme
KS Kogut–Susskind

Acknowledgments

I am very grateful to Hugo Reinhardt for introducing me to lattice QCD and offering me this interesting research project. My special acknowledgments are due to Giuseppe Burgio who always had a sympathetic ear and gave me helpful advice and assistance. Furthermore, I want to address thanks to Markus Quandt for his support with the new computer rack at our institute. I also express gratitude to Jan Heffner and Markus Pak for helpful discussions and thanks are also due to Davide Campagnari for critical reading of the manuscript.

I want to thank my girlfriend Isabel Voigtländer for all the patience which I demanded from her during my studies of physics.

Last but not least, I wish to extend special thanks to my parents for supporting and funding me during my studies of physics in Tübingen, as well as during my year abroad at the State University of New York at Stony Brook.

Appendix A

Appendix

A.1 Natural units

Throughout this work we set the speed of light $c = 1$, as well as Planck's constant $\hbar = 1$. From the former follows that length and time have the same dimensions,

$$[\text{length}] = [\text{time}]. \tag{A.1}$$

Because $\hbar = 1$, we obtain that the dimension of energy equals the inverse dimension of time,

$$[\text{energy}] = [\text{time}]^{-1}. \tag{A.2}$$

Moreover, the relativistic relation between mass and energy

$$E^2 = m^2c^4 + p^2c^2 \tag{A.3}$$

yields that energy, mass and momentum have the same dimensions and, in conclusion,

$$[\text{mass}] = [\text{length}]^{-1} \tag{A.4}$$

whereas the latter reads quantitatively

$$1 = \hbar c \simeq 197.327\,\text{MeV fm} \iff 1\,\text{fm}^{-1} \simeq 197.327\,\text{MeV}. \tag{A.5}$$

A.2 Green's integration formula

Theorem A.1. *Let ϕ, ψ be two times continuously differentiable within the domain $\Omega \subseteq \mathbb{R}^n$. Then*

$$\int_\Omega d^n x \nabla\phi \cdot \nabla\psi = -\int_\Omega dx\, \phi\, \Delta\psi + \int_{\partial\Omega} dS\, \phi\, \partial_n \psi, \tag{A.6}$$

where ∂_n is the derivative in the outer normal direction.

Proof see, e.g., [50].

A.3 Chiral symmetry

A.3.1 Invariance of the massless Dirac operator

We consider the fermionic action

$$\begin{aligned} S_F[\psi,\overline{\psi},A] &= \int \mathrm{d}^4x\, \overline{\psi}(x) D(x) \psi(x), \\ D(x) &= \gamma_\mu \left(\partial_\mu + iA_\mu(x)\right) \end{aligned} \tag{A.7}$$

where D is the massless Dirac operator. We define *chiral rotations* of the fermion fields as

$$\psi(x) \to \psi'(x) = \mathrm{e}^{i\alpha\gamma_5}\, \psi(x), \quad \overline{\psi}(x) \to \overline{\psi}'(x) = \mathrm{e}^{i\alpha\gamma_5}\, \overline{\psi}(x) \tag{A.8}$$

with $\gamma_5 \equiv \gamma_1\gamma_2\gamma_3\gamma_4$ and $\alpha \in \mathbb{R}$. Then the Lagrangian in (A.7) is invariant under this transformation since $\{\gamma_5,\gamma_\mu\} = 0$, and a mass term would obviously break this symmetry.

Define right- and left-handed projectors

$$P_R = \frac{1}{2}\left(\mathbb{1} + \gamma_5\right), \quad P_L = \frac{1}{2}\left(\mathbb{1} - \gamma_5\right) \tag{A.9}$$

which project onto orthogonal subspaces $P_R P_L = P_L P_R = 0, P_L + P_R = \mathbb{1}$ and for which

$$\gamma_\mu P_L = P_R \gamma\mu, \quad \gamma_\mu P_R = P_L \gamma\mu. \tag{A.10}$$

Therewith we define right- and left-handed fermion fields

$$\psi_R(x) = P_R\psi(x), \quad \psi_L(x) = P_L\psi(x) \tag{A.11}$$

and equivalently for $\overline{\psi}(x)$. Calculate

$$\begin{aligned}\overline{\psi}D\psi &= \overline{\psi}(P_R+P_L)D(P_L+P_R)\psi \\ &= \gamma_\mu P_R\overline{\psi}\left(\partial_\mu + iA_\mu\right)P_L\psi + \gamma_\mu P_L\overline{\psi}\left(\partial_\mu + iA_\mu\right)P_R\psi \\ &+ \gamma_\mu P_R\overline{\psi}\left(\partial_\mu + iA_\mu\right)P_R\psi + \gamma_\mu P_L\overline{\psi}\left(\partial_\mu + iA_\mu\right)P_L\psi \\ &= P_L\gamma_\mu\overline{\psi}\left(\partial_\mu + iA_\mu\right)P_L\psi + P_R\gamma_\mu\overline{\psi}\left(\partial_\mu + iA_\mu\right)P_R\psi \\ &+ P_L\gamma_\mu\overline{\psi}\left(\partial_\mu + iA_\mu\right)P_R\psi + P_R\gamma_\mu\overline{\psi}\left(\partial_\mu + iA_\mu\right)P_L\psi \\ &= \overline{\psi}_L D\psi_L + \overline{\psi}_R D\psi_R.\end{aligned} \tag{A.12}$$

Thus we see that the Dirac operator can be decomposed into a left- and a right-handed part.

A.3.2 The chiral condensate

Consider the vacuum expectation value $\left\langle\overline{\psi}_R(x)\psi_L(x)\right\rangle$, where $\overline{\psi}_R(x)\psi_L(x)$ transforms under (A.8) as

$$\overline{\psi}_R(x)\psi_L(x) \to \mathrm{e}^{i(\alpha-\alpha')\gamma_5}\,\overline{\psi}_R(x)\psi_L(x). \tag{A.13}$$

When the vacuum expectation value $\left\langle\overline{\psi}_R(x)\psi_L(x)\right\rangle$ or equivalently $\left\langle\overline{\psi}_L(x)\psi_R(x)\right\rangle$ is left invariant under such a transformation, it must vanish. Thus the *chiral condensate*

$$\left\langle\overline{\psi}(x)\psi(x)\right\rangle = \left\langle\overline{\psi}_R(x)\psi_L(x)\right\rangle + \left\langle\overline{\psi}_L(x)\psi_R(x)\right\rangle \tag{A.14}$$

is a measure of spontaneous breaking of chiral symmetry.

A.4 Coulomb gauge and gauge functionals

We prove that the continuum Coulomb gauge condition $\partial_i A_i(x)$ is equivalent to maximizing

$$\tilde{F}_G[A](x_4) = \sum_{i=1}^{3}\int \mathrm{d}^3\boldsymbol{x}\ \mathrm{tr}\left[\left(G(x)A_i(x)G^\dagger(x)\right)^2\right]. \tag{A.15}$$

for all x_4 with respect to gauge transformations $G(x) \in \mathrm{SU}(3)$.

Consider infinitesimal gauge transformations

$$G(x) = \mathrm{e}^{i\varepsilon H(x)}, \quad G^\dagger(x) = \mathrm{e}^{-i\varepsilon H(x)} \tag{A.16}$$

with $\varepsilon \in \mathbb{R}$ small and $H(x)$ an arbitrary traceless hermitian matrix. Under this infinitesimal

gauge transformation the gauge field $A_\mu(x)$ transforms as, cf. (3.62c),

$$\begin{aligned} A_\mu(x) \to A'_\mu(x) &= G(x)A_\mu(x)G^\dagger(x) + i\left(\partial_\mu G(x)\right)G^\dagger(x) \\ &= \mathrm{e}^{i\varepsilon H(x)}\, A_\mu(x)\, \mathrm{e}^{-i\varepsilon H(x)} - \varepsilon\partial_\mu H(x) \\ &= (\mathbb{1} + i\varepsilon H(x))\, A_\mu(x)\, (\mathbb{1} - i\varepsilon H(x)) - \varepsilon\partial_\mu H(x) \\ &= A_\mu(x) + \varepsilon\left\{i\left[H(x), A_\mu(x)\right] - \partial_\mu H(x)\right\} + \mathcal{O}(\varepsilon^2). \end{aligned} \tag{A.17}$$

Plugging this into (A.15) for $G(x)A_i(x)G^\dagger(x)$ and taking the periodicity of the trace into account, which makes the contributions from the commutator vanish, yields for the transformation of the gauge functional

$$\begin{aligned} \tilde{F}_G[A'](x_4) &= \sum_{i=1}^{3} \int \mathrm{d}^3\boldsymbol{x}\ \mathrm{tr}\left[A_i^2(x) - \varepsilon A_i(x)\partial_i H(x) - \varepsilon\partial_i H(x) A_i(x)\right] + \mathcal{O}(\varepsilon^2) \\ &= \tilde{F}_G[A](x_4) - 2\varepsilon \sum_i \int \mathrm{d}^3\boldsymbol{x}\ \mathrm{tr}\left[A_i(x)\partial_i H(x)\right] + \mathcal{O}(\varepsilon^2) \\ &= \tilde{F}_G[A](x_4) + 2\varepsilon \sum_i \int \mathrm{d}^3\boldsymbol{x}\ \mathrm{tr}\left[(\partial_i A_i(x))H(x)\right] + \mathcal{O}(\varepsilon^2). \end{aligned} \tag{A.18}$$

In the last step we performed an integration by parts under the assumption that $H(x)$ vanishes for large x. It is now obvious from (A.18) that the gauge functional is in an extremum if and only if $\sum_i \partial_i A_i(x)$ vanishes.

An equivalent condition on the lattice is the prescription to extremize

$$F_G[U](n_4) = a^2 \sum_{i=1}^{3} \sum_{\boldsymbol{n}} \mathrm{tr}\left[G(n)U_i(n)G^\dagger(n+\hat{i}) + G(n+\hat{i})U_i^\dagger(n)G^\dagger(n)\right] \tag{A.19}$$

with respect to $G(n)$, which is equivalent to (A.15) since

$$U_\mu(n) \approx \mathbb{1} + iaA_\mu(n) - \frac{a^2}{2}A_\mu^2(n) + \mathcal{O}(a^3). \tag{A.20}$$

In order to see that space independent gauge transformations $G(x_4)$ leave the Coulomb gauge undisturbed, consider a subsequent infinitesimal gauge transformation $G(x_4) = \mathrm{e}^{i\varepsilon H(x_4)}$,

$$\begin{aligned} A_i(x) \to A''_i(x) &= A_i(x) + \varepsilon\left\{i\left[H(x_4), A_i(x)\right] - \partial_i H(x_4)\right\} + \mathcal{O}(\varepsilon^2) \\ &= A_i(x) + \varepsilon i\left[H(x_4), A_i(x)\right] + \mathcal{O}(\varepsilon^2) \end{aligned} \tag{A.21}$$

of (A.18). Since $\partial_i H(x_4)$ vanishes and the commutator does not contribute under the trace, we obtain

$$\tilde{F}_G[A''](x_4) = \tilde{F}_G[A'](x_4). \tag{A.22}$$

A.5 On the connection of the dressing functions of the propagator and its inverse

We have to prove that

$$D^2(p) = \frac{A_t(p)}{\mathcal{A}_t(p)} = \frac{A_s(p)}{\mathcal{A}_s(p)} = \frac{A_d(p)}{\mathcal{A}_d(p)} = \frac{B_m(p)}{\mathcal{B}_m(p)} \iff \mathcal{D}^2(p) = \frac{\mathcal{A}_t(p)}{A_t(p)} = \frac{\mathcal{A}_s(p)}{A_s(p)} = \frac{\mathcal{A}_d(p)}{A_d(p)} = \frac{\mathcal{B}_m(p)}{B_m(p)}, \tag{A.23}$$

with

$$D^2(p) := k_4^2 A_t^2(p) + \sum_i k_i^2 A_s^2(p) + k_4^2 \sum_i k_i^2 A_d^2(p) + B_m^2(p), \tag{A.24}$$

$$\mathcal{D}^2(p) := k_4^2 \mathcal{A}_t^2(p) + \sum_i k_i^2 \mathcal{A}_s^2(p) + k_4^2 \sum_i k_i^2 \mathcal{A}_d^2(p) + \mathcal{B}_m^2(p) \tag{A.25}$$

It is sufficient to show one direction, e.g., "$\Longrightarrow$", since the other direction can be shown in an analogues way. We start by inverting the left set of equations

$$\frac{1}{D^2(p)} = \frac{\mathcal{A}_t(p)}{A_t(p)} = \frac{\mathcal{A}_s(p)}{A_s(p)} = \frac{\mathcal{A}_d(p)}{A_d(p)} = \frac{\mathcal{B}_m(p)}{B_m(p)}, \tag{A.26}$$

so we can see that if we want (2) following from (1), we have to show that

$$\mathcal{D}^2(p) D^2(p) = 1. \tag{A.27}$$

By assumption we have

$$\mathcal{A}_t^2(p) = \frac{A_t^2(p)}{D^4(p)}, \quad \mathcal{A}_s^2(p) = \frac{A_s^2(p)}{D^4(p)}, \quad \mathcal{A}_d^2(p) = \frac{A_d^2(p)}{D^4(p)}, \quad \mathcal{B}_m^2(p) = \frac{B_m^2(p)}{D^4(p)}, \tag{A.28}$$

what we may plug into $\mathcal{D}^2(p)$ to yield

$$\left(\frac{k_4^2 A_t^2(p) + \sum_i k_i^2 A_s^2(p) + k_4^2 \sum_i k_i^2 A_d^2(p) + B_m^2(p)}{D^4(p))} \right) D^2(p) \equiv 1. \tag{A.29}$$

A.6 Formulas for $Z(\boldsymbol{p})$ and $M(\boldsymbol{p})$

Using Feynman's slash notation, $\not{k} \equiv \gamma_i k_i$ and $\not{k}_4 \equiv \gamma_4 k_4$, we have

$$S^{-1}(p) = i\not{k} a A_s(p) + i\not{k}_4 a A_t(p) + B_m(p) \tag{A.30}$$

$$= i\not{k} a \frac{\mathcal{A}_s(p)}{\mathcal{D}^2(p)} + i\not{k}_4 a \frac{\mathcal{A}_t(p)}{\mathcal{D}^2(p)} + \frac{\mathcal{B}_m(p)}{\mathcal{D}^2(p)} \tag{A.31}$$

and

$$S(p) = -i\not{k} a \mathcal{A}_s(p) - i\not{k}_4 a \mathcal{A}_t(p) + \mathcal{B}_m(p) \tag{A.32}$$

$$= -i\not{k} a \frac{A_s(p)}{D^2(p)} - i\not{k}_4 a \frac{A_t(p)}{D^2(p)} + \frac{B_m(p)}{D^2(p)} \tag{A.33}$$

where

$$D^2(p) \equiv \boldsymbol{k}^2 a^2 A_s^2(p) + k_4^2 a^2 A_t^2(p) + B_m^2(p), \tag{A.34}$$

$$\mathcal{D}^2(p) \equiv \boldsymbol{k}^2 a^2 \mathcal{A}_s^2(p) + k_4^2 a^2 \mathcal{A}_t^2(p) + \mathcal{B}_m^2(p). \tag{A.35}$$

Integration over k_4 yields ($A_t(p)$ even function with respect to k_4)

$$\overline{S}^{-1}(\boldsymbol{p}) = i\not{k} a \int_{-\pi}^{\pi} \frac{\mathrm{d}\hat{p}_4}{2\pi} A_s(p) + \int_{-\pi}^{\pi} \frac{\mathrm{d}\hat{p}_4}{2\pi} B_m(p) \tag{A.36}$$

$$= i\not{k} a \int_{-\pi}^{\pi} \frac{\mathrm{d}\hat{p}_4}{2\pi} \frac{\mathcal{A}_s(p)}{\mathcal{D}^2(p)} + \int_{-\pi}^{\pi} \frac{\mathrm{d}\hat{p}_4}{2\pi} \frac{\mathcal{B}_m(p)}{\mathcal{D}^2(p)} \tag{A.37}$$

and

$$\overline{S}(\boldsymbol{p}) = -i\not{k} a \int_{-\pi}^{\pi} \frac{\mathrm{d}\hat{p}_4}{2\pi} \mathcal{A}_s(p) + \int_{-\pi}^{\pi} \frac{\mathrm{d}\hat{p}_4}{2\pi} \mathcal{B}_m(p) \tag{A.38}$$

$$= -i\not{k} a \int_{-\pi}^{\pi} \frac{\mathrm{d}\hat{p}_4}{2\pi} \frac{A_s(p)}{D^2(p)} + \int_{-\pi}^{\pi} \frac{\mathrm{d}\hat{p}_4}{2\pi} \frac{B_m(p)}{D^2(p)}. \tag{A.39}$$

Invert (A.36):

$$\overline{S}(\boldsymbol{p}) = \frac{-i\not{k} a \int_{-\pi}^{\pi} \frac{\mathrm{d}\hat{p}_4}{2\pi} A_s(p) + \int_{-\pi}^{\pi} \frac{\mathrm{d}\hat{p}_4}{2\pi} B_m(p)}{P^2(\boldsymbol{p})}, \tag{A.40}$$

$$P^2(\boldsymbol{p}) \equiv \boldsymbol{k}^2 a^2 \left(\int_{-\pi}^{\pi} \frac{\mathrm{d}\hat{p}_4}{2\pi} A_s(p) \right)^2 + \left(\int_{-\pi}^{\pi} \frac{\mathrm{d}\hat{p}_4}{2\pi} B_m(p) \right)^2. \tag{A.41}$$

Invert (A.38):

$$\overline{S}^{-1}(\boldsymbol{p}) = \frac{i\not{k} a \int_{-\pi}^{\pi} \frac{\mathrm{d}\hat{p}_4}{2\pi} \mathcal{A}_s(p) + \int_{-\pi}^{\pi} \frac{\mathrm{d}\hat{p}_4}{2\pi} \mathcal{B}_m(p)}{\mathcal{P}^2(\boldsymbol{p})}, \tag{A.42}$$

$$\mathcal{P}^2(\boldsymbol{p}) \equiv \boldsymbol{k}^2 a^2 \left(\int_{-\pi}^{\pi} \frac{\mathrm{d}\hat{p}_4}{2\pi} \mathcal{A}_s(p) \right)^2 + \left(\int_{-\pi}^{\pi} \frac{\mathrm{d}\hat{p}_4}{2\pi} \mathcal{B}_m(p) \right)^2. \tag{A.43}$$

Compare (A.36) with (A.42) to obtain

$$\int_{-\pi}^{\pi} \frac{\mathrm{d}\hat{p}_4}{2\pi} A_s(p) = \frac{\int_{-\pi}^{\pi} \frac{\mathrm{d}\hat{p}_4}{2\pi} \mathcal{A}_s(p)}{\mathcal{P}^2(\boldsymbol{p})}, \tag{A.44}$$

$$\int_{-\pi}^{\pi} \frac{\mathrm{d}\hat{p}_4}{2\pi} B_m(p) = \frac{\int_{-\pi}^{\pi} \frac{\mathrm{d}\hat{p}_4}{2\pi} \mathcal{B}_m(p)}{\mathcal{P}^2(\boldsymbol{p})}. \tag{A.45}$$

Compare (A.38) with (A.40) to obtain

$$\int_{-\pi}^{\pi} \frac{\mathrm{d}\hat{p}_4}{2\pi} \mathcal{A}_s(p) = \frac{\int_{-\pi}^{\pi} \frac{\mathrm{d}\hat{p}_4}{2\pi} A_s(p)}{P^2(\boldsymbol{p})}, \tag{A.46}$$

$$\int_{-\pi}^{\pi} \frac{\mathrm{d}\hat{p}_4}{2\pi} \mathcal{B}_m(p) = \frac{\int_{-\pi}^{\pi} \frac{\mathrm{d}\hat{p}_4}{2\pi} B_m(p)}{P^2(\boldsymbol{p})}. \tag{A.47}$$

We write the static propagator as

$$\overline{S}(\boldsymbol{p}) = Z(\boldsymbol{p}) \frac{-i\not{\boldsymbol{k}} a + M(\boldsymbol{p})}{\boldsymbol{k}^2 a^2 + M^2(\boldsymbol{p})}, \tag{A.48}$$

$$\overline{S}^{-1}(\boldsymbol{p}) = Z^{-1}(\boldsymbol{p}) \left(i\not{\boldsymbol{k}} a + M(\boldsymbol{p})\right). \tag{A.49}$$

Compare (A.42) and (A.49):

$$Z(\boldsymbol{p}) = \frac{\mathcal{P}^2(\boldsymbol{p})}{\int_{-\pi}^{\pi} \frac{\mathrm{d}\hat{p}_4}{2\pi} \mathcal{A}_s(p)} = \left(\int_{-\pi}^{\pi} \frac{\mathrm{d}\hat{p}_4}{2\pi} A_s(p) \right)^{-1}, \tag{A.50}$$

$$M(\boldsymbol{p}) = \frac{\int_{-\pi}^{\pi} \frac{\mathrm{d}\hat{p}_4}{2\pi} \mathcal{B}_m(p)}{\int_{-\pi}^{\pi} \frac{\mathrm{d}\hat{p}_4}{2\pi} \mathcal{A}_s(p)} = \frac{\int_{-\pi}^{\pi} \frac{\mathrm{d}\hat{p}_4}{2\pi} B_m(p)}{\int_{-\pi}^{\pi} \frac{\mathrm{d}\hat{p}_4}{2\pi} A_s(p)}. \tag{A.51}$$

Or compare alternatively (A.40) and (A.48), then

$$\frac{\int_{-\pi}^{\pi} \frac{\mathrm{d}\hat{p}_4}{2\pi} A_s(p)}{P^2(p)} = \frac{Z(\boldsymbol{p})}{\boldsymbol{k}^2 a^2 + M^2(\boldsymbol{p})} \iff Z(\boldsymbol{p}) = \left(\boldsymbol{k}^2 a^2 + M^2(\boldsymbol{p})\right) \int_{-\pi}^{\pi} \frac{\mathrm{d}\hat{p}_4}{2\pi} \mathcal{A}_s(p) \tag{A.52}$$

$$\frac{\int_{-\pi}^{\pi} \frac{\mathrm{d}\hat{p}_4}{2\pi} B_m(p)}{P^2(p)} = \frac{Z(\boldsymbol{p}) M(\boldsymbol{p})}{\boldsymbol{k}^2 a^2 + M^2(\boldsymbol{p})} \iff M(\boldsymbol{p}) = \frac{\int_{-\pi}^{\pi} \frac{\mathrm{d}\hat{p}_4}{2\pi} \mathcal{B}_m(p)}{\int_{-\pi}^{\pi} \frac{\mathrm{d}\hat{p}_4}{2\pi} \mathcal{A}_s(p)}. \tag{A.53}$$